
Wayne State University Dissertations

January 2019

Self-Delivery Drug Amphiphilics In Chemotherapy And Immunotherapy

Jingchao Xi
Wayne State University

Follow this and additional works at: https://digitalcommons.wayne.edu/oa_dissertations

 Part of the [Chemical Engineering Commons](#)

Recommended Citation

Xi, Jingchao, "Self-Delivery Drug Amphiphilics In Chemotherapy And Immunotherapy" (2019). *Wayne State University Dissertations*. 2341.

https://digitalcommons.wayne.edu/oa_dissertations/2341

This Open Access Embargo is brought to you for free and open access by DigitalCommons@WayneState. It has been accepted for inclusion in Wayne State University Dissertations by an authorized administrator of DigitalCommons@WayneState.

**SELF-DELIVERY DRUG AMPHIPHILIES IN CHEMOTHERAPY AND
IMMUNOTHERAPY**

by

JINGCHAO XI

DISSERTATION

Submitted to the Graduate School

of Wayne State University,

Detroit, Michigan

in partial fulfillment of the requirements

for the degree of

DOCTOR OF PHILOSOPHY

2019

MAJOR: CHEMICAL ENGINEERING

Approved By:

Advisor

Date

ACKNOWLEDGEMENTS

I am not sure whether it was a meaningful day. But time flew. I could still remember the day I arrived at Detroit. Throughout the five years study and life at Wayne State University, I have received a great deal of support and assistance.

First of all, I would like to thank my parents, family and Mr. Chao Zhang who gave me suggestions and supported me under any circumstances.

I would like to express my special appreciation and thanks to my advisor Professor Haipeng Liu, you have been a tremendous mentor for me. I would like to thank you for encouraging my research and for allowing me to grow as a research scientist. Your advice on both research as well as on my career have been invaluable.

Besides my advisor, I would like to thank the rest of my thesis committee: Prof. Guangzhao Mao, Prof. Zhiqiang Cao, and Pro. Fei Chen, for their insightful comments and encouragement, but also for the hard question which incited me to widen my research from various perspectives.

Special thanks are also extended to all professors at Wayne State University I have worked with during my doctoral research: Dr. Yingxi Zhu at Chemical Engineering, Dr. Mai T. Lam and Dr. Weiping Ren at Biomedical Engineering whose supervision, expertise and suggestions greatly aided the completion of my research in the past 5 years.

I thank my labmates, Yiwei Chen, Myunggi An, Benxin Jing, Chunsong Yu and Cameron B. Pinnock in for the stimulating discussions, for the sleepless nights we were working together before deadlines, and for all the fun we have

had in the last four years. In particular, I am grateful to Dr. Meng Li for enlightening me the first glance of research.

Last, I would also like to thank the Department of Chemical Engineering and The Graduate School at Wayne State University for their financial support during my tenure as a graduate student.

TABLE OF CONTENTS

ACKNOWLEDGEMENTS	i
LIST OF FIGURES	viii
LIST OF TABLES	xvi
Chapter 1. Introduction and literature review	1
1.1 Overview	1
1.2 The design principles of self-delivery drug amphiphiles	5
1.2.1 Amphiphilic drug modification: conjugation strategies and types of linkers	5
1.2.2 Amphiphilic modification enhances circulation half-life and tissue/organ targeting	7
1.2.3 Amphiphilic modification improves oral bioavailability.	9
1.2.4 Amphiphilic modification overcomes blood-brain barrier	10
1.2.5 Amphiphilic modification facilitates drug uptake and targeting at subcellular level.	11
1.3 Clinical and preclinical examples of drug amphiphiles.	13
1.3.1 Amphiphilic oligonucleotides (ODNs).	13
1.3.2 Amphiphilic peptides.	15
1.3.3 Amphiphilic Small Molecular Drugs.	21
Chapter 2. Self-delivery of chemotherapeutic agents to tumor via ‘albumin-hitchhiking’	25
2.1 Introduction	25
2.1.1 Albumin as a fatty acid transporter.	25
2.1.2 Albumin as a drug carrier in cancer therapy.	26
2.2 Method	31

2.2.1 Materials, cells and animals.	31
2.2.2 Synthesis of amphiphilic doxorubicin and doxorubicin loaded micelles.	31
2.2.3 Dynamic light scattering (DLS).	33
2.2.4 Electrophoretic mobility shift assay (EMSA).	33
2.2.5 Fluorescence resonance energy transfer assay ¹	34
2.2.6 Membrane insertion and cellular uptake studies.	34
2.2.7 Mechanism of cellular entrance.	35
2.2.8 <i>In vivo</i> pharmacokinetics values.	35
2.2.9 <i>In vivo</i> biodistribution study.	36
2.2.10 Tumor model.	37
2.2.11 Hematoxylin and eosin (H&E) staining.	37
2.2.12 Statistical analysis.	37
2.3 Results and discussions.	39
2.3.1 Design of albumin-based self-delivery amphiphilic conjugates. ...	39
2.3.2 Amphiphilic doxorubicin avidly binds to circulating serum albumin.	43
2.3.4 Three-way equilibriums of amphiphilic doxorubicin.	47
2.3.5 Analysis of uptake pathway under three-way equilibrium.	49
2.3.6 Albumin binding amphiphilic DOX extends half-life, alteration drug distribution and improves the therapeutic anti-tumor efficacy.	53
2.4 Conclusions.	58
Chapter 3. Amphiphilic doxorubicin specifically targets cell mitochondria.	60
3.1 Introduction.	60

3.1.1 Targeting mitochondria for cancer therapy.	60
3.2 Method.....	64
3.2.1 Materials, cells and animals.	64
3.2.2 Design and conjugation of amphiphilic doxorubicin.	65
3.2.3 Synthesis of pH sensitive amphiphilic doxorubicin.....	66
3.2.4 Preparation of doxorubicin loaded DSPE-PEG ₂₀₀₀ micelles.	66
3.2.5 <i>In vitro</i> cytotoxicity.	67
3.2.6 Cellular uptake studies.	67
3.2.7 Subcellular tracking study.	68
3.2.8 <i>In vitro</i> colocalization analysis.....	69
3.2.9 Mitochondria and nuclei isolation.	69
3.2.10 Measurement of reactive oxygen species (ROS) generation.	70
3.2.11 Tumor model and confocal microscopy images of tumor tissue.	70
3.2.12 Statistical analysis.	71
3.3 Results and discussions.....	72
3.3.1 Amphiphilic modification increases DOX-induced antitumor effect in multiple murine cell lines.	72
3.3.2 Amphiphilic modification overcomes drug resistance in breast adenocarcinoma cells.....	73
3.3.3 Amphiphilic DOX accumulates in mitochondrial area <i>in vitro</i>	74
3.3.4 Discussion of potential mitochondrial targeting mechanism.	79
3.3.5 Albumin is not engaged as a participant of the intracellular sorting of amphiphilic DOX.	84
3.3.6 Amphiphilic modification is not a universal strategy for mitochondria drug delivering.....	86

3.3.7 Amphiphilic DOX generates massive reactive oxygen species (ROS) in mitochondria.	90
3.3.8 Amphiphilic DOX achieves tumoral -mitochondrial targeting <i>in vivo</i>	91
3.4 Conclusions.	93
Chapter 4. Enhancing Antigen Presentation and Inducing Antigen-Specific Immune Tolerance with Amphiphilic Peptides.	95
4.1 Introduction.	95
4.1.1 Type 1 diabetes(T1D) and peptide therapy.	96
4.1.2 Autoantigen presentation plays a key role in triggering peripheral tolerance of T1D.	97
4.2 Method.	100
4.2.1 Materials.	100
4.2.2 Cells and animals.	100
4.2.3 Preparation and purification of amphiphilic antagonists.	101
4.2.5 <i>In vitro</i> characterization.	102
4.2.6 Electrophoretic mobility shift assay (EMSA).	103
4.2.7 Lymph nodes draining and cellular uptake.	103
4.2.8 <i>Ex vivo</i> antigen presentation assay.	104
4.2.9 <i>In vivo</i> tolerization with amphiphilic peptide.	104
4.2.10 <i>In vivo</i> tolerization with amphiphilic antagonists and antigen.	105
4.2.12 Antigen-specific cytotoxic T lymphocyte (CTL) detection.	105
4.2.14 Enzyme-linked immunosorbent assay (ELISA).	106
4.2.15 Monitoring blood glucose levels.	107
4.2.16 Statistical analysis.	107

4.3 Results and discussions.....	108
4.3.1 Synthesis of amphiphilic antagonists.	108
4.3.2 Synthesis of amphiphilic peptides.	109
4.3.3 Amphiphilic antagonists downregulate the expression of CD40, CD80.....	110
4.3.4 Immunosuppression with amphiphilic antagonists <i>in vivo</i>.....	113
4.3.5 Study of antigen-specific immune tolerance	117
4.3.6 Immunosuppression with amphiphilic peptides.	118
4.3.7 Amphiphilic peptide antigen binds albumin, accumulates in the antigen presenting cells in the draining lymph nodes.....	122
4.3.8 Amphiphilic peptide antigen anchors on cell membrane and increase the interaction between peptide and major histocompatibility complex (MHC) complex.....	124
4.3.9 Membrane anchored amphiphilic peptide enhances the antigen presentation.....	126
4.3.10 Albumin-hitchhiking amphiphilic vaccines in animal models of Type 1 Diabetes (T1D).....	129
4.4 Conclusions.....	131
Chapter 5. Conclusions and Future Perspectives.	132
References	134
ABSTRACT	177
Autobiographical Statement	179

LIST OF FIGURES

- Figure 1.1.1 Improving drug delivery by amphiphilic drug conjugate.** (A) Schematic illustration of the design of drug amphiphiles. A typical drug amphiphile can be divided into three individual fractions: a pharmaceutical payload, a linker, and a chemical modification which renders the drug amphiphilic. (B) The interactions between drug amphiphiles and their biological surroundings can be controlled by molecular engineering which governs the drug molecules' physicochemical properties.....4
- Figure 1.3.1.1 Representative examples of oligonucleotide amphiphiles.** Amphiphilic immunostimulatory oligonucleotide equilibrates between membrane insertion state and albumin binding state and can be used to directly label tumor cells (intratumoral injection) or target draining lymph nodes (subcutaneous injection).³⁴ 15
- Figure 1.3.2.1. Examples of peptide amphiphiles.** (A) Molecular structure of Daptomycin.⁸⁰ (B) Model of action of cholesterol-C34 peptide in HIV fusion inhibition. Cholesterol-C34 anchors on the surface of host cells and increases both the affinity and duration of ligand-receptor interactions.⁸⁷⁻⁸⁸ (C) Amphiphilic peptide epitopes self-assemble into cylindrical micelles and facilitate the uptake of antigen presenting cells.⁹⁴⁻⁹⁵ (D) Structure of long-acting insulin detemir (Levemir). Insulin is modified with myristic acid at the lysine amino acid at position B29. This modification causes protein self-association as well as albumin protein binding, which prolongs the duration of action.⁹⁶ 18
- Figure 1.3.3.1. Example of small molecule drug amphiphiles.** (A) molecular structures and TEM images of self-assembling camptothecin and peptide conjugates.¹⁰³ (B) self-assembling irinotecan-chlorambucil drug-drug conjugate.¹⁰⁵ (C) Molecular structure and confocal image of mitochondria-targeting amphiphilic doxorubicin.⁷⁰ 22
- Figure 2.1.1 Fatty acid (FA) binding sites in human serum albumin (HSA).** 26
- Figure 2.1.2.1 Accumulation of the Evans blue in sarcoma180 tumors over 72 h.**¹² 27
- Figure 2.3.1.1 Target lymph node by albumin-based self-delivery vaccines.**²⁵ (A) Schematic of the design of albumin-based self-delivery vaccines. (B) Size-exclusion chromatography of CpGs, Cho-CpGs, C18-CpGs or Lipo-CpGs alone or following incubation with FBS for 2h. (C) Fluorescent amphiphiles were injected s.c. at the tail base, lymph nodes were isolated and imaged 24 hours post injection. (D) SIINFEKL tetramer of C57BL/6 mice (n = 4–8/group) after immunization with ovalbumin (10 µg) + CpG (1.24 nmol)..... 39
- Figure 2.3.1.1 Synthesis and Nuclear Magnetic Resonance (NMR) characterization of amphiphilic doxorubicin.**⁴⁵ (A) Amphiphilic DOX was

synthesized by conjugating of doxorubicin hydrochloride (DOX) to DSPE-PEG₂₀₀₀-NHS. (B) ¹H-NMR spectra of amphiphilic DOX. The proton peaks of DOX (c, d, and e) and DSPE-PEG (a, b) were observed at 8.5~7.0 ppm and 0.9~3.6 ppm, respectively..... 41

Figure 2.3.2.1 Albumin-binding properties of doxorubicin hydrochloride (DOX) and amphiphilic doxorubicin were assayed by fluorescence resonance energy transfer^{1,45} 40 μM Alexa 660 labeled bovine serum albumin (BSA-Alexa 660) were incubated with either DOX or amphiphilic DOX in PBS (pH 7.4) for four h at 37 °C. After incubation, samples were excited at 470 nm using spectrofluorometer (JASCO FP-6500), and the emission were collected ranging from 540 to 750 nm..... 43

Figure 2.3.2.2 A majority of amphiphilic DOX, instead of free DOX can bind to serum albumin in blood.⁴⁵ (A-C) Fresh isolated blood from mice were incubated with DOX or amphiphilic DOX at a final concentration 0.5 μM for 4 h. After separation, whole blood cells were analyzed by flow cytometry (A) and sera were isolated to quantify the content of drug via fluorescence spectroscopy (B) and binding status were visualized by gel shift assay (C). 45

Figure 2.3.4.1 The membrane insertion property of amphiphilic doxorubicin.⁴⁵ (A) DOX or amphiphilic DOX (1 μM) were co-cultured with B16F10 cells in 10% FBS at 4 °C or 37 °C. Uptake was quantified by flow cytometry. (B) Cellular distribution was analyzed by confocal microscope. 47

Figure 2.3.4.2 Self-assemble, membrane-insertion, and albumin-binding properties of amphiphilic DOX.⁴⁵ In aqueous solution, spherical micelles are self-assembled from amphiphilic DOX with a DOX-PEG sunglow and a lipid core. In the presence of albumin and cells, the micelle structure is disrupted by binding to albumin (albumin hitchhiking) or inserting on plasma membrane (membrane insertion). The structure of lipid-polymer (e.g., the length of lipid and PEG) and albumin concentration govern the equilibrium partitioning between albumin binding state or membrane insertion state. Current structure (DSPE-PEG₂₀₀₀) was optimized for albumin-binding based on our previous finding. At high concentrations of albumin (e.g., 640 μM in blood), the equilibrium strongly favors albumin-binding..... 48

Figure 2.3.5.1 The amphiphilic DOX can exist in three statuses *in vitro* and the uptake pathway were complicated.⁴⁵ (A) Cellular uptake of amphiphilic DOX and DOX loaded DSPE-PEG₂₀₀₀ micelle in 10% FBS. (B and C) B16F10 cells were pretreated with different inhibitors and then incubated with amphiphilic DOX or DSPE-PEG₂₀₀₀ micelles. Cellular uptake was measured by flow cytometry. 49

Figure 2.3.5.2 BSA competed with cells to bind amphiphilic DOX in a certain time but was not a hinder of internalization.⁴⁵ (A and B) B16F10 cells uptake of free DOX and amphiphilic DOX in different concentrations of FBS was examined

by flow cytometry. (C) Uptake of amphiphilic DOX in the presence of low (1 μ M) or high (1 mM) bovine serum albumin..... 51

Figure 2.3.6.1 *In vivo* plasma pharmacokinetic evaluation and biodistribution of amphiphilic DOX in B16F10 tumor bearing C57BL/6 mice model.⁴⁵ (A) Time-drug concentration profile in plasma of DOX and amphiphilic DOX. Plasma doxorubicin concentrations resulting from a single injection free doxorubicin (10 mg/kg) or amphiphilic DOX (10 mg/kg equivalent doxorubicin) as a function of time post injection. (B and C) Tissues (kidney, heart, tumor, liver, spleen) content of drug 2 h (B) and 24 h (C) after a single injection of either DOX and amphiphilic DOX (equivalent doxorubicin at 10 mg/kg). The values are the mean \pm SEM (n = 4)..... 53

Figure 2.3.6.2 *In vivo* anti-tumor activity of amphiphilic DOX in melanoma bearing mice model.⁴⁵ (A and B) Tumor growth inhibition by amphiphilic DOX. Mice were injected with doxorubicin hydrochloride, or amphiphilic DOX, or PBS. All groups (n = 8) of mice received above treatments (5 mg/kg equivalent doxorubicin, 10 μ L/g of the body weight) on days 5, 8 and 11 by intravenous injection in the lateral tail vein. Tumor volumes (A) and body weight (B) were regularly measured during the experimental period. (C) Tumor photographs of whole animals (day 15 after tumor inoculation) and after isolation. To evaluate cardiotoxicity, C57BL/6 mice tumor free were treated with DOX or amphiphilic DOX (10 mg/kg of body weight) at days 5, 8, and 11, and a maximum dose of 20 mg/kg on day 16. Representative photomicrographs of heart sections of DOX and amphiphilic DOX treated. (D) H&E staining of myocardium sections from tumor-free mice. Vacuole structures are indicated with black arrows..... 56

Figure 3.2.1.1 Structures and anticancer drugs as substrates of P-glycoprotein (P-gp) transporter.⁴³⁻⁴⁵ 62

Figure 3.2.3.1 Molecular structure of amphiphilic doxorubicin (amph- DOX).⁵⁸ 65

Figure 3.3.1.1 Amphiphilic DOX induced cytotoxicity in murine cell lines.⁵⁸ (A-C) *In vitro* cell viability of B16F10 (A), 4T1 (B), or EG7 (C) cells against unmodified DOX and amphiphilic DOX for 24 h after exposure. 72

Figure 3.3.2.1 Amphiphilic DOX overcame drug resistance in breast adenocarcinoma cells.⁵⁸ (A and B) *In vitro* DOX sensitive OVCAR-8 (A) and drug resistance NCI/ADR-RES cells against unmodified DOX and amphiphilic DOX for 48 h exposure. 73

Figure 3.3.3.1 Amphiphilic DOX accumulated in B16F10 cellular mitochondrial area *in vitro*.⁵⁸ Subcellular tracking of unmodified DOX and amphiphilic DOX at the incubating concentration of 1 μ M in B16F10 cells. Cells treated with either free DOX (red, from DOX intrinsic fluorescence) or amphiphilic DOX were incubated with Mito-Tracker Green (green, upper two panels) or

Mitochondria-RFP (green, lower two panels). Cell nuclei were tracking with DAPI². Noting that some cells were not transfected in the Mitochondria-RFP treated group. Scale bar = 10 μm 75

Figure 3.3.3.2 Amphiphilic DOX selectively accumulated in both B16F10 and 4T1 cellular mitochondria.⁵⁸ (A-C) Pharmacokinetic quantification of relative drug tracking total cells (A), mitochondria (B) and (C) nuclei of DOX or amphiphilic DOX treated B16F10 cells. B16F10 cells at the density of 1×10^8 per well were incubated with 10 μM DOX or amphiphilic DOX for 1, 4, 12 or 24 h. Mitochondria and nuclei compartments were isolated by commercial isolating kits. The fluorescent intensity of each drugs was quantified by fluorescence spectrophotometer after extraction. (D) CLSM images of amphiphilic DOX (concentration of 1 μM) treated 4T1 cells showing the cellular uptake and intracellular distribution of free doxorubicin or amphiphilic DOX at four hours. Mitochondria tracking of 4T1 cells was employed MitoTracker Green reagent. Scale bar = 10 μm 77

Figure 3.3.3.3. Confocal microscopy imagines colocalization of amphiphilic DOX with mitochondria or lysosomes.⁵⁸ (A and B) B16F10 cells were treated with 1 μM amphiphilic DOX and tracked mitochondria by MitoTracker Green (A) or lysosome LysoTracker Green (B). Cell nuclei were stained with DAPI². Scale bar = 5 μm 78

Figure 3.3.4.1 *In vitro* antitumor activity and subcellular location of DOX capsulated DSPE-PEG₂₀₀₀ micelles.⁵⁸ (A-C) Cells internalization of DOX loaded DSPE-PEG₂₀₀₀ micelles was examined by flow cytometry (A and B) and subcellular location at 4h were analyzed by confocal microscope (C). B16F10 cells (5×10^5 cells per well) were seeded to 96-well plate at 37 °C for overnight. Cells were incubated with DOX loaded DSPE-PEG₂₀₀₀ micelles (DOX concentration of 1.0 μM) at for different time periods before flow cytometry analysis. (C) B16F10 cells at the density of 1×10^5 cells per well were seeded to 6-well plate for overnight. Cells were treated with DOX loaded DSPE-PEG₂₀₀₀ micelles and MitoTracker Green for mitochondria tracking, whereas cell nuclei were stained with DAPI². Scale bar = 10 μm 80

Figure 3.3.4.2 Design of pH sensitive amphiphilic DOX, and its intracellular distribution and cytotoxicity.⁵⁸ (A) Amphiphilic NHNH-DOX was synthesized by conjugating of doxorubicin hydrochloride (DOX) to DSPE-PEG₂₀₀₀-NHNH₂. (B) B16F10 cells at the density of 1×10^5 cells per well were seeded to a 6-wells plate for overnight. Cells were treated with DOX loaded DSPE-PEG₂₀₀₀ micelles and MitoTracker Green for mitochondria tracking whereas cell nuclei² were stained with DAPI. Scale bar = 10 μm . (C) *In vitro* cytotoxicity of free DOX, amphiphilic DOX and amphiphilic NHNH-DOX against B16F10 cells 24 h. B16F10 cells at the density of 5×10^5 were incubated with either amphiphilic DOX or free doxorubicin with varying concentrations for 24h. Cell proliferation was evaluated by AlamarBlue assay. 82

Figure 3.3.5.1 Influence of serum on amphiphilic DOX uptake and distribution.⁵⁸ B16F10 cells at the density of 1×10^5 cells per well were seeded to a 6-wells plate at 37 °C. After overnight adhesion, cell medium was removed and replaced with 0% FBS and 10% FBS medium with DOX and amphiphilic DOX at a final concentration of 1.0 μ M for 4 hours. Cells were treated with free DOX, and amphiphilic DOX. Cell nuclei and mitochondria were tracked by DAPI² and MitoTracker, respectively. Scale bar = 5 μ m. 84

Figure 3.3.5.1 Subcellular location of amphiphilic DOX/ bovine serum albumin (BSA).⁵⁸ Bovine serum albumin-Alexa 660 (BSA-Alexa 660) were pre-incubated with amphiphilic DOX in PBS (pH 7.4) for 4 h at 37 °C. B16F10 cells seeded on the a 6-wells plated were incubated with BSA/amphiphilic DOX complex for 4 h amphiphilic DOX (1.0 μ M) in FBS free cell culture medium. 85

Figure 3.3.6.1 Structure of amphiphilic fluorescein and its intracellular distribution.⁵⁸ B16F10 cells were incubated with amphiphilic Fluorescein for 24 h and imaged to detect its intracellular distribution. 87

Figure 3.3.6.2 Subcellular location of Cholesterol-PEG₂₀₀₀-DOX at 4 h.⁵⁸ B16F10 cells at the density of 1×10^5 cells per well were seeded on cover glasses in 6-wells plates for adhesion. Cells were treated with Cholesterol-PEG₂₀₀₀-DOX for 4 h. Cell nuclei and mitochondria were tracked by DAPI² and Mito-Tracker, respectively. Scale bar = 5 μ m. 88

Figure 3.3.7.1 Amphiphilic DOX generated reactive oxygen species (ROS) in cellular mitochondria.⁵⁸ (A) B16F10 cells were incubated with 10 μ M DOX and amphiphilic DOX for 4h. After drug treated, ROS generation was quantified by a ROS indicator, H2DCFDA (DCF, green) which was incubated with cells at a final concentration of 20 μ M for 30 min. Scale bar of CLSM is 10 μ m. (B) Flow cytometer quantification of ROS generation was assigned in B16F10 cells treated with DOX or amphiphilic DOX at the final concentration at 1, 5 and 10 μ M. 90

Figure 3.3.8.1 Amphiphilic DOX achieved dual target *in vivo*.⁵⁸ Melanoma tumor bearing mice were injected with doxorubicin hydrochloride, or amphiphilic DOX, or PBS. All groups (n = 8) of mice received above treatments (5 mg/kg equivalent doxorubicin, 10 μ L/g of the body weight) on days 5, 8 and 11 by intravenous injection in the lateral tail vein. At the end of experimental period, tumor tissues were isolated, frozen and sliced in to sections. Mitochondria and cell nuclei were stained with MITO-ID RED and DAPI. Scale bar = 10 μ m. 91

Figure 4.3.1.1 Schematic diagram and chemical formula of DEX, amphiphilic DEX, MTX, amphiphilic MTX, Myco and amphiphilic Myco. Synthesis procedures are dropped in the method part. Briefly, DEX was firstly coupled with succinic anhydride. The DEX-succinic acid was further activated by NHS and conjugated to DSPE-PEG₂₀₀₀-amine. The MTX and Myco was pre-activated with NHS and coupled to DSPE-PEG₂₀₀₀-amine directly. 109

Figure 4.3.2.1 Schematic diagram of amphiphilic peptides. Synthesis procedures are dropped in the method part. Briefly, peptides with amino-terminal cysteines and DSPE-PEG₂₀₀₀-Maleimide were dissolved in dimethylformamide (DMF) and agitated at room temperature for 24 hours, following the addition of triethylamine (TEA) for their coupling..... 110

Figure 4.3.3.1 Amphiphilic antagonists downregulated the expression of CD40, CD80. ³ DCs were incubated with DEX (10 nM) and CpG (1 nM), or amphiphilic DEX (10 nM) and CpG (1 nM), or CpG (1nM) only, or medium (No treatment) alone for 24 h. Expression of the membrane markers CD80 (A and C) and CD40 (B and D) were assessed by flow cytometric analysis. Data shown the mean values ± SEM. *, p < 0.05; **, p < 0.01; ***, p < 0.001; ****, p < 0.0001 by one-way ANOVA with Bonferroni post-test. 111

Figure 4.3.3.2 Amphiphilic antagonists inhibited TNF-α production *in vitro*. (A-C) DCs harvested on day 6 were incubated for 24 hours with various concentration of antagonists or their amphiphilic conjugation and CpG (1 nM), CpG (1 nM) only, or medium (No treatment) alone. At the end of the incubation, supernatants were analyzed by ELISA for TNF-α content. 112

Figure 4.3.4.1 Amphiphilic antagonists or antigen alone induced immunosuppression in the cytotoxicity T cell response. (A) Mice were immunized with 10ug OVA protein and 1.25nmol lipo-G₂-CpG at day 0. Mice were received s.c. immunizations with 10 µg OVA and 10ug free antagonists or amphiphilic conjugation on day 7 and double dose on day 14. (B-D) Mice were sacrificed (SAC) and blood was collected 7 days post challenge and assayed for cytotoxicity OVA-specific CD8⁺ T cell..... 115

Figure 4.3.4.2 Amphiphilic antagonists or antigen alone induced immunosuppression in humoral response. Blood was collected 7 days post challenge and assayed for ELISA. The IgG titers were defined as the half maximal effective dose (EC₅₀) of a 4-parameter logistic (4PL) curve fit curve. 116

Figure 4.3.5.1 Treatment with amphiphilic antagonists did not result in broad immunosuppression. (A) Mice were immunized with OVA and lipo-G₂-CpG in the right limbs and with anti-agonists or amphiphilic antagonists with amphiphilic HPV peptide and lipo-G₂-CpG in the left limbs twice on day 0 and day 14. (B and C) HPV-specific CD8⁺ T cells (B) and OVA-specific CD8⁺ T cells (C) were isolated from blood seven-days post the vaccination boost. 117

Figure 4.3.6.1 Amphiphilic peptides induction antigen-specific immunological tolerance. (A) One week after immunized with OVA protein mixed with lipo-G₂-CpG, animals were separated into two subgroups and tolerized with 10 µg dominant MHC-II peptide (OVA₃₂₃₋₃₃₉) vaccine, or lipo-OVA₃₂₃₋₃₃₉, respectively. (B-D) Blood was collected 7 days post immunological challenge and assayed for IFN-γ secreting CD4⁺ T cell (B), CD4⁺ CD25⁺ Foxp3⁺ Treg cells (C) and anti-OVA IgG responses (D). 119

Figure 4.3.6.2 Immunization with lipo-OVA₃₂₃₋₃₃₉ deleted OT-II T cells and promoted the induction of regulatory T cells. (A-C) CD4⁺ OT-II T cells labeled with CFSE and were i.v. transferred into C57BL/6 mice on day -1. At day 0, animal received s.c. immunizations with PBS (no treatment), ovalbumin protein (OVA, 10 µg), OVA₃₂₃₋₃₃₉ peptide (10 µg), or amphiphilic OVA₃₂₃₋₃₃₉ (equal amount peptide). Six days later, inguinal nodes were harvested and the frequencies of OT-II T cells (B) as well as the percentage of Foxp3⁺CD25⁺CD4⁺ T cells were quantified(C) (n = 3 per group). 121

Figure 4.3.7.1 Albumin-binding lipo-peptide remarkably increased LNs drainage and DCs uptake. (A) Fluorescein labeled lipo-OVA₃₂₃₋₃₃₉, or OVA₃₂₃₋₃₃₉ were incubated with FBS at 37 °C for 4 hours and analyzed by native gel electrophoresis (0.8% agarose). The peptide bands were visualized by photograph under UV; protein bands were stained with Coomassie blue. (B) Fluorescein labeled peptides were injected s.c. at the tail base (n = 4 LNs/group), inguinal and axillary nodes were isolated 24 h after injection and analyzed by flow cytometry. 123

Figure 4.3.8.1 Enhanced interaction of peptide to MHC complex expressed on cell surface of DCs. (A and B) Confocal images (A) and uptake quantifications (B) of BMDCs after 1h incubation with fluorescence dye labeled OVA₃₂₃₋₃₃₉ (A, left) or lipo-OVA₃₂₃₋₃₃₉ (A, right) showing red color on cell membrane equatorial periphery. (C) Schematic illustration showing CD4 lipo-peptide anchors on the cell surface and directly loads onto MHC-II. Unmodified peptide displays transient interaction (low affinity and short half-live) with MHC, resulting in insufficient presentation to T cells (upper panel). In contrast, membrane anchored peptide acts as an antigen reservoir, enhancing the binding and presentation via an additional association with cell membrane. Membrane-anchor enables rebind as peptide and MHC disengage (lower panel). Scale bar = 20 µm. 125

Figure 4.3.9.1 Amphiphilic OVA₃₂₃₋₃₃₉ peptide recognized CD4 epitope and can be presented to T cells without antigen processing. (A and B) BMDCs pre-treated with NH₄Cl, or fixed with paraformaldehyde (PFA), were pulsed with low dose of 2 µg/mL (A) or high dose of 10 µg/mL lipo-OVA₃₂₃₋₃₃₉ (B) or unmodified OVA₃₂₃₋₃₃₉ for 2 h. OT-II T cells were then added and co-cultured for 48 h. IL-2 production were quantified by ELISA measurement of IL-2 production. Data show the mean values ± SEM. *p < 0.05; **p < 0.01; ***p < 0.001; ****p < 0.0001 by unpaired student's t-test..... 126

Figure 4.3.9.2 Amphiphilic OVA₃₂₃₋₃₃₉ peptide enhanced antigen presentation to T cells. (A) BMDCs were incubated with different concentrations of lipo-OVA₃₂₃₋₃₃₉, or unmodified OVA₃₂₃₋₃₃₉, washed and co-cultured with OT-II T cells. IL-2 was measured at 48 h. (B) BMDCs were pulsed with 10 µg/mL lipid-OVA₃₂₃₋₃₃₉ or unmodified OVA₃₂₃₋₃₃₉ for 2 h, washed, and cultured for the indicated times to allow peptide/MHC to decay. OT-II T cells were then added and co-cultured for another 48 h. T cell responses to DCs loaded with CD4 epitope were quantified by ELISA measurement of IL-2 productions. 127

Figure 4.3.10.1 Amphiphilic peptide vaccine protected mice from T-cell induced autoimmune type 1 diabetes at the early period. (A-C) NOD mice were treated with two (on week 6 and 8) s.c. injections of 20 µg B₉₋₂₃ peptide, LN-targeting B₉₋₂₃ peptide (lipo- B₉₋₂₃) or PBS, blood glucose concentrations were monitored. (A) Percentage of diabetic mice (n = 12 for each group, p values were shown by log-rank test). (B) At the age of week 10, percentage of IFN-γ secreting CD4⁺ T cells and Foxp3⁺ CD25⁺ CD4⁺ T cells in blood. (C) At week 10, serum cytokine levels were measured by ELISA. 129

LIST OF TABLES

Table 2.2.2.1 HPLC gradient for purification of DSPE-PEG₂₀₀₀-DOX.⁴⁵	32
Table 3.2.7.1 Confocal microscopy setting for mitochondria tracking.⁵⁸	69
Table 3.3.1.1 Amphiphilic modification increases DOX-induced antitumor effect in multiple murine cell lines.⁵⁸	73
Table 3.3.2.1 Amphiphilic DOX overcame drug resistance in breast adenocarcinoma cells.⁵⁸	74
Table 3.3.3.1 Pearson's Correlation Coefficients and Manders' coefficients.⁵⁸	76

Chapter 1. Introduction and literature review.

1.1 Overview

Recent developments of novel drug delivery systems are driven by the requirements that target specific disease, maximize therapeutic efficacy while minimizing side effects⁴⁻⁵. Among various therapeutics, a large portion of the drug molecules exhibit physicochemical drawbacks such as poor solubility and bioavailability, short circulation half-lives and nonspecific distribution that limited their clinical applications⁶⁻⁷. To balance the effect of these limitations, drugs are administered usually at high treating frequencies or at high doses. This, however, leads to adverse side effects or induces autoimmune reactions^{5, 8-10}. One potential approach to address these issues is to incorporate therapeutic drugs in to a tailored delivery matrix, which controls the dosage, duration, and distribution of the drug molecules after administration. For systemic administration, the delivery system increases the circulating half-life and accumulation in target tissues. For drugs administered locally, the delivery vehicles intensively retain at the local site to prolong the retention time. These attributes potentially enhance the performance as well as reduce dosing frequency or concentration, which ultimately lead to increased patient compliance^{7, 9, 11-13}.

While existing drug delivery systems (e.g., liposomes) have fulfilled some needs in the field, it remains challenging to design drug carriers which meet all the criteria for delivery¹⁴⁻¹⁶. Possible loading efficiency, stability, toxicity and immunogenicity issues greatly restrict the clinical applications of some of the delivery systems in the short-term. An emerging strategy to overcome the above

limitations is the design of drug amphiphiles which have the potential for self-delivery. Self-delivery drugs¹⁷⁻²⁰ eliminates the need for external delivery systems. A typical drug amphiphile²¹⁻²³ can be divided into three distinct segments: a pharmaceutical payload, a linker, and a chemical modification which renders the whole amphipathicity (**Figure 1.1.1A**). Drug amphiphiles can be synthesized by amphiphilic modification which alters the drug molecule's physicochemical properties and targets disease sites through several mechanisms. Because a range of amphiphiles with great structural diversity are available for conjugation, the physicochemical properties of a particular drug can be fine-tuned to achieve desired characteristics such as solubility, stability, biodistribution, membrane permeability and intracellular accumulation (**Figure 1.1.1B**). Tailoring the drug amphiphiles' structure and/or hydrophilic/lipophilic balance²⁴ leads to different interactions with biological surrounding environment after administration. For example, drug amphiphiles²¹ with appropriate HLB are capable of self-assembling into stable supramolecular nanostructures under physiological conditions. Compared to soluble drugs, these self-assembled drug nanostructures have demonstrated to be superior in protecting labile drugs from degradation, controlling the release of drugs, as well as site-specific drug accumulation. In general, drugs delivered by nanoparticles exhibit reduced toxicity while maintaining or enhancing the therapeutic effects. On the other hand, drug amphiphiles can be engineered to bind plasma proteins (e.g., albumin or lipoprotein)²²⁻²³. Endogenous proteins are natural carriers which are known to have long circulation half-life and improved site-specific targeting. For example, drugs that bind to albumin accumulate in solid

tumors by the enhanced permeation and retention (EPR) effects and more importantly, by elevated metabolic activities in tumor in response to the need for amino acids and energy ²⁵⁻²⁷. Protein binding has also been used for lymphatic targeting: following subcutaneous injection, vaccinal amphiphiles transport through binding to the albumin and accumulate in the draining lymph nodes. Understanding and controlling the molecular interactions between plasma proteins and drugs in a complex biological environment is the key to harness this endogenous pathway for targeted drug/vaccine delivery. Finally, the interplay between the drug amphiphiles and biological membranes/or membrane transporter proteins/enzymes is known to enhance the membrane permeability, which allows the crossing of critical barriers such as blood-brain barriers, intestinal absorption barriers and specific targeting at the cellular or intracellular level.

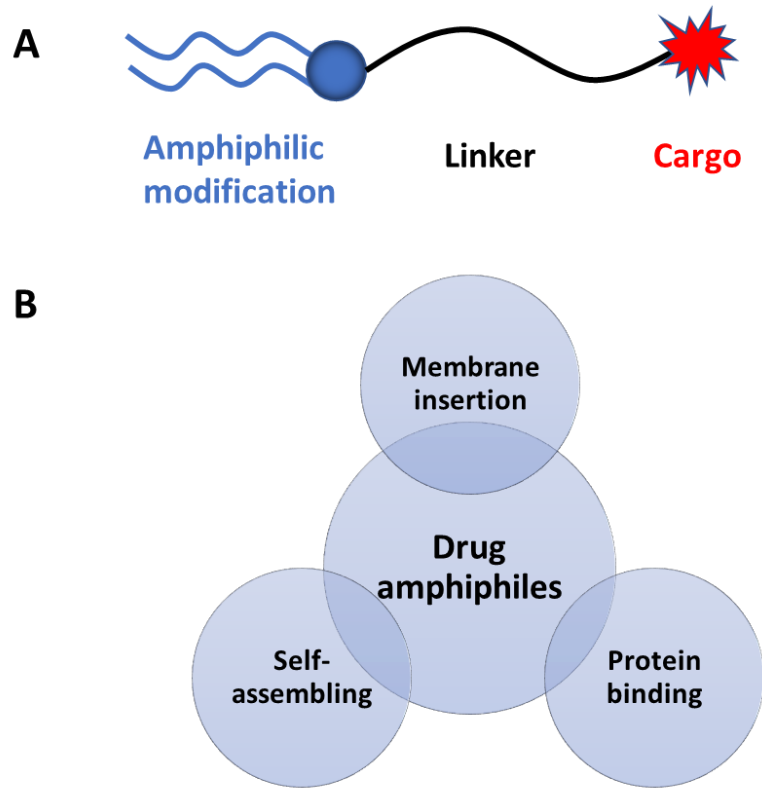


Figure 1.1.1 Improving drug delivery by amphiphilic drug conjugate. (A) Schematic illustration of the design of drug amphiphiles. A typical drug amphiphile can be divided into three individual fractions: a pharmaceutical payload, a linker, and a chemical modification which renders the drug amphiphilic. (B) The interactions between drug amphiphiles and their biological surroundings can be controlled by molecular engineering which governs the drug molecules' physicochemical properties.

1.2 The design principles of self-delivery drug amphiphiles.

For a long period of time, amphiphilic modification has been harnessed to improve the biological activity of the parent compounds, providing decades of referential experience to guide the current designs. For example, lipid-nucleoside conjugates (nucleolipids) have been used since the 1970s to overcome drug resistance.²⁸ Generally, the novel amphiphilic modification provides superior pharmacological properties compared to the parent compounds, including improved oral bioavailability, increased stability and circulating half-life, facilitated targeting at the organ, cellular and subcellular levels. The past decade has seen tremendous progress in the exploration of amphiphilic modification to improve both efficacy and safety of drugs. New drug amphiphiles are emerging as paradigms to guide the rational design for therapeutic applications, some of which are summarized in the following discussion.

1.2.1 Amphiphilic drug modification: conjugation strategies and types of linkers.

Depending on the hydrophobicity of the drug, a hydrophobic or hydrophilic modification is selected to be employed for the conjugation. The pharmaceutical payload must contain reactive group(s) for covalent conjugation. There are a variety of conjugation strategies available, including the formation of ester bond, amide bond, thiol-ene reaction, azide-alkyne click reaction, bioreducible disulfide, and many others.²⁹⁻³⁰ The conjugation can form drug amphiphiles with cleavable or non-cleavable linkage. Although non-cleavable linkers have the advantage of increased plasma stability and reduced off-target toxicity, non-cleavable drug

conjugation might compromise the performance by altering the binding affinity or intrinsic activity of the drug. Recently, the use of stimuli-responsive linkages designed for the traceless release of drugs from their conjugates has gained significant attention.³¹⁻³² In these cases, payloads are released upon linker cleavage in response to the environmental signals at the disease areas to achieve spatiotemporal drug control and maximal drug efficacy. A large variety of environmental signals such as biological, physical, or chemical stimuli and the corresponding chemical linkers have been extensively explored in the past.³¹⁻³² In many cases, conjugation to cleavable linkers produces prodrugs that are inactive before drug release. However, the choice of conjugation strategies for a specific payload depends on the availability of appropriate functional groups on drug for coupling, the metabolic pathways of the drug for *in vivo* stability, as well as the requirement for drug release for maximal therapeutic potency. Importantly, the functions of the linker molecules extend beyond payload connection and controlled release.³³⁻³⁷ As demonstrated in previous examples, an appropriately designed linker is also critical to the overall physicochemical properties of the whole conjugate, which controls the stability of self-assembled supramolecular structure, the ability for plasma protein binding, and cell membrane interactions.³⁴⁻³⁷ For example, in a complexed biological environment, the molecular weight of polyethyleglycol (PEG) in a diacyl lipid-PEG-peptide conjugate controls the delicate balance between an albumin-binding state and a membrane insertion state.³⁵ In the late case where the payload needs to be anchored on the membrane surface, a relative long, flexible linker enables the payload to extend from the cell

surface, minimizing the potential steric hindrance which affects the receptor-ligand interaction.³⁶

1.2.2 Amphiphilic modification enhances circulation half-life and tissue/organ targeting.

To achieve a high therapeutic index, drug is expected to accomplish sufficient circulation time in blood for target exposure, and site-specific accumulation following parenteral administration. Due to their low molecular weights, small molecule drugs are rapidly cleared from the blood through renal excretion. Additionally, many biotherapeutics (peptides, oligonucleotides) have extremely short *in vivo* half-life due to their susceptibility to enzymatic degradation. Amphiphilic modification can prolong the plasma half-life of the drug by several distinct mechanisms. First, drug amphiphiles self-assemble into nanostructures with different shapes and sizes. Molecular assemblies with a hydrodynamic diameter greater than 5.5 nm exceed the renal filtration threshold and prevent the rapid clearance via renal filtration and urinary excretion.³⁸⁻³⁹ Therefore, self-assembled drug amphiphiles are larger in size than monomeric drug alone, making them more likely to have long blood circulation time. Second, amphiphilic modification and molecular self-assembling protect the vulnerable drugs from enzymatic degradation, improving the drug molecules' stability in circulation. The third mechanism is that certain drug amphiphiles are designed to bind tightly to serum albumin or lipoprotein. Albumin has a hydrodynamic size of approximately 7 nm and is one of the plentiful protein in the blood and interstitial fluids.⁴⁰⁻⁴¹ Compared to molecular drug alone, albumin binding forms an albumin-drug

complex with greater size and prevents the drug from renal clearance. Importantly, albumin has an extraordinarily long circulation half-life (~19 days) in human due to its unique neonatal Fc receptor-driven recycling pathway (avoid lysosomal degradation).⁴² Similarly, lipoproteins are natural nanoparticles which have long residence time in the circulation.⁴² Therefore, drug amphiphiles transportation via the albumin or lipoproteins is an effective approach to extend the circulation time *in vivo*.

Apart from increasing the circulating half-life, amphiphilic modification can affect the delivery of drugs to the target sites. Increasing the molecular sizes by self-assembling or protein-binding is known to preferentially accumulate the drug in tumor tissue or inflammatory site via EPR effect.⁴³ This passive targeting approach (EPR) is the primary mechanism of the majority of current nanomedicine for the treatment of solid tumors. In addition to passive targeting, it is known that under conditions of cellular stress, albumin is taken up as a source of amino acid and energy due to increased catabolic activities at disease sites. Although the exact cellular receptors for albumin remain to be identified, albumin-based self-delivery drugs have been used to target solid tumor as well as inflammatory conditions such as rheumatoid arthritis.⁴⁴⁻⁴⁵ Finally, self-delivery amphiphilic vaccines which bind to albumin accumulated in the antigen presenting cells (APCs) in the lymph gland after subcutaneous injection.³⁵ In contrast to unmodified vaccines, which rapidly diffuse into blood circulation due to their small molecular weights, amphiphilic vaccines bind to albumin, drain to the lymphatic capillaries and filtered by APCs in the lymph nodes. Because of its ability to efficiently deliver

vaccine components to lymph node, this novel amphiphilic vaccine approach elicited a dramatic increase in antigen-specific T cells compared to unmodified vaccines.³⁵

1.2.3 Amphiphilic modification improves oral bioavailability.

Oral administration of therapeutic agents is highly preferred because of the convenience with non-invasive and self-administration. However, drugs administered orally must overcome a series of harsh environments and absorption barriers in the gastrointestinal tract. For example, the numerous enzymes and acidic pH in the digestive tract are designed to break down molecules including drugs before they can be absorbed and enter the bloodstream. Many drug compounds do not have the physicochemical characteristics required for oral administration. Amphiphilic modification of drugs can help improving oral delivery by maintaining the drug molecules' structure integrity in gastric environment and increasing intestinal permeability.⁴⁶ Depending on their distribution and metabolism, orally administered drug molecules can enter the systemic circulation through the intestinal lymphatic system or absorption in portal blood capillaries after intestinal epithelium permeation.⁴⁶⁻⁴⁷ In both routes, drugs must cross the epithelium barrier, a single layer of cells with selective permeability for dietary nutrients and other substances. In this process, membrane permeation is a quite complex process and has encompassed a wide range of passive and active mechanisms. However, drug lipophilicity plays a dominate role in the absorptive membrane permeability and subsequent blood absorption.⁴⁸⁻⁴⁹ Molecules with higher lipophilicity generally exhibit better permeability than hydrophilic drugs.⁴⁸⁻⁴⁹

Current methods for addressing the permeability associated with hydrophilic drugs have focused on chemical modifications which increase the lipophilicity of drugs. Intestinal lymphatic absorption and transport is a unique pathway for oral drugs to enter systemic circulation.⁵⁰⁻⁵¹ The mammalian intestine is intensively perfused with lymphatic capillaries, which absorb dietary lipids and vitamins from the gastrointestinal tract.⁵⁰⁻⁵¹ In this pathway, orally administered lipids or lipophilic drugs are transported to intestinal lymphatic system by associating with lipoproteins. These lipoproteins associated drugs subsequently enter blood circulation, thus avoiding the potential first-pass metabolism in the liver.⁵⁰ Appropriate lipophilic modification on drug is essential to hijack this lymphatic uptake pathway for oral drug delivery.

1.2.4 Amphiphilic modification overcomes blood-brain barrier.

Passing the blood-brain barrier (BBB) is one of the important steps for drug to reach the brain following systemic administration. However, the BBB consists of a monolayer of tightly packed endothelial cells expressing efflux transporter proteins (e.g. P-glycoprotein, Pgp), blocking most drugs administered systematically from entering the brain and central nervous system.⁵²⁻⁵³ Although transport across the endothelium by ligand-receptor binding is possible, passive diffusion of the drug across brain endothelial cells remains the predominant route.⁵³ Structurally, many factors can affect the passive permeability of drugs crossing BBB. Studies have shown that compounds with high lipophilicity (higher Log P), less hydrogen bonds (< 8-10), and low molecular weight (<500) have better permeability to BBB.⁵³ Thus, amphiphilic modification which reduces Pgp protein

efflux and increases lipophilicity will likely increase BBB permeation.⁵⁴ It is generally believed that plasma protein binding limits the diffusion of the drugs, especially for drugs with high association rate⁵⁵ and low dissociation rate (K_{off}).⁵⁶ However, several plasma proteins (e.g., transferrin and low density lipoproteins) can penetrate BBB by receptor mediated transcytosis, a mechanism which has been explored for enhancing BBB permeability.⁴⁹ Therefore, care should be taken in terms of plasma protein binding when designing drug amphiphiles to cross BBB.

1.2.5 Amphiphilic modification facilitates drug uptake and targeting at subcellular level.

In addition to the above extracellular barriers, targeted delivery of therapeutics requires transportation across the cell membrane, and ultimately to a defined subcellular structure. Several biological barriers must be permeated to achieve efficient subcellular disposition. Amphiphilic modification has also been explored to enhance the cellular uptake, to anchor the drug molecules on plasma membrane, and to direct the drugs to specific subcellular compartments. Amphiphilic especially lipophilic conjugation was reported to be used of as an uptake enhancing approach for hydrophilic drugs.⁵⁷ This attribution heavily relies on the hydrophobic interactions between the lipophilic moieties and cellular membranes.⁵⁸ Passive diffusion across membrane bilayers is the most important permeability mechanism. The ability to associate and dissociate with the hydrophobic membrane interior is one of the dominant parameters governing transmembrane diffusion.⁵⁸ While highly hydrophilic molecules fail to enter membrane, extremely lipophilic molecules are trapped within the lipid bilayers and

fail to diffuse out. Thus, balancing the hydrophobicity of drug amphiphiles is critical in transmembrane diffusion. In addition to simple diffusion, lipid-based amphiphiles have been shown to spontaneously insert their hydrophobic lipid tail into the lipid bilayer of membrane as a precursor for subsequent cellular uptake.⁵⁹⁻⁶⁰ This mechanism enables the membrane translocation of otherwise impermeable molecules. In contrast to direct diffusion, membrane inserted drug amphiphiles either remain in the membranes (plasma and intracellular membranes) or release the drug payload by appropriate mechanisms. The final mechanism associated with enhanced cellular uptake of drug amphiphiles is the receptor-mediated uptake. Lipoprotein- or albumin-bound drug amphiphiles are recognized by endocytic receptors on the plasma membrane, followed by rapid internalization.⁶¹⁻⁶²

Transmembrane protein receptors are important drug targets as cells use them for signal transduction, molecules transport, and cell-cell interactions. Anchoring drug amphiphiles on the cell surface has been harnessed to enhance the affinity and stability of ligand-receptor binding.⁶³⁻⁶⁵ These membrane anchored amphiphiles firmly anchor the drug molecules on the surface of the cells, increasing the local ligand concentrations around the receptors by restricting the ligand diffusion. Thanks to the unique bi-valent interactions between cell surface receptor and ligand, both binding affinity and stability can usually be improved.⁶³

Besides being an appropriate membrane targeting approach, recent advances have identified amphiphilic drug modification as a novel strategy for subcellular targeting of drugs.⁶⁶ The exact mechanisms of how amphiphilic modification leads to subcellular organelle accumulation remain poorly established,

but it is believed that the overall physicochemical properties and ligand-receptor interactions govern the intracellular sorting and trafficking pathways.⁶⁶ Therefore, amphiphilic modification can be utilized to enhance or reroute the drug molecules to specific organelles. For example, amphiphilic modification is an effective way for cytosolic targeting of small interfering RNAs (siRNA).⁶⁷⁻⁶⁹ Lipophilic ligands modified siRNA associate with high density lipoproteins and cross the membrane directly into cytoplasm via non-endocytotic pathway mediated by the scavenger receptor BI.⁷⁰ A wide range of lipophilic moieties including cholesterol, fatty acids, steroids were used for siRNA conjugation and some of them have reached clinical stage.⁶⁹ Amphiphilic modification has also been utilized for the endosomal entrapment in drug delivery. Due to its high affinity toward membrane bilayer, diacyl lipid-immunostimulatory oligonucleotide conjugates were designed to target Toll-like receptor (TLR) 9, which are exclusively expressed within the endosomal compartments of antigen presenting cells.³⁵ The enhanced cellular uptake and intracellular targeting by amphiphilic modification have been utilized to overcome the drug-resistance, one of the major challenges in current cancer chemotherapy.⁷¹⁻⁷⁵ This is achieved by amphiphilic conjugation which alters the internalization pathways, or delivers and anchors the drug to intracellular organelles where the P-glycoprotein efflux pump cannot access.^{71, 75}

1.3 Clinical and preclinical examples of drug amphiphiles.

1.3.1 Amphiphilic oligonucleotides (ODNs).

The albumin-hitchhiking approach has been recently applied to deliver immunostimulatory oligonucleotides (ODNs) to the lymph nodes after

subcutaneous injection.^{35, 76-77} Liu et.al. conjugated diacyl lipid to the single-stranded oligonucleotides CpG DNA (**Figure 1.3.1.1**), consisted of unmethylated cytosine-guanine motifs that bind Toll-like receptor-9 (TLR-9) and do the duty for potent immunological adjuvants.³⁵ Amphiphilic CpG accumulates in the antigen presenting cells in the lymph nodes by transporting and trafficking by the help of endogenous albumin protein. Albumin binding prevents CpG ODN from rapidly spreading into the blood circulation and re-target them to the lymphatics and draining lymph nodes, where they are filtered by various antigen presenting cells. Interestingly, both the molecular weight of the diacyl lipid and ODN affect the albumin binding and subsequent lymph node accumulation: longer diacyl lipids than sixteen carbons, which exhibit a high affinity for albumin showed intense accumulation in LN. At the same time, shorter diacyl lipids than fourteen carbons with low affinity exhibited markedly reduced retentions.³⁵ The optimal length of ODN was determined to be 15-30 nucleotides.³⁵ This vaccine approach elicited extensive antigen-specific T cell priming and improved anti-tumor proliferation effects. In addition to albumin-binding, diacyl lipid modification of ODNs provides a consolidating and embedding pathway for intercellular entrance by interacting with plasma membrane. Due to the inherent affinity toward membrane bilayers, lipid-ODNs are able to spontaneously insert onto the surface of the membrane.^{34, 37} This property has been utilized for localized ODN delivery. In an attempt to augment the anti-tumor immune response, Liu et.al. used diacyl lipid conjugated immune stimulatory ODNs for in situ tumor cell modification (**Figure 1.3.1.1**).³⁷ Intratumoral injected diacyl lipid modified CpG DNA spontaneously insert into the

plasma membrane of tumor cells, leading to significantly increased local retention time in tumor. This approach also promotes the association of immune adjuvant (CpG) with tumor antigens. In situ stimulation of malignant cells will be favourable for the local activation of antigen presenting cells such as dendritic cells responding to apoptotic tumor cells.³⁷ Finally, diacyl lipid-ODNs were dominantly accumulated in the endosomes, where TLR-9 are expressed. In a murine melanoma tumor model, cell membrane anchored CpG ODNs with nuclease-resistant phosphorothioate backbone displayed markedly enhanced immune co-stimulatory activity and improved anti-tumor efficacy compared to soluble CpG.³⁷

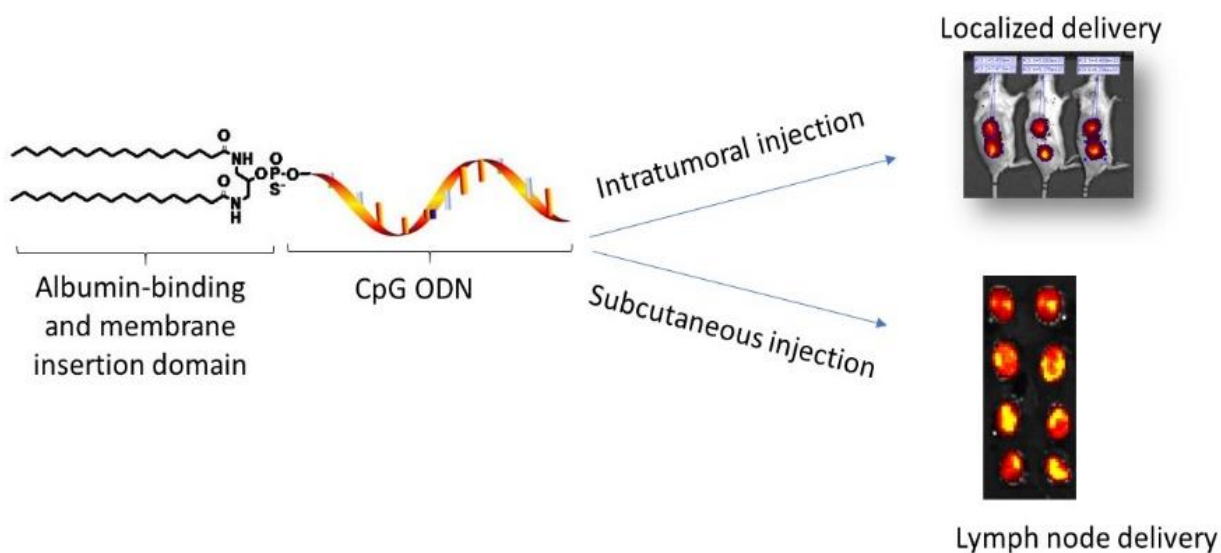


Figure 1.3.1.1 Representative examples of oligonucleotide amphiphiles. Amphiphilic immunostimulatory oligonucleotide equilibrates between membrane insertion state and albumin binding state and can be used to directly label tumor cells (intratumoral injection) or target draining lymph nodes (subcutaneous injection).

1.3.2 Amphiphilic peptides.

Peptide amphiphiles⁴⁷ are amphiphilic molecules that contain bioactive peptides. PAs can be synthesized by linking amino acids into hydrophilic and

hydrophobic domains, or by conjugating oligopeptide to hydrophobic hydrocarbon chain (lipopeptide).⁷⁸⁻⁸⁰ Due to their amphiphilic properties, PAs self-assemble into nanostructures under certain conditions. The self-assembly of PAs is believed to be driven by a combination of molecular interactions such as hydrogen bonding, hydrophobic interactions, van der Waals force, and electrostatic interactions.⁸⁰⁻⁸¹ Combining the amphiphilic features with the bioactive peptides, PAs have been shown great promise in biomedical applications and can be utilized to act as anti-pathogenic agents to treat infections, as vaccines/immunotherapy agents or as cosmeceuticals.⁷⁹

The antibacterial, antifungal and antiviral activity of naturally expressed PAs from bacteria were extensively studied in the past.⁸² The first PA-based antibiotic, Cubicin[®] (Daptomycin, **figure 1.3.2.1A**), was approved for the treatment of complicated skin infections by Food and Drug Administration (FDA) in 2003 in USA.⁸³ Daptomycin is an amphiphilic peptide and consists of cyclic 13 amino acids peptide linked to a decanoyl lipid chain. Despite years of study, its exact molecular mechanism of activity remains unclear.⁸⁴ Accumulated evidences suggest that by inserting of its hydrophobic decanoyl chain into bacterial membrane, daptomycin causes membrane permeabilization and potassium ions outflow, leading to rapid bacteria cell death.⁸⁴ The formation of spherical micelles by daptomycin has been proposed to facilitate bacterial-targeted delivery.⁸⁵ However, studies also shown that more than 90% of the total amount of daptomycin in blood is protein-bound,⁸⁶⁻⁸⁷ which in turn, may affect its antibacterial activity, as demonstrated in protein-free media.⁸⁸ Yet these in vitro protein binding studies failed to predict

clinical efficacy of daptomycin, suggesting other important characteristics, such as favorable pharmacokinetics are of vital clinical importance to the success of antibiotic therapy. Several other PAs such as caspofungin, anidulafungin, and micafungin have been approved as antifungal antibiotics.⁸⁹

PAs are also designed to anchor peptide ligands on the surface of cell membrane, creating a cooperative receptor-ligand binding and increasing the local ligand concentrations around receptors. Conjugating cholesterol to HIV fusion inhibitory peptide (C34) creates a peptide amphiphile capable of membrane insertion.⁹⁰⁻⁹¹ The amphiphilic modification anchored C34 on the cholesterol-enriched lipid rafts, resulting in dramatically enhanced potency in terms of HIV inhibition (**Figure 1.3.2.1B**).⁹⁰⁻⁹¹ Importantly, anchoring C34 peptide on cell surface also enhance the peptide's stability, as the antiviral activity appeared to be persistent following extensive wash.⁹⁰ Similar lipid peptide-based HIV fusion inhibitors were reported.⁹¹⁻⁹² The dramatically enhanced inhibitory potency and stability, combined with the >300-fold increase in plasma concentration, make this amphiphilic strategy attractive in blocking many other virus entry during infections.

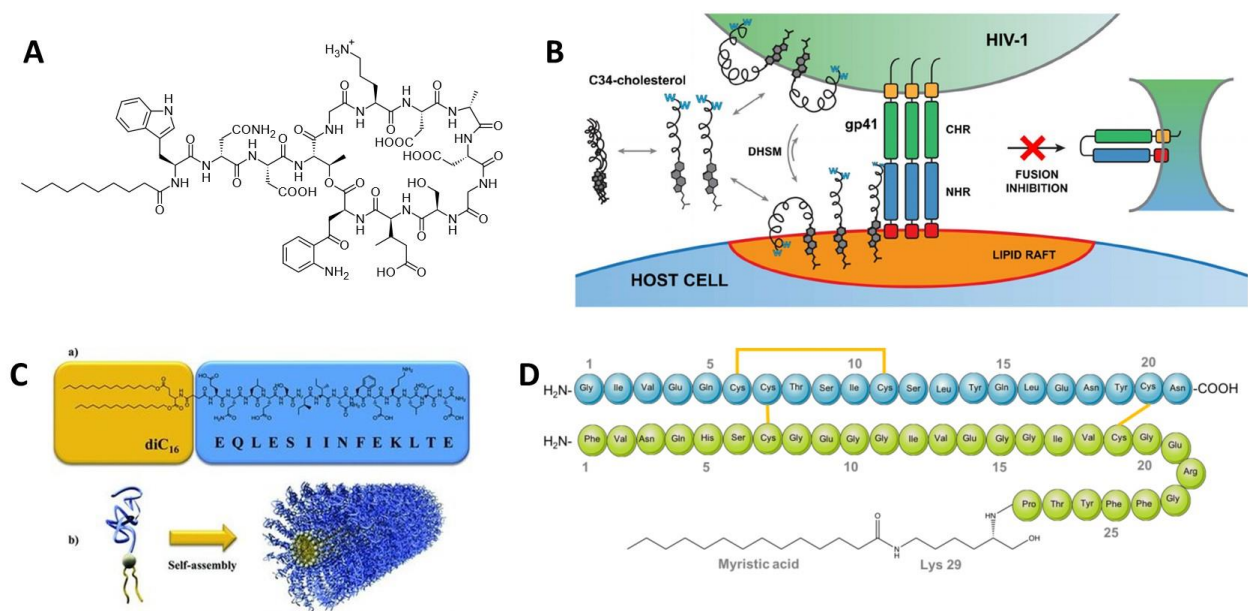


Figure 1.3.2.1. Examples of peptide amphiphiles. (A) Molecular structure of Daptomycin. (B) Model of action of cholesterol-C34 peptide in HIV fusion inhibition. Cholesterol-C34 anchors on the surface of host cells and increases both the affinity and duration of ligand-receptor interactions. (C) Amphiphilic peptide epitopes self-assemble into cylindrical micelles and facilitate the uptake of antigen presenting cells. (D) Structure of long-acting insulin detemir (Levemir). Insulin is modified with myristic acid at the lysine amino acid at position B29. This modification causes protein self-association as well as albumin protein binding, which prolongs the duration of action.

PAs are also extensively explored in vaccine applications primarily due to their abilities to self-assemble into nano-sized structures. The peptide epitopes displayed on the surface of nano-structures closely mimic the highly repetitive antigens on the pathogen surface, which are believed to be critical in B cell receptor clustering.⁹³ In addition to directly activate B cells, the PA-based self-assembled nano-vaccines have been frequently used to target antigen presenting cells (APCs).⁹⁴ This is achieved by two distinct pathways: first, nano-vaccine formulations promote lymph nodes draining through lymphatic capillaries.^{51, 93} Unlike small molecule epitopes, which quickly diffuse into blood circulation after subcutaneous or intramuscular injection, nano-vaccines preferentially drain to the

lymph nodes. Alternatively, the physicochemical properties of nano-vaccines also facilitate the uptake by APCs.⁹⁵ Because of this targeting mechanism, a variety of fully synthetic PAs with both B-cell and T-cell epitopes have been synthesized and tested. The first example of PAs in vaccine application was reported in 1984. Hopp and co-workers pioneeringly synthesized PAs by conjugating dipalmitoyl-lysine moiety to a peptide bearing hepatitis virus epitopes.⁹⁶ The amphiphilic modification significantly improved the production of antibodies against hepatitis surface antigen.⁹⁶ Tirrell and coworkers conjugated dialkyl lipid with two palmitic chains to a series of peptide containing B cell or T cell epitopes (**Figure 1.3.2.1C**).⁹⁷⁻⁹⁸ These lipid conjugated peptides self-assembled into cylindrical micelles and elicited potent humoral and cellular responses in mice. In many of these examples, the synthetic assemblies are able to elicit potent immune responses without the need for additional molecular adjuvants, which make them attractive in the design of safe vaccines.

In addition to the self-assemble property, PAs can be carefully engineered to bind albumin protein. Insulin is widely used to treat diabetes mellitus type 1. However, insulin is quickly degraded (half-life 4-6 minutes) after its release into blood. Insulin detemir (Levemir[®]) is a long-lasting insulin analogue in which myristic acid is conjugated to the B29 lysine (**Figure 1.3.2.1D**). It binds to albumin in the blood and lasts 18 to 23 hours after injection.⁹⁹ Insulin degludec (Tresiba[®]) is ultralong-acting insulin (up to 42 hours) in which a longer fatty acid (hexadecanedioic acid) was used for B29 lysine conjugation.¹⁰⁰ Increasing the hydrophobicity of the lipid results in the formation of self-assembled multi-

hexamers in subcutaneous tissues which prolong the release of insulin into blood circulation.¹⁰⁰ Similarly, Liraglutide (Victoza®) is a fatty acid modified Glucagon-like peptide-1 (GLP-1) agonist used to treat type 2 diabetes.¹⁰¹ Endogenous GLP-1 has an extremely short half-life in blood (1.5-2 minutes). However, attaching an albumin-binding fatty acid dramatically prolongs its circulation life. Albumin-binding also facilitate therapeutic peptide transport to lymph nodes.⁵¹ Instead of forming the micelle structure, peptide antigens conjugated to a long chain (>16 carbons) diacyl phospholipid via a long PEG (Mw > 2000) linker preferentially bind to albumin after s.c. injection.³⁵ This new lymphatic system targeting approach dramatically improved the peptide vaccine's efficacy and safety.

Lipopeptides derived from microbial origin are important molecular adjuvants which potently stimulate the innate immune system via Toll-like receptors. For example, bacterial lipoprotein derivatives that contain dipalmitoyl-S-glycerol cysteine (Pam₂Cys) or tripalmitoyl-S-glycerol cysteine (Pam₃Cys) can trigger TLR1/2 and TLR2/6 activation.¹⁰² Covalently conjugating low molecular weight haptens, B cell and T cell epitopes to lipopeptide adjuvants has been shown to elicit improved humoral and cellular immune responses in experimental animals and human clinical trials, providing protections against infection and cancer. In 1998, FDA approved LYMERix™ as a general vaccine for Lyme disease. LYMERix™ is Pam₃Cys linked to outer surface protein A (OspA) of *Borrelia burgdorferi*. Despite the fact that clinical trials in over 10906 individuals showed a 76% reduction in Lyme disease, with no significant adverse effects, LYMERix™ was withdrawn from market by the manufacturer due to press coverage of vaccine

risks which led to poor market performance.¹⁰³ In general, attaching fatty acids such as palmitic acid (palmitoylation) to peptide epitopes enhances the hydrophobicity of antigens, and contributes to their membrane interactions which facilitate TLR engagement (TLR1/2 and TLR2/6 are surface TLRs).

1.3.3 Amphiphilic Small Molecular Drugs.

Amphiphilic modification of anti-cancer low-molecular-weight drugs which enables self-delivery of drugs to tumor cells has attracted significant research interests. Amphiphilic drugs conjugation leads to the formation of stable supramolecular assemblies, which improves the stability, circulating time, and tumor penetration/retention of parent drugs. For example, linear amphiphilic polymer was conjugated to hydrophobic camptothecin (CPT) analog SN38.¹⁰⁴ The amphiphilic modification leads to micelle forming PEG₂₀₀₀-SN38. Compared with soluble SN38, micellar SN38 showed enhanced cytotoxicity in vitro and antitumor efficacy in vivo.¹⁰⁴ Similarly, Shen and coworkers conjugated oligomeric ethylene glycol to one or two copies camptothecin. Instead of forming micelles, these amphiphilic camptothecins formed nanovesicles due to the reduced hydrophilic/lipophilic balance.¹⁰⁵ The vesicles can encapsulate other hydrophilic drugs such as doxorubicin for combination therapy.¹⁰⁵ The formation of nano-sized nanoparticles (typically micelles) by linking multiple copies of drugs to PEG-containing polymeric scaffolds is also extensively explored. In addition to PEG, fully synthetic peptides have been used to aid the amphiphilic self-assembly. Cui and coworkers conjugated hydrophilic peptides to camptothecin (**Figure 1.3.3.1A**).¹⁰⁶ Besides the simply hydrophobic interactions, this design also takes

advantages of the highly predictable self-assemble properties of peptides, by which multiple molecular interactions including van der Waals forces, ionic bonds, hydrogen bonds are involved in the self-assembly.⁸⁰ The addition of a reducible disulfide linker allows the release of CPT upon tumor cell uptake and internalization, resulting greater cytotoxic effect *in vitro*.¹⁰⁶

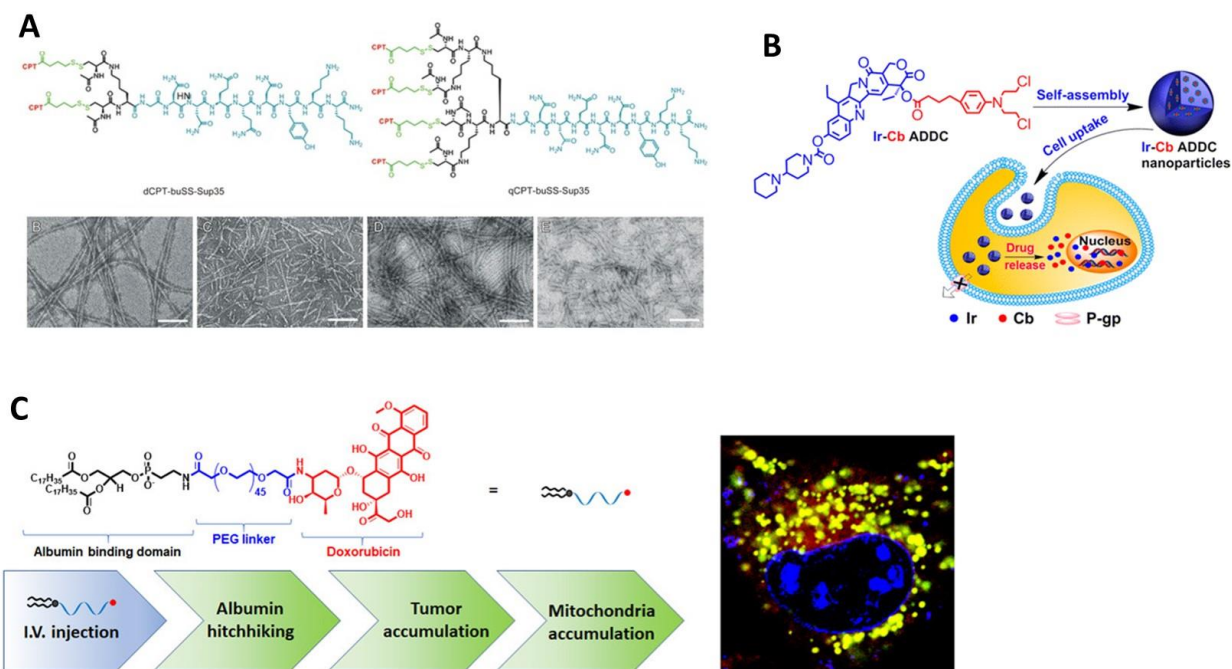


Figure 1.3.3.1. Example of small molecule drug amphiphiles. (A) molecular structures and TEM images of self-assembling camptothecin and peptide conjugates. (B) self-assembling irinotecan-chlorambucil drug-drug conjugate. (C) Molecular structure and confocal image of mitochondria-targeting amphiphilic doxorubicin.

Hydrophobic modification (typical lipid modification) on hydrophilic drugs leads to the formation of nanostructures by self-aggregation. Conjugating doxorubicin to squalene led to the formation of squalenoyl doxorubicin nanoaggregations with a mean diameter of 130-nm.¹⁰⁷ Compared to unmodified doxorubicin, this simple conjugate dramatically improved the therapeutic anti-

cancer efficacy *in vivo*. Similar amphiphilic lipid-drug conjugates are extensively reviewed.⁷⁵

An emerging new strategy in the design of self-delivery drugs is the amphiphilic drug-drug conjugation. In this strategy, self-assemble amphiphiles consisting of hydrophilic and hydrophobic drugs were conjugated. Huang and coworkers covalently conjugated hydrophilic irinotecan and hydrophobic chlorambucil (Ir-Cb) via a cleavable ester bond (**Figure 1.3.3.1B**).¹⁰⁸ In aqueous buffer Ir-Cb self-assembles into nanoparticles and facilitates the delivery to tumor. Both irinotecan and chlorambucil were released from the prodrug due to hydrolysis by intracellular esterases. Since then, different amphiphilic drug-drug conjugates with self-assemble capacities have been designed.¹⁰⁹ Targeting multiple anti-cancer drugs to tumor site synergize the cytotoxic effect and overcome the multiple drug resistance, especially when drugs with different mechanisms of action were used.

Intracellular organelle targeting by lipid-drug conjugates is a new, yet exciting strategy to improve drug delivery. Lipids spread the entire cell, trafficking from the cell surface to/ within the various organelle membranes where lipid metabolism occurs. Increasing evidence demonstrated that internalized lipid-drug conjugates were distributed to various subcellular organelles in a lipid- and/or drug-specific manner.¹¹⁰⁻¹¹¹ By varying the lengths of acyl chain and altering the order of domains, M Koivusalo and co-workers demonstrated the ordered-domain sphingomyelins with long chain was observed in endosomes and then recycled to the plasma membrane, while short-chain, disordered sphingomyelins were

trapped in late endosomal compartments.¹¹⁰ Depending on the nature of the amphiphilic modification, the small molecule chemotherapeutic drug doxorubicin can be targeted to different intracellular locations. Maksimenko et al. conjugated doxorubicin to squalene via a cleavable ester bond.¹⁰⁷ Squalene-doxorubicin self-assembled into nanoassemblies of ~130-nm diameter, and efficiently deliver doxorubicin to the nuclei, presumably by releasing the free drug after intracellular entry. In a separate study, Xi et al. conjugated the amine group of doxorubicin to 1,2-Distearoyl-sn-glycero-3-phosphoethanolamine (DSPE) linked with a polyethylene glycol linker (amph-DOX, **Figure 1.3.3.1D**).⁷⁴ Interestingly, this simple molecular conjugate achieved high levels of tumor- and mitochondria-selective accumulation of doxorubicin. Although it is not clear how amphiphilic modification impacts doxorubicin's cellular uptake and intracellular trafficking, it is concluded that amphiphilic modification altered the physicochemical properties of doxorubicin, which in turn retargets it to mitochondria.⁷⁴

Chapter 2. Self-delivery of chemotherapeutic agents to tumor via 'albumin-hitchhiking'.

2.1 Introduction.

2.1.1 Albumin as a fatty acid transporter.

Fatty acids play critical roles as a source of biological supplement in mammalian bodies and boundary of physiological membranes¹⁻¹¹². Due to low solubility of fatty acids in blood plasma and interstitial fluid, albumin, a main transporter, binds with FAs to increase their concentration in vascular bundle and interstitial subdivision. As the most abundant plasma protein (35 - 50 g/L human serum), albumin has a molecular weight of 66.5 kDa and a heart-shaped structure which is folded from a single polypeptide chain.² Interaction between fatty acids and human serum albumin (HSA) was firstly reported in 1941. In this study, after four-times' crystallization, albumin was still observed to be yellow, a color from the existing impurity of plasma dyestuffs, which was further recognized to be FA.¹¹³ In the following years, several studies unveiled the binding properties of albumin to FA. It is known that albumin protein comprises three homologous domains, each containing two distinct subdomains. Curry and colleagues demonstrated plasma albumin possessed seven FA-binding sites (FA1-FA7)¹¹⁴⁻¹¹⁵, which were asymmetrically distribute throughout the albumin protein (**Figure 2.1.1.1**)⁴⁻⁵. There are seven bindings sites (FA1-7) lying in subdomain IB, subdomain IIIB, between IA and IIA or IIA and IIB, and within subdomain IIIA and subdomain IIA. Among these sites, FA4 and FA5 entirely located within domain III, which are highly appealing to FAs allowing the lipid tail to bind in a nearly linear formation. Residues

located outside of subdomain IIIA in FA4 will bind the carboxylate head-groups of FAs through hydrogen force, whereas the lipid tail convolves into the hydrophobic cuniculus throughout subdomain IIIA ^{113-114, 116}. FA5 resided in subdomain IIIB provides spaces for the side-chains of residues (Tyr401 and Lys525) binding to the carboxylate head-group of the FA, meanwhile methylene tail protrudes further into the long linear cavity, resulting in a unique structure and a comprehensive view of binding properties. ¹¹⁷ On the other hand, complexes with different parts such as small molecules reveal the appearance of small sub-hole within this crevice ¹¹⁸.

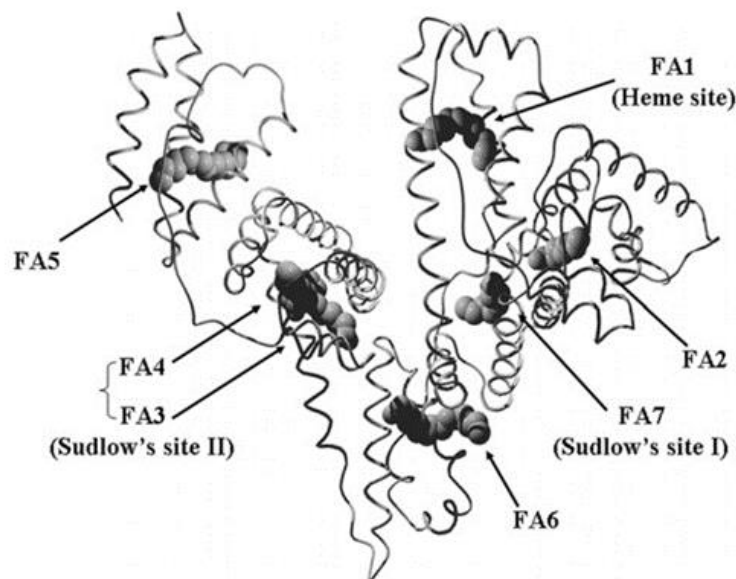


Figure 2.1.1 Fatty acid (FA) binding sites in human serum albumin (HSA).⁴⁻⁵

2.1.2 Albumin as a drug carrier in cancer therapy.

Drugs administrated in various routine are transported by the blood or interstitial fluid. They firstly encounter are not only the miscellaneous interstitial compounds or originations and cellular components, but also a multitude of plasma proteins. Plasma albumin has been emerged as a versatile protein carrier for improving the pharmacokinetic profile and targeting of cancer drugs.

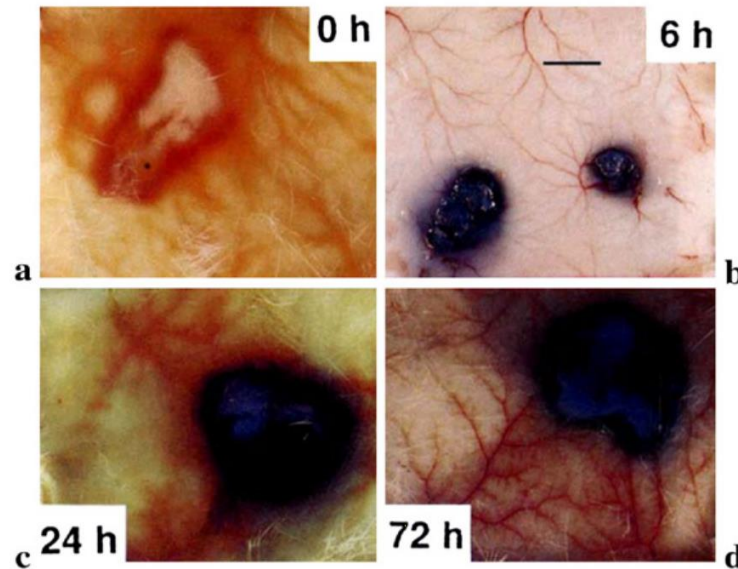


Figure 2.1.2.1 Accumulation of the Evans blue in sarcoma180 tumors over 72 h.¹²

For all cancers, a common method of growth is to parasitize the hosts for energy and nutrients ¹¹⁹, not only a variety of small molecular nutrients such as fatty acid and amino acids but also some large molecular proteins such as albumin. Compared with normal tissue, tumors act as ‘nitrogen traps’ in protein metabolism and uptake most of the proteins by pinocytosis ¹²⁰⁻¹²¹. Even under the stress of starvation, there is no release of tumor proteins for the body.¹²² Seepy ciliary vascular combined with a vacant or defective lymphatic drainage of solid tumor also trap albumin in such tissues. Matsumura and Maeda firstly demonstrated that Evans blue dye that had avidity to albumin accumulated in tumor after intravenous injection. ²¹ After 6 hours, blue color from Evans blue dye was observed in the tumor area in in preclinical models, which intensified over 72 hours (**Figure 2.1.2.1**).¹²³ The tumorigenic accumulation of proteins with various molecular sizes from 12 to 150 kDa were also explored. However, there was no significant

differences observed between the uptake of albumin (MW 66.5 kDa) and immunoglobulin (MW 150 kDa). They concluded that due to the tumoral hypervascularity, macromolecules had an enhanced permeability and little recovery through either blood vessels or lymphatic vessels. In addition, a certain time of drug circulating in blood was also speculated to be the prerequisite for an increased accumulation tumor uptake of the protein. Based on such reports, macromolecules passively target tumor via enhanced permeability and retention (EPR) are further developed.¹²³ Tumor vessels are poorly aligned with endothelial cells leading to the formation of wide fenestrations whose size varies from 100 to 1200 nm in diameter¹²⁴⁻¹²⁵ Associating with tumor vascular fluid and components transportation, macromolecules introduced as drug carriers having hydrodynamic size between 2 nm to 10 nm in radius (e.g., serum albumin has a radius of 3.6 nm) are permitted to spill over into tumor tissue instead of normal tissue. Thus, macromolecules permeate through the impaired and defective blood vessels in tumor tissue whereas healthy veins only grant small molecule flow across the endothelial barrier. Another factor of the intensive uptake of large molecular weight (> 40 kDa) components in tumor tissue is the reduced clearance¹²⁶. The macromolecules are retained in the interstice of tumor tissue leading to a high intratumor concentrations which is primarily caused by a lack of lymphatic drainage in such defective lymphatic system. Hence, both an enhanced permeability and retention (EPR) and reduced clearance effects of macromolecules are contributing to the accumulation and retention of albumin in solid tumors.

2.1.2.2 Drug delivery via albumin-hitchhiking.

Methotrexate-albumin conjugate (MTX-HSA) was one of albumin-based drug delivery system evaluated in clinical studies¹²⁷. Directly conjugating the MTX to lysine residues of human serum albumin, discrepant antitumor proliferation properties in Walker-256 carcinoma bearing rats were observed and only coupling ratio close to one MTX to one albumin exhibited the high-level performance of tumor specific accumulation comparative with unmodified albumin¹²⁸⁻¹²⁹. A prominent observation of this study was the remedial responses to MTX-HSA therapy from three patients with kidney cancer or mesothelioma (one partial response, two minor responses). However, no objective results were identified in the following phase II study that 17 patients with metastatic kidney carcinoma¹³⁰. Combinational therapy of MTX-HSA with another chemotherapy cisplatin was conducted as the first line treatment to the carcinoma of urinary bladder in another phase II study. Although obviously remissions were confirmed in seven patients, there is no evidence that the clinical application of this therapy is being further applied.¹³¹

Kratz and co-workers modified the albumin conjugation methods of drug derivatives and obtained high-purity drug albumin coupling components with a constant drug coupling ratio. This approach set the breaking point of protein in advance to reduce alteration in three-dimensional structure.¹³² The resulting conjugate was distinctly superior against murine kidney cancer compared to mice treated with free doxorubicin at equitoxic dose¹³². Their further work stated a prodrug concept that exploited endogenous albumin as a self-delivery platform by

which the prodrug was designed to rapidly and specifically bond to circulating plasma albumin after intravenous injection. The albumin/drug complex was spontaneously generated and transported as the normal albumin in situ through the vein¹³³⁻¹³⁴. Employing endogenous albumin as a transporter can avoid possibly immunogenicity from pathogenic albumin. In addition, there is a broad range of drugs can be designed as albumin-binding drugs which are comparatively primitive and inexpensive to develop in engineering. For example, acid-sensitive doxorubicin prodrugs (DOXO-EMCH) was reported to follow such strategy and showed dramatically improved antitumor efficacy in preclinical murine cancer models¹³².

2.2 Method.

2.2.1 Materials, cells and animals.

Doxorubicin hydrochloride salt was obtained from LC laboratories (Woburn, MA). 1,2-Distearoyl-sn-Glycero-3-Phosphoethanolamine (DSPE) conjugated polyethylene glycol (PEG 2000) with active succinimidyl ester (DSPE-PEG₂₀₀₀-NHS) was purchased from Biochempeg scientific Inc (Watertown, MA). Cholesterol polyethylene glycol (PEG 2000) NHS and DSPE-PEG₂₀₀₀-NHNH₂ were ordered from Nanocs Inc (New York, NY). Triethylamine (TEA), N-hydroxysuccinimide (NHS), bovine serum albumin (BSA), filipin (FLP), ethyl-isopropyl amiloride (EIPA) and sucrose were purchased from Sigma-Aldrich (St Louis, MO). Alexa Fluor 660 NHS Ester (Succinimidyl Ester) was obtained from Thermo Fisher Scientific (Waltham, MA). Cells were cultured in complete medium (RPMI1640, 10% fetal bovine serum (Greiner Bio-one), 100 U/mL penicillin G sodium and 100 µg/mL streptomycin (Pen/Strep). Mouse skin melanoma (B16F10) cell line, mouse mammary carcinoma (4T1) cell lines were ordered from ATCC. Animals were housed in the United States Department of Agriculture (USDA)-inspected Wayne State University animal facility under federal, state, local and NIH guidelines for animal care. Female C57BL/6 mice (5-8 weeks) were obtained from the Jackson Laboratory.

2.2.2 Synthesis of amphiphilic doxorubicin and doxorubicin loaded micelles.

Doxorubicin hydrochloride (DOX, 5 mg, 8.6 mmol) were dissolved in 0.5 mL dimethyl sulfoxide (DMSO) solvent and DSPE-PEG₂₀₀₀-NHS (38 mg, 5.7 mmol) were added to 4.5 mL of the same solvent. These two solutions were

homogeneously mixed with addition of 3 μ L triethylamine (TEA). After stirred in the dark at room temperature (RT) for 12 hours, most of the DMSO solvent was removed in a stream of air for 72 h. The product residues were re-dissolved in 5 mL D.I water for high performance liquid chromatography (HPLC) purification. Amphiphilic doxorubicin (amph-DOX) was purified by a C4 reverse-phase HPLC column (Thermo Scientific, 250 x 4.6 mm, 5 μ m). 200 μ L samples were injected and separation using a solvent gradient (**Table 2.2.2.1**) with methanol and triethylammonium acetate (TEAA, 0.1 M pH = 7.4) buffer. The elution and concentration of DSPE-PEG₂₀₀₀-DOX was monitored by measurement of the UV absorbance at 260 nm and 485 nm. The chromatography spectra of product were eluted at 13min and product was collected from 12 min to 14 min. After that resulting component was sir dried and dissolve in DMSO again. ¹H-NMR (Varian, 400 MHz) and Mass spectrum (Bruker Daltonics MALDI Ultraflex Extreme TOF/TOF) were used to characterize DSPE-PEG₂₀₀₀-DOX (amph-DOX).

Table 2.2.2.1 HPLC gradient for purification of DSPE-PEG₂₀₀₀-DOX.⁴⁵

Time	Methanol	0.1 M TEAA
0.00	50.0	50.0
10.00	100.0	0.0
15.00	100.0	0.0
15.01	0.0	100.0
20.00	0.0	100.0

Doxorubicin were loaded into DSPE-PEG₂₀₀₀ micelles by the single solvent film casting method. Briefly, doxorubicin hydrochloride (2 mg, 3.5 mmol) pre-activated with triethylamine (TEA, 7 mg ,7 mmol) at a 1:2 molar ratio in methanol

for 1 h at RT, subsequently was mixed with 20 mg DSPE-PEG₂₀₀₀ in chloroform. Solvent in the mixture was air dried at RT for overnight, resulting a thin film. The dried film was then mixed with 1 mL D.I water and stirring at 60 °C for 20 min. Free un-entrapped doxorubicin existing in the supernatant were separated by centrifugation (5500 rpm, 15 min).

2.2.3 Dynamic light scattering (DLS).

The size of amphiphilic DOX micelles was analyzed by zetasizer (Nanosizer ZS, Malvern Instrument) at 25 °C. 10 µM amphiphilic DOX was dissolved in PBS and incubated in presence of or absence of BSA at 37 °C for 4 h. Micelles were added to the microcuvette (ZEN0040, Malvern Instrument) and started the Zeta sizer measurement to measure the products hydrodynamic diameter (DH). The hydrodynamic diameter was determined using Stokes–Einstein equation: $DH = (kT/3\pi\eta D)$. In Stokes–Einstein equation, D is diffusion coefficient, referring via the cumulant fitting from autocorrelation function; T is temperature, 25 °C; η is viscosity; k is the Boltzmann constant.

2.2.4 Electrophoretic mobility shift assay (EMSA).

An agarose gel EMSA technique was used to characterize the binding between albumin protein and amphiphilic DOX. 10 µM free DOX and amphiphilic DOX dissolved in phosphate buffered saline (PBS, pH 7.4) were incubated with mouse blood for 4 hours at 37 °C, resulting in 1 mL mixtures in total volume. 0.5 mL of the samples were used for fluorescent analysis and gel electrophoresis shift assay and the other 0.5 mL were used for flow cytometry analysis. After centrifugation, 20 µL samples were premixed with glycerin and loaded for

electrophoresis and the all gels were run under 200 V for 30 min. Images were recorded using a digital camera (Canon EOS) under UV illustration.

2.2.5 Fluorescence resonance energy transfer assay ¹.

Fluorescence resonance energy transfer ¹ assay was employed to demonstrate the binding between albumin and amphiphilic DOX. 30 mg of BSA dissolved in PBS was firstly labeled with 2.1 mg of Alexa 660 dissolved in DMSO for 4 h at RT. After coupling, the product was purified using gel-filtration column (MidiTrap G-25, Sigma-Aldrich) and analyzed by HPLC. 10 μ M amphiphilic DOX or free DOX were incubated with above Alexa 660 labelled bovine serum albumin-(BSA-Alexa660) complex in PBS (pH 7.4) buffer for 4 h at 37 °C. After that, samples were analyzed by spectrofluorometer (JASCO FP-6500). DOX or amphiphilic DOX were excited at 470 nm and the fluorescence spectra were monitored from 550 nm to 650 nm in wavelength.

2.2.6 Membrane insertion and cellular uptake studies.

The membrane insertion and cellular uptake of unmodified DOX and amphiphilic DOX were quantified in B16F10 cells by flow cytometry (Applied Biosystems). Cells with a density of 1×10^6 cells per well were seeded in a 96-wells plate for overnight. For membrane insertion determination, the cell medium was removed and replaced with 1.0 μ M DOX and amphiphilic DOX in cold cell culture medium for different time periods at 4 °C. For uptake quantification, the cell medium was removed and replaced with 1.0 μ M DOX or amphiphilic DOX in cell culture medium for different time periods at 37 °C. After washing three times with PBS, cells were harvested in fluorescence-activated cell sorting (FACS) buffer and

analyzed by Attune acoustic focusing cytometer. Each assay was performed in triplicate.

2.2.7 Mechanism of cellular entrance.

1×10^6 B16F10 cells were seeded in full cell culture medium in 96-wells plate at 37°C. After overnight incubation, cells were incubated in the presence or absence of 5 µg/mL filipin (FLP), 10 µg/mL ethyl-isopropyl amiloride (EIPA), or 0.1 M sucrose for 30 min. 1 µM amphiphilic DOX or DOX loaded micelles were added to each well and incubated for another 4 h. After incubation, cells were centrifugated and washed three time using PBS for flow cytometry analysis.

2.2.8 *In vivo* pharmacokinetics values.

To measure the pharmacokinetics *in vivo*, 100 µL B16F10 melanoma cells (10^7 cells/mL) suspended in sterilized PBS were subcutaneously (s.c.) inoculated in the flank region of 5-weeks C57BL/6 mice. When the tumor size reached ~500 mm³, mice were randomly divided into three groups (n = 8 mice per group). Free doxorubicin (10 mg/kg), amphiphilic DOX (10 mg/kg equivalent doxorubicin) or PBS were intravenously administrated at tail vein into the tumor bearing mice. 50 µL blood samples (n = 4 at each time point) were collected into the heparinized tubes at 30 and 60 min, 2, 4, 6, 12 and 24 h after drug administration and then centrifuged at 15,000 × g for 10 min to isolate the blood plasma. Sera were mixed with two equal volumes of PBS and drug concentrations in sera were interpolated from standard curve by measuring the fluorescence intensity at 585 nm in each sample, normalized with sera from non-treated animals. The standard curve of drug was established by mixed known concentration of DOX to homogenates of

mixture of PBS and non-treated sera samples. Half-life ($t_{1/2}$) was interpolated from doxorubicin concentrations in the area vs. time curve and stimulated by one-phase exponential decay method (Graphpad prism).

2.2.9 *In vivo* biodistribution study.

For tracking the *in vivo* distribution, a total number of twenty-four B16F10 melanoma tumor bearing C57BL/6 mice (tumor volume $\sim 500 \text{ mm}^3$) were randomly separated into three groups. Mice injected intravenously with either free doxorubicin (10 mg/kg), amphiphilic DOX (10 mg/kg equivalent doxorubicin) or the same volume of PBS. In each treatment group, mice were euthanized under carbon dioxide inhalation at 2 or 24 h after drug administration ($n = 4$ at each time point). The tumor, spleen, heart, brain, lung, kidney, and liver tissues were collected. Tissue samples were liquid nitrogen frozen and stored at $-80 \text{ }^\circ\text{C}$ until drug extraction.

To extract drug from tissues, each sample were weighed and smashed by tissue homogenizer (Biomasher II tube, Kimble) and sonicated with nine parts (v/w) of PBS. 200 μL homogenate were combined with 50 μL Triton X-100 solution (10%, v/v, BioVision, Inc.) and 750 μL HCl (0.75 N, Sigma-Aldrich) in dichloromethane (DCM). The mixture was incubating at $-20 \text{ }^\circ\text{C}$ for 12 h in the dark and vortexed at room temperature after thawing. Samples containing drug were isolated by centrifugation at $20,000 \times g$ for 20 min ($4 \text{ }^\circ\text{C}$). Fluorescence intensity was measured and corrected against extracts from tissue samples of non-treated animals. A standard curve was interpolated by titration known concentration of

doxorubicin to homogenates of mixture of PBS and non-treated tissue samples prior to extraction.

2.2.10 Tumor model.

B16F10 (5.0×10^5 cells in 100 μ L PBS) were subcutaneously inoculated into the left flank of 5-6-weeks C57BL/6 mice. When the tumor volumes reached 30 mm³ (on day 5), mice were divided into three treatment groups (n = 8). The tumor-bearing mice were intravenously injected with either 5 mg/kg doxorubicin hydrochloride, amphiphilic DOX or PBS every 72 h (on days 5, 8, and 11) in total three times. Tumor length(L) and width(W) were measured with calipers, and the tumor volume was calculated using the following equation: Tumor volume (V) = $0.5 \times L \times W^2$.

2.2.11 Hematoxylin and eosin (H&E) staining.

Heart samples were isolated and performed formaldehyde-fixed and paraffin-embedded. Hematoxylin and eosin immunohistochemical (H&E) staining was applied on the fixed heart samples. After staining, pathology was observing the slides under a microscope, cell nuclei were colored purple-blue and positive area were orange. Figures of each slide were selected randomly and analyzed using Fiji ImageJ (Bethesda, Maryland) image analysis software.

2.2.12 Statistical analysis.

The mean values of two groups were performed using unpaired Student's t tests. The statistical difference between groups were determined using a one-way analysis of variance²⁰ with Bonferroni post-test. All the values were expressed as means \pm standard error of mean. GraphPad Prism (San Diego, CA) software was

used for all the statistical analyses. *** $p < 0.001$, ** $p < 0.01$, * $p < 0.05$, NS, not significant.

2.3 Results and discussions.

2.3.1 Design of albumin-based self-delivery amphiphilic conjugates.

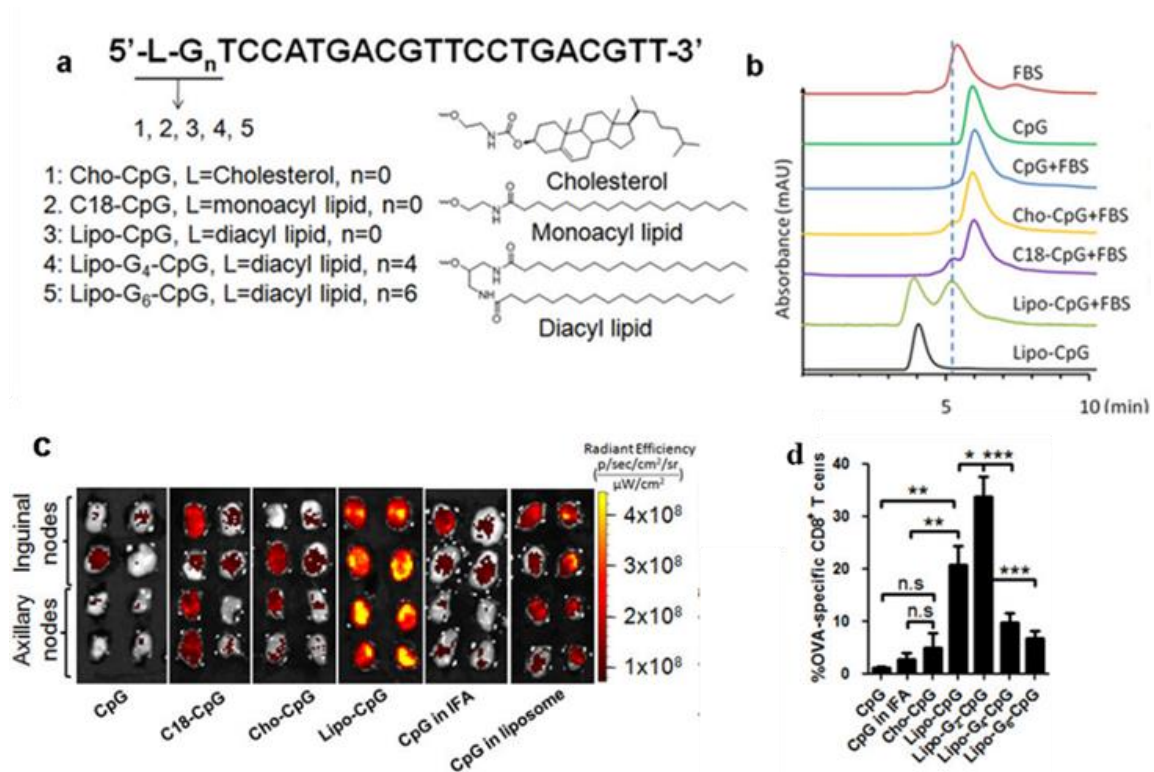


Figure 2.3.1.1 Target lymph node by albumin-based self-delivery vaccines. (A) Schematic of the design of albumin-based self-delivery vaccines. (B) Size-exclusion chromatography of CpGs, Cho-CpGs, C18-CpGs or Lipo-CpGs alone or following incubation with FBS for 2h. (C) Fluorescent amphiphiles were injected s.c. at the tail base, lymph nodes were isolated and imaged 24 hours post injection. (D) SIINFEKL tetramer of C57BL/6 mice (n = 4-8/group) after immunization with ovalbumin (10 µg) + CpG (1.24 nmol).²⁵

Endogenous albumin protein based self-delivering system is a promising approach in targeting tumor tissues *in vivo*.^{120, 130} We recently proposed an 'albumin-hitchhiking' approach which efficiently delivered therapeutic agents to lymph nodes (LNs).³⁵ As we illustrated in **Figure 2.3.1.1A**²⁵, subunit vaccines were covalently conjugated to a lipophilic tail which optimized for albumin binding in structure through a solubility-promoting polar polymer. Following subcutaneous injection, this amphiphilic vaccine has a high affinity to endogenous albumin

protein, draining to the lymph node through lymphocytic fluid³⁵. Lipid-based amphiphiles self-assembling into micelles were observed in aqueous buffer¹³⁵. However, these micelles were supposed to be formed at a higher concentration of monomer (above the critical micelle concentration, CMC) and were kinetically unstable especially in the presence of proteins such as albumin^{35, 76, 135}. In addition to protein absorption, these amphiphilic molecules with a lipid tail also exhibited plasma membrane insertion property, as demonstrated by the rapid uptake and intracellular delivery^{35, 136-137}. Thus, in the presence cells and serum, there existed a complicated three-way equilibriums: micelles were self-assembled from amphiphiles, amphiphiles in the single chain state can also insert their diacyl tails into cell membranes or bind to albumin protein. This three-way equilibrium was delicately regulated by 1), the length of both lipid tails and PEG that a long diacyl lipid (≥ 16 carbons) and a long polyethylene glycol (≥ 36 EG units) favors the albumin binding *in vivo*^{35, 135, 138}; 2) The *in situ* albumin concentration. In order to translate this 'albumin-hitchhiking' approach to deliver anti-cancer drugs, we modified doxorubicin with a structural optimized albumin-binding diacyl lipid linked by a polyethylene glycol linker (**Figure 2.3.1.1A**)²⁵. Instead of chemically conjugating the anti-cancer drugs to an albumin *ex vivo*, we proposed to design a novel amphiphilic drug which can bind rapidly to endogenous albumin. Albumin binding dramatically increased the molecular drug's size and transported the drug to disease site via enhanced permeation and retention effect (EPR)¹²⁵ or receptor mediated uptake. We hypothesized that the amphiphilic functionalization can alter doxorubicin's physicochemical properties, which in turn re-defined its

pharmacological characteristics, improved its therapeutic anti-tumor efficacy and reduced DOX-associated side effects.

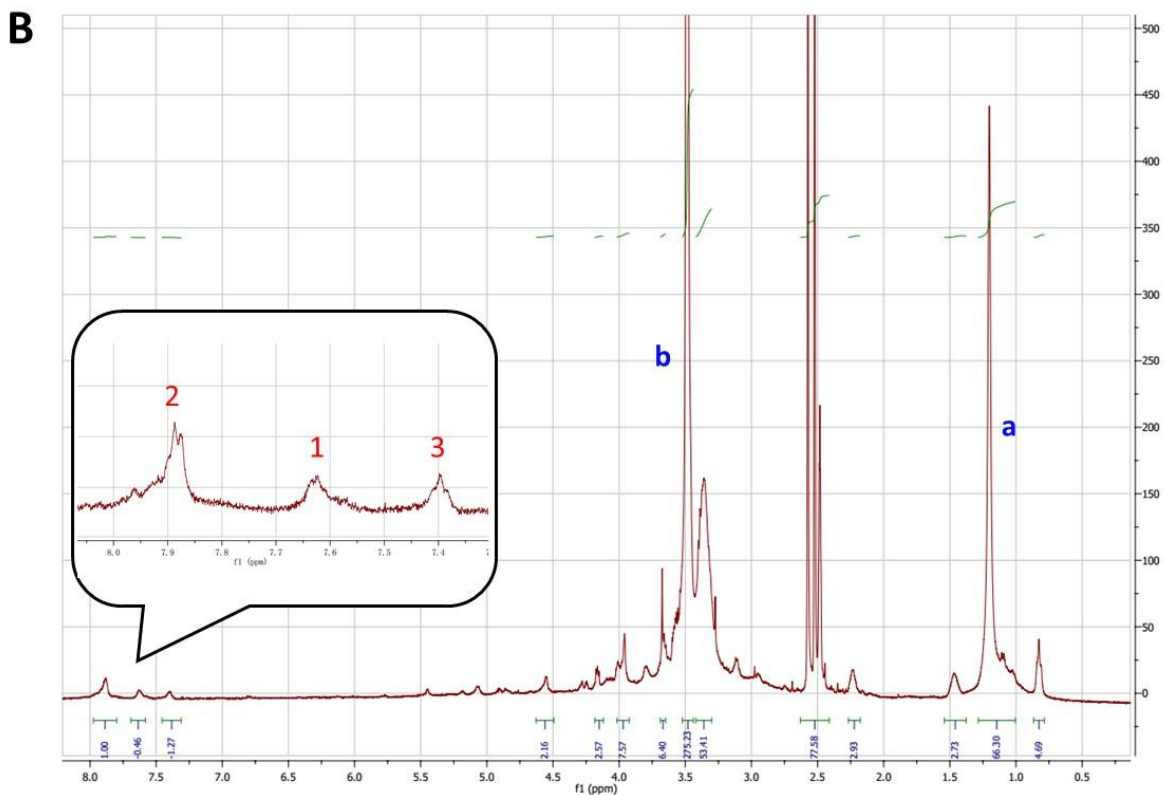
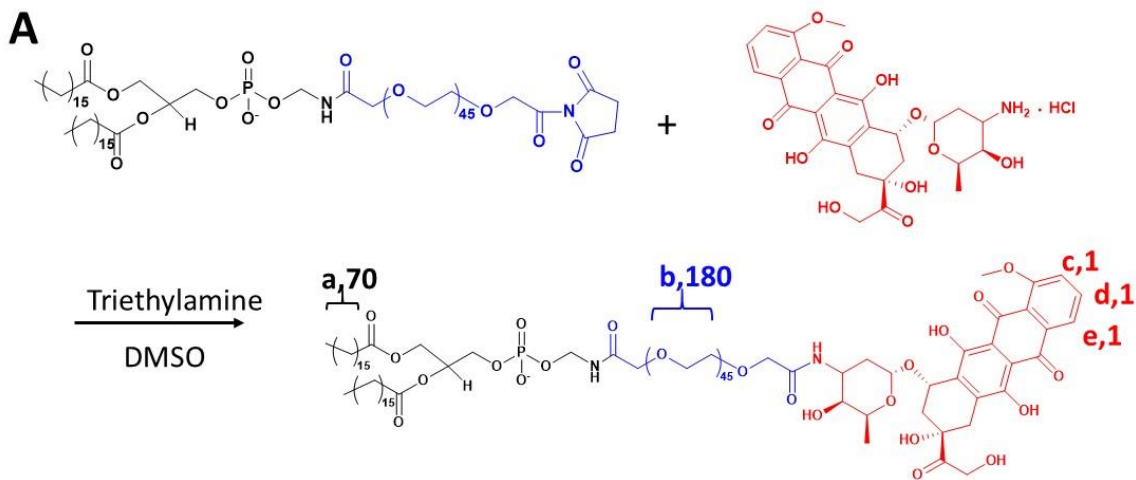


Figure 2.3.1.1 Synthesis and Nuclear Magnetic Resonance (NMR) characterization of amphiphilic doxorubicin.⁴⁵ (A) Amphiphilic DOX was synthesized by conjugating of doxorubicin hydrochloride (DOX) to DSPE-PEG₂₀₀₀-NHS. (B) ¹H-NMR spectra of amphiphilic DOX. The proton peaks of DOX (c, d,

and e) and DSPE-PEG (a, b) were observed at 8.5~7.0 ppm and 0.9~3.6 ppm, respectively.

The structure of amphiphilic doxorubicin can be divided into three distinct segments (**Figure 2.3.1.1A**)⁴⁵: a diacyl lipid tail as albumin-binding and membrane-anchor domain, a central repeat block containing ethylene glycol³⁵ units and DOX conjugated to the end of EG. The synthetic route of DSPE-PEG₂₀₀₀-DOX was simply coupling doxorubicin hydrochloride and 1,2-Distearoyl-sn-Glycero-3-phosphoethanolamine (DSPE) conjugated polyethylene glycol (PEG 2000) with active succinimidyl ester (DSPE-PEG₂₀₀₀-NHS) via amide linkage. The final conjugates were analyzed and purified by reverse phase HPLC chromatography. As shown in **Figure 2.3.1.1B**⁴⁵, the Nuclear Magnetic Resonance (NMR) of amphiphilic DOX was measured in DMSO-d₆. The proton peaks of DOX (c, d, and e) and DSPE-PEG (a, b) were observed at 8.5~7.0 ppm and 0.9~3.6 ppm, respectively. The original integration of peak 4 was set broadly which contains the water peak at 3.3 ppm.

2.3.2 Amphiphilic doxorubicin avidly binds to circulating serum albumin.

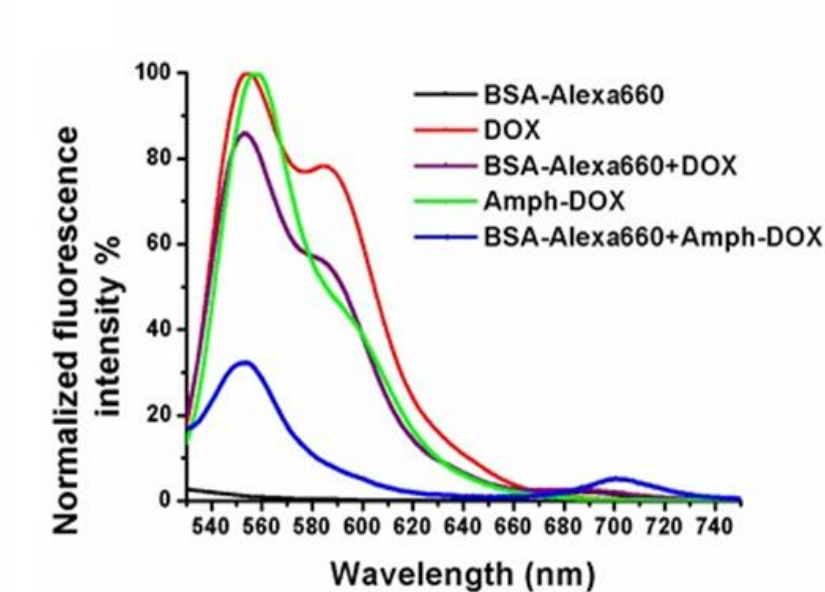


Figure 2.3.2.1 Albumin-binding properties of doxorubicin hydrochloride (DOX) and amphiphilic doxorubicin were assayed by fluorescence resonance energy transfer ^{1,45} 40 μ M Alexa 660 labeled bovine serum albumin (BSA-Alexa 660) were incubated with either DOX or amphiphilic DOX in PBS (pH 7.4) for four h at 37 $^{\circ}$ C. After incubation, samples were excited at 470 nm using spectrofluorometer (JASCO FP-6500), and the emission were collected ranging from 540 to 750 nm.

To demonstrate the albumin binding property of amphiphilic DOX, albumin-binding properties of doxorubicin hydrochloride (DOX) and amphiphilic DOX were assayed by fluorescence resonance energy transfer ¹ binding assay ¹³⁹. Alexa 660 labeled bovine serum albumin (BSA-Alexa 660) were synthesized by coupling BSA and Alexa 660 in the presence of TEA. Binding assays were prepared by adding excess BSA-Alexa 660 (40 μ M) in PBS buffer with 10 μ M either DOX or amphiphilic DOX at 37 $^{\circ}$ C. After 4 hours of incubation time, the mixtures were transferred in 1 cm path length quartz cuvettes and analyzed by spectrofluorometer (JASCO FP-6500). **Figure 2.3.2.1** ⁴⁵ displayed the emission spectra excited for these samples. Emission spectra obtained from PBS buffer of pure 10 μ M DOX (red line),

amphiphilic DOX (green line) and 40 μ M Bovine serum albumin (BSA)-Alexa 660 (black line) were also exhibited for comparison. The maximum excitation wavelength of DOX at 470 nm was used for all samples. At this wavelength, DOX or amphiphilic DOX excitation occurred with high efficiency, while direct BSA-Alexa 660 excitation was negligible. In the absence of BSA-Alexa 660, the solution of amphiphilic DOX and DOX mainly showed the fluorescence emission from DOX (565 nm) when excited at 470 nm. However, the increase in emission from BSA-Alexa 660 (690 nm) with concomitant suppression of amphiphilic DOX (565 nm) was observed in the presence of BSA-Alexa 660, clearly indicating FRET occurring from amphiphilic DOX to BSA-Alexa 660.

To test whether amphiphilic DOX conjugates can bind to endogenous serum albumin, free doxorubicin hydrochloride or its amphiphilic conjugates were incubated with freshly isolated mouse blood. The quantification and interaction of drug with serum albumin were analyzed by fluorescence spectroscopy (**Figure 2.3.2.2B**)⁴⁵ and gel shift electrophoresis (**Figure 2.3.2.2C**)⁴⁵. Parallely, the whole blood samples were analyzed by flow cytometry. Upon co-cultured with blood containing cells and plasm proteins, 9.8% of free DOX was detected in the erythrocytes, which was almost three times more than that of amphiphilic DOX (**Figure 2.3.2.2A**)⁴⁵.

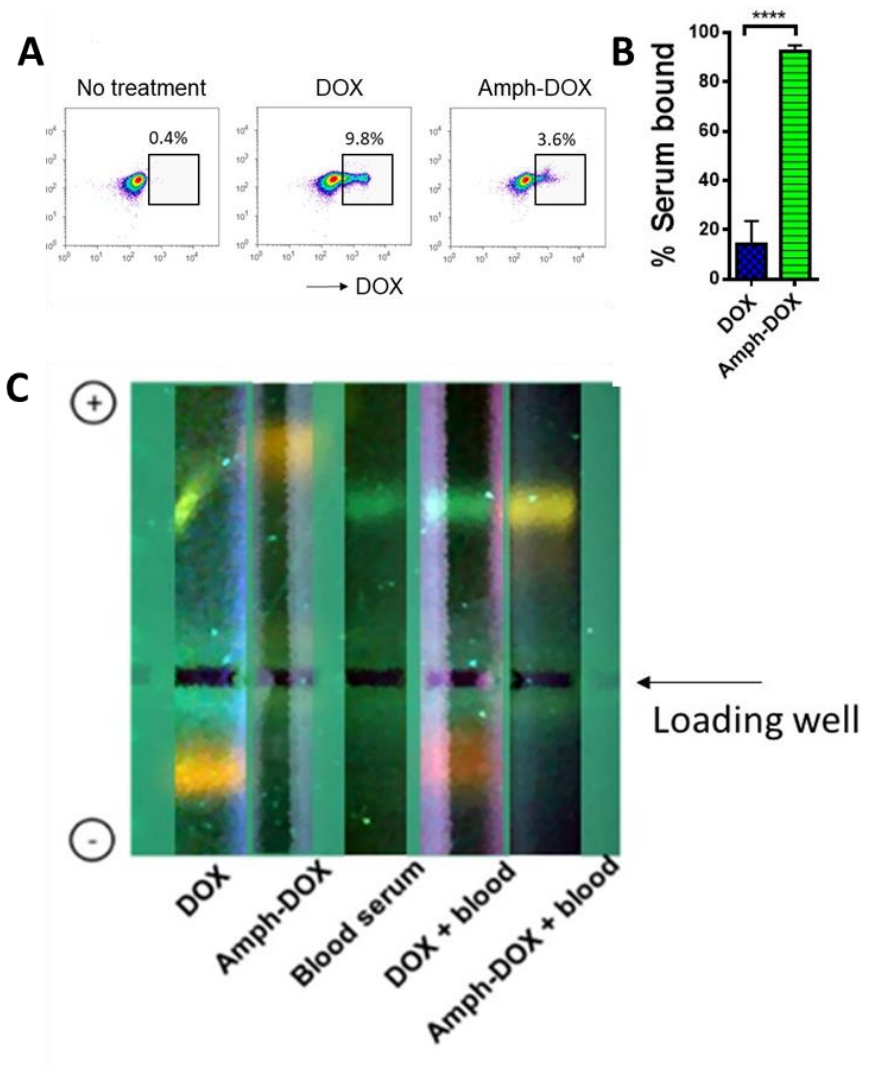


Figure 2.3.2.2 A majority of amphiphilic DOX, instead of free DOX can bind to serum albumin in blood.⁴⁵ (A-C) Fresh isolated blood from mice were incubated with DOX or amphiphilic DOX at a final concentration 0.5 μ M for 4 h. After separation, whole blood cells were analyzed by flow cytometry (A) and sera were isolated to quantify the content of drug via fluorescence spectroscopy (B) and binding status were visualized by gel shift assay (C).⁴⁵

This observation was consistent with previous publications and suggested adriamycin interacts with blood cells^{138, 140-142} By comparison, despite being in the possession of lipid tail for membrane insertion, amphiphilic DOX had less association with the cells in the blood (3.6%). Fluorescence spectroscopy

measurements indicated that 92% of amphiphilic DOX and 18% of free DOX remained in the blood serum (**Figure 2.3.2.2B**)⁴⁵. Further, gel electrophoresis analysis (**Figure 2.3.2.2C**)⁴⁵ of drug incubated with blood showed a light-orange fluorescent band from amphiphilic DOX co-migrated with albumin (**Figure 2.3.2.2C**, lane 5)⁴⁵, suggesting that the majority of the amphiphilic DOX existing in serum albumin/ amphiphilic DOX status. This band was distinct from albumin as pure serum showing a green color under ultraviolet light (254 nm) which came from protein autofluorescence. In contrast, two individual band in the opposite direction of loading well were observed in free DOX incubated with blood. DOX possesses a single positive charge and migrated as a single band toward the negative electrode (**Figure 2.3.2.2C**, lane 4)⁴⁵, indicating a lack of interaction with negative charged albumin protein in the gel. Size exclusion HPLC spectra (data not shown) showed that amphiphilic DOX was eluted at 6.7 min indicating a large size aggregation. While incubating with mouse blood, the aggregation was disassembling and co-eluted with serum at 9 min. These results strongly demonstrated that, unlike unmodified DOX, which extensively interacted with cells in blood, amphiphilic DOX can bind to plasma albumin in blood vessel and warrant further investigation of albumin-based self-delivery platform for drug delivery.

2.3.4 Three-way equilibriums of amphiphilic doxorubicin.

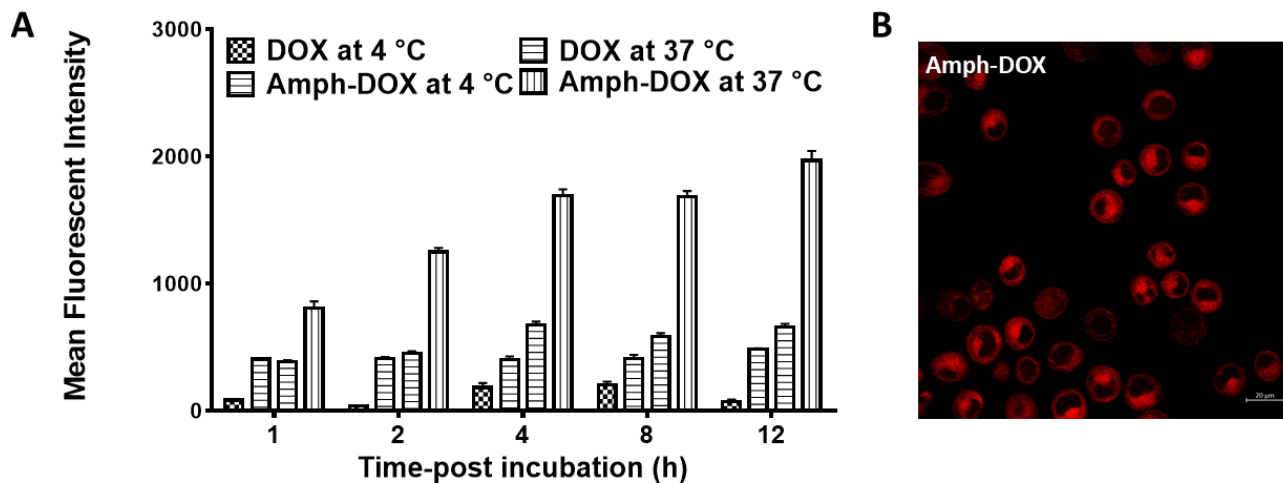


Figure 2.3.4.1 The membrane insertion property of amphiphilic doxorubicin.

⁴⁵ (A) DOX or amphiphilic DOX (1 μ M) were co-cultured with B16F10 cells in 10% FBS at 4 °C or 37 °C. Uptake was quantified by flow cytometry. (B) Cellular distribution was analyzed by confocal microscope.

DSPE lipid was observed to spontaneously anchor and penetrate cells driving by the hydrophobic effect indicating the importance of lipid-membrane fusion as a forerunner to cell entrance. To explore the membrane insertion property of amphiphilic DOX, freshly trypsinized B16F10 cells were incubated with DOX salt or amphiphilic DOX at 4 °C to maximally inhibit internalization and the uptake were determined by flow cytometry. Amphiphilic DOX showed a rapid internalization at 1h and peaked after 4 h incubation. The uptake of amphiphilic DOX was more than four-fold than that of free DOX. Confocal images also indicated membrane insertion and rapid internalization of amphiphilic DOX via endocytic recycling (**Figure 2.3.4.1B**)⁴⁵. These results suggested amphiphilic modification enhanced cell entry partially due to the membrane insertion and it was suspected that multiple routes were involved in the internalization process. The

uptake of amphiphilic DOX *in vitro* (e.g., cell culture environment) was very complicated in that: there exists a three-way equilibrium (**Figure 2.3.4.2**)⁴⁵ when amphiphilic DOX was incubated with cells. Amphiphilic DOX can exist as micelle states, albumin-binding state, and cell membrane insertion state. This has made the mechanism study very difficult as *in vitro* (typically, 10% FBS, note that the albumin concentration is approximately ten times less than that in blood), all these states can enhance the cellular uptake as compared to free DOX.

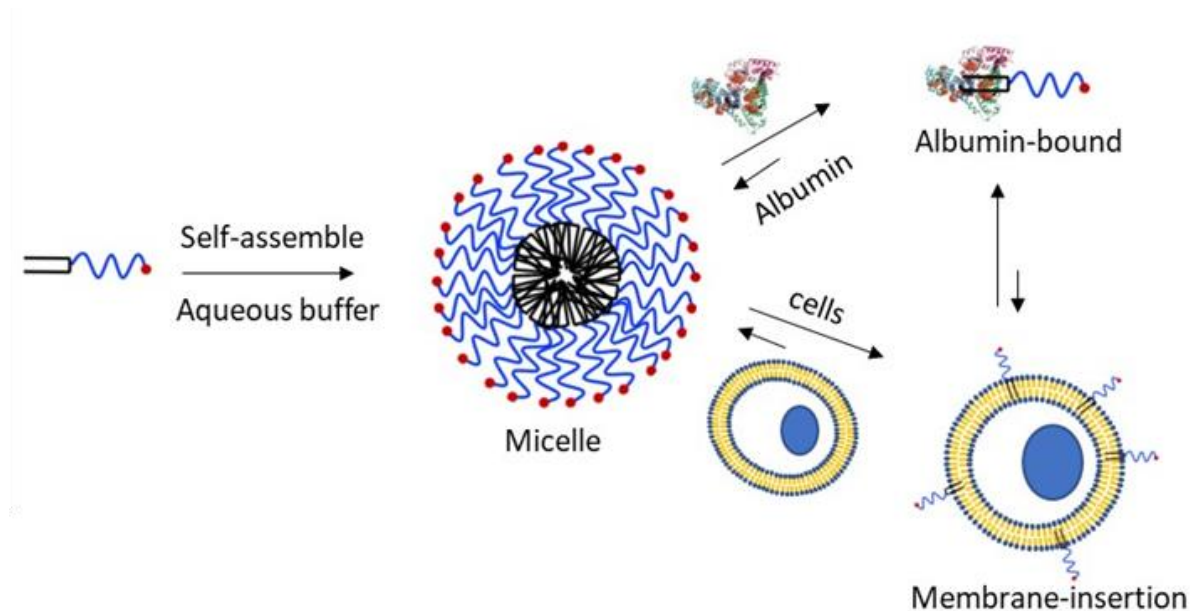


Figure 2.3.4.2 Self-assemble, membrane-insertion, and albumin-binding properties of amphiphilic DOX. ⁴⁵In aqueous solution, spherical micelles are self-assembled from amphiphilic DOX with a DOX-PEG sunflower and a lipid core. In the presence of albumin and cells, the micelle structure is disrupted by binding to albumin (albumin hitchhiking) or inserting on plasma membrane (membrane insertion). The structure of lipid-polymer (e.g., the length of lipid and PEG) and albumin concentration govern the equilibrium partitioning between albumin binding state or membrane insertion state. Current structure (DSPE-PEG₂₀₀₀) was optimized for albumin-binding based on our previous finding. At high concentrations of albumin (e.g., 640 μM in blood), the equilibrium strongly favors albumin-binding. ⁴⁵

2.3.5 Analysis of uptake pathway under three-way equilibrium.

In the three-way equilibrium (**Figure 2.3.4.2**)⁴⁵ we proposed, amphiphilic DOX can enter cell in three different formulas: self-assembling particle, albumin/amphiphilic DOX complex or single-chain amphiphilic DOX. We firstly compared the cell internalization of amphiphilic DOX with DOX loaded DSPE-PEG₂₀₀₀ micelles. Doxorubicin were entrapped into DSPE-PEG₂₀₀₀ micelles by the film casting method¹⁴³. Briefly, doxorubicin hydrochloride (2 mg, 3.5 mmol) in methanol was pre-treated with triethylamine (TEA, 7 mg, 7 mmol) at a 1:2 molar ratio for one hour at RT, then mixed with 20 mg DSPE-PEG₂₀₀₀ in chloroform. The DOX loaded DSPE-PEG₂₀₀₀ micelles were obtained under a stream of air form a thin film and hydrated with D.I water. Cells were incubated with 1 μ M DOX, amphiphilic DOX or equal molar DOX loaded micelle for 4 h at 37 °C. Cellular uptake was evaluated using mean fluorescence intensity quantified by flow cytometry of treated cells. Consistent with previous study, increased uptake was observed in amphiphilic DOX compared with cells treated with DOX (**Figure 2.3.5.1A**)⁴⁵. As we expected, amphiphilic DOX showed a superior cell entrance ability comparing with DOX loaded micelles, indicating amphiphilic DOX uptake through multiple channel which was not entirely the same with DSPE-PEG encapsulated DOX nanoparticles.

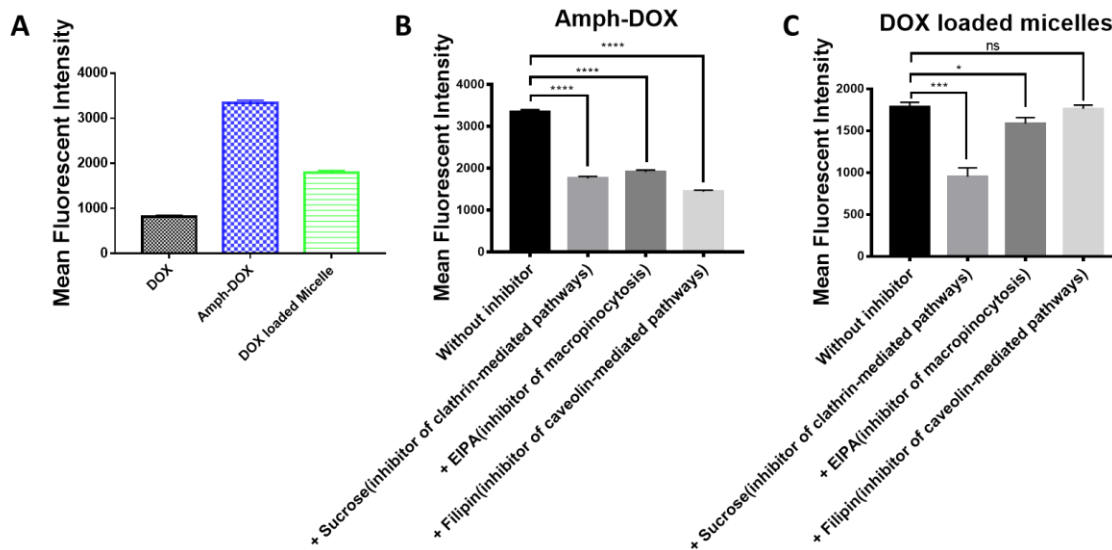


Figure 2.3.5.1 The amphiphilic DOX can exist in three statures *in vitro* and the uptake pathway were complicated.⁴⁵ (A) Cellular uptake of amphiphilic DOX and DOX loaded DSPE-PEG₂₀₀₀ micelle in 10% FBS. (B and C) B16F10 cells were pretreated with different inhibitors and then incubated with amphiphilic DOX or DSPE-PEG₂₀₀₀ micelles. Cellular uptake was measured by flow cytometry.

Endocytosis or endocytosis-like internalization routine are the main pathways of entrances for lipoplexes. To investigate the difference of uptake pathway between amphiphilic DOX and DOX loaded DSPE-PEG₂₀₀₀ micelles in a cell culture condition, cells were cultured with filipin, the caveolae transport inhibitor, or sucrose, the clathrin-mediated inhibitor, or EIPA (inhibitor of macropinocytosis). 50-65% of internalization were inhibited by sucrose, filipin and EIPA suggesting multiple mechanisms were involved in the uptake of amphiphilic DOX (**Figure 2.3.5.1B**)⁴⁵. In contrast, the uptake of DOX loaded DSPE-PEG₂₀₀₀ micelles were primarily affected by the inhibitor of clathrin-mediated pathway (**Figure 2.3.5.1C**)

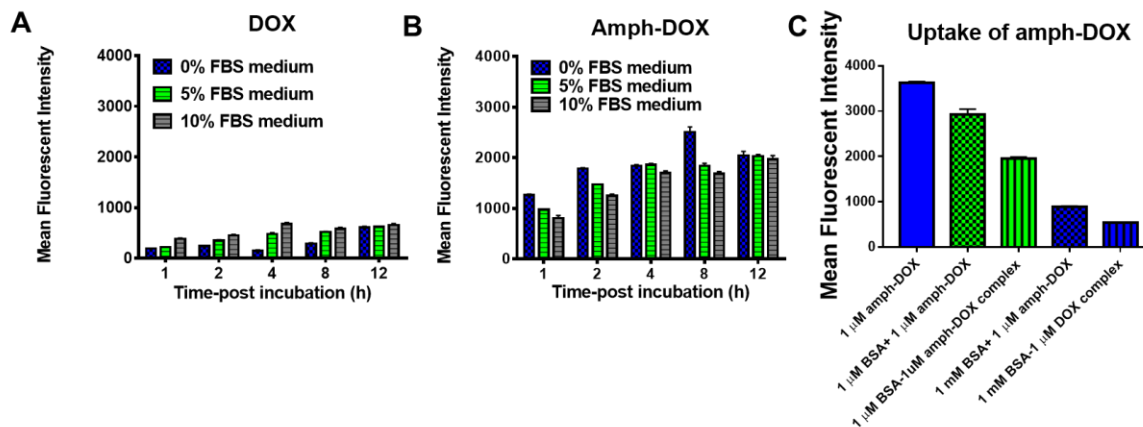


Figure 2.3.5.2 BSA competed with cells to bind amphiphilic DOX in a certain time but was not a hinder of internalization.⁴⁵ (A and B) B16F10 cells uptake of free DOX and amphiphilic DOX in different concentrations of FBS was examined by flow cytometry. (C) Uptake of amphiphilic DOX in the presence of low (1 μ M) or high (1 mM) bovine serum albumin.

The stability of self-assembling amphiphilic dox micelles were characterized by DLS, demonstrating deconstruction of particle in the in the presence of serum albumin. To investigate the role of albumin in amphiphilic DOX internalization process, we evaluated the uptake and intracellular distribution of amphiphilic DOX in the presence and absence of albumin in a cell culture environment. *In vitro*, at first two hours, uptake of amphiphilic DOX showed negatively correlated with FBS content, reflecting the shift of equilibrium lay to the direction of cellular membrane insertion at low albumin concentrations (**Figure 2.3.5.2 A and B**)⁴⁵. However, after longer time incubation, partition between cellular uptake and albumin binding was observed for amphiphilic DOX in the various of FBS content (the major protein in FBS is albumin) in B16F10 cells. The results suggested that high concentrations of albumin would 1) drive the equilibrium toward an albumin-binding state and 2) the free albumin would compete with albumin-bound amphiphilic DOX for uptake, reducing the amphiphilic DOX's cellular uptake. **Figure 2.3.5.2C**⁴⁵ showed the

uptake results from low concentration (1 μ M) or high concentration (1 mM) albumin protein. As expected, the presence of extra albumin greatly reduced the uptake of amphiphilic DOX (**Figure 2.3.5.2C**)⁴⁵, suggesting the amphiphilic DOX was indeed bound to albumin. However, these data should not be simply interpreted as albumin does not facilitate the tumor uptake. Rather, it demonstrated that the uptakes were at similar levels no matter what state amphiphilic DOX was. In each state, the uptake was significantly better when compared to unmodified DOX. It is also worthy to mentioned that the concentration of albumin in blood is at least ten times higher than that in a typical cell culture environment (10% FBS). At this concentration, the majority of amphiphilic DOX binds to albumin protein (**Figure 2.3.2.2**)⁴⁵. Taken together, the data we collected suggested amphiphilic DOX reached tumor cells by binding and trafficking with albumin protein. *In vitro*, the uptake of amphiphilic DOX in its micellar formulation appeared to be equally efficient when compared with albumin-binding formulation, both of which were significantly greater compared with free DOX.

2.3.6 Albumin binding amphiphilic DOX extends half-life, alteration drug distribution and improves the therapeutic anti-tumor efficacy.

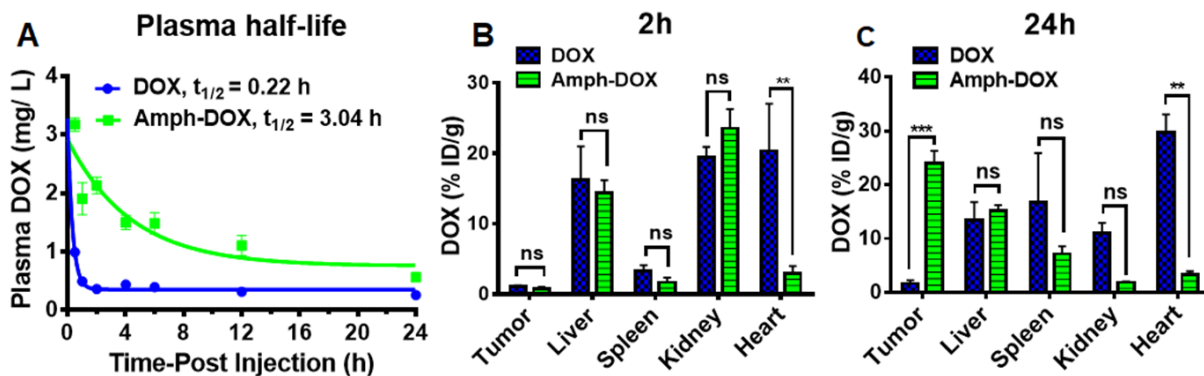


Figure 2.3.6.1 *In vivo* plasma pharmacokinetic evaluation and biodistribution of amphiphilic DOX in B16F10 tumor bearing C57BL/6 mice model.⁴⁵ (A) Time-drug concentration profile in plasma of DOX and amphiphilic DOX. Plasma doxorubicin concentrations resulting from a single injection free doxorubicin (10 mg/kg) or amphiphilic DOX (10 mg/kg equivalent doxorubicin) as a function of time post injection. (B and C) Tissues (kidney, heart, tumor, liver, spleen) content of drug 2 h (B) and 24 h (C) after a single injection of either DOX and amphiphilic DOX (equivalent doxorubicin at 10 mg/kg). The values are the mean \pm SEM (n = 4).

Albumin based self-delivery systems are known to enhance drug residence time in circulating blood.¹⁴⁴⁻¹⁴⁶ To test whether the amphiphilic DOX can prolong serum half-life via associated with albumin, mice were i.v. administrated with unmodified DOX or amphiphilic DOX. At various duration following injection, sera were isolated from drug treated mice blood samples for evaluating the profile of time-drug concentration. *In vivo*, unmodified DOX exhibited a rapid clearance from the plasma and its concentration was negligible (less than 1 mg/L) in 30 min post injection (**Figure 2.3.6.1A**)⁴⁵. In contrast, amphiphilic DOX with same dosage exhibited higher serum concentration and extended retention time, with a half-life (3.0 h) in blood increased approximately 60-fold compared with that of free

doxorubicin (0.22 h). Besides reducing clearance, albumin-based self-delivery amphiphilic DOX is also expected to accumulate in tumor via multiple principles: 1) due to the EPR effect, albumin/drug complex favorably accumulates in tumor relative to normal tissues; 2) albumin protein has an extraordinarily universal penetration capability via Fc receptor-mediated transcytosis in both normal and malignant tissues.^{145, 147} iii) Under the pressure of malignant cellular metabolism, tumor cells and tissues take up albumin protein as a source of amino acid and nutrient.^{145, 147} Meanwhile, the recruit of albumin protein in health organs are supposed to be relatively low due to the clathrin-mediated albumin recycling pathway.¹⁴⁸ Compared with unmodified drug, B16F10 tumor bearing mice treated with amphiphilic DOX were exhibited 15-fold amount of drug extracted from tumor tissue 24 h post injection (**Figure 2.3.6.1C**)⁴⁵. Moreover, amphiphilic DOX resulted in a significantly lower heart accumulation of drug compared to unmodified DOX (**Figure 2.3.6.1B and C**)⁴⁵, suggesting amphiphilic DOX might lead to a reduction of the potential DOX- related temporary and permanent cardiotoxicity.

We next evaluated the antitumor activities of amphiphilic DOX by therapeutically treating B16F10 melanoma tumor bearing C57BL/6 mice. At day 0, amount of 5×10^5 B16F10 cells in PBS were subcutaneously inoculated into the right flank of the mice. Mice received three injections of 5 mg/kg of unmodified DOX, or amphiphilic DOX, or PBS on days 5, 8, and 11. As shown in **Figure 2.3.6.2A**⁴⁵, administration of unmodified DOX showed a transient inhibition of B16F10 tumor at the early stage of the treatment, while therapeutic effect quickly regress when treatment termination on day 11. In contrast, mice treated with the

same doses of amphiphilic DOX markedly delayed the tumor growth, suggesting a progress of DOX- related chemotherapy (**Figure 2.3.6.2A and C**)⁴⁵. Treatment with amphiphilic DOX also diminished doxorubicin-induced losses in total body weight (**Figure 2.3.6.2B**)⁴⁵.

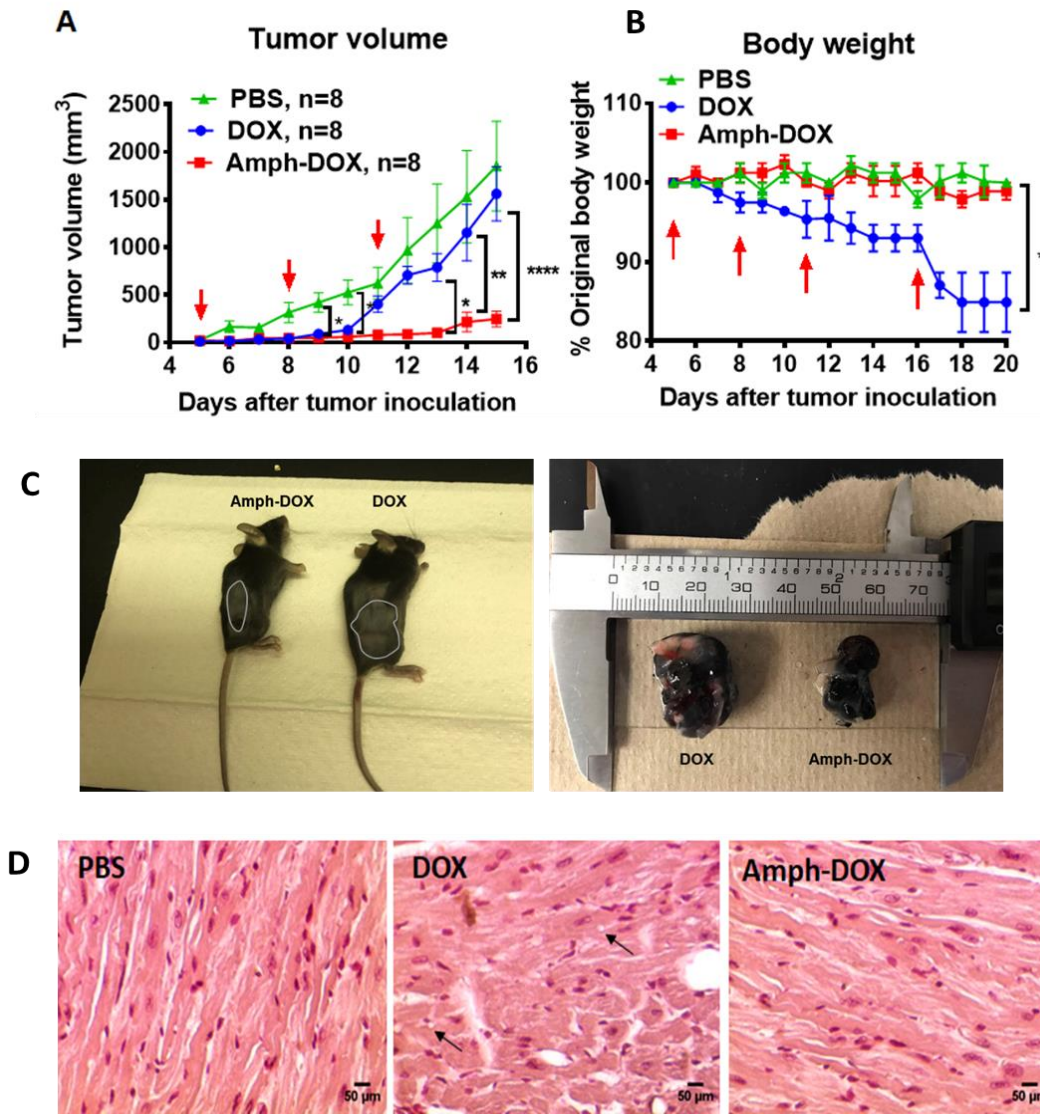


Figure 2.3.6.2 *In vivo* anti-tumor activity of amphiphilic DOX in melanoma bearing mice model.⁴⁵ (A and B) Tumor growth inhibition by amphiphilic DOX. Mice were injected with doxorubicin hydrochloride, or amphiphilic DOX, or PBS. All groups (n = 8) of mice received above treatments (5 mg/kg equivalent doxorubicin, 10 μL/g of the body weight) on days 5, 8 and 11 by intravenous injection in the lateral tail vein. Tumor volumes (A) and body weight (B) were regularly measured during the experimental period. (C) Tumor photographs of whole animals (day 15 after tumor inoculation) and after isolation. To evaluate cardiotoxicity, C57BL/6 mice tumor free were treated with DOX or amphiphilic DOX (10 mg/kg of body weight) at days 5, 8, and 11, and a maximum dose of 20 mg/kg on day 16. Representative photomicrographs of heart sections of DOX and amphiphilic DOX treated. (D) H&E staining of myocardium sections from tumor-free mice. Vacuole structures are indicated with black arrows.⁴⁵

In clinical, doxorubicin-induced cardiotoxicity can be highly possible and acute.¹⁴⁹ To investigate the cardiomyopathy established by DOX, H&E staining of cardiac muscle sections was analyzed of mice after administrations on days 5, 8 and 11. Histopathological analysis of heart section (on day 15) of amphiphilic DOX treated mice showed no sign of defective heart muscle and negligible cardiotoxicity, similar to those with no treatment control (**Figure 2.3.6.2D**). However, DOX treated animals showed noticeable, albeit mild damage to cardiac tissue, characterized by increased cytoplasmic vacuolization and distorted myocardial cell arrangement (**Figure 2.3.6.2D**). In conclusion, these results demonstrated the albumin-based self-delivery amphiphilic DOX can prolong drug circulating period, increase drug delivery to tumor tissue via associated with endogenous albumin protein leading to enhanced antitumor efficacy. Though the permanent DOX-related side-effect and cardiotoxicity cannot be determined by our model, the reduced mouse cardiac tissue accumulation and no cardiomyocyte pathology also guarantees a potential security profile for myocardial tissue in the preclinical model.

2.4 Conclusions.

In recent years, anti-cancer drugs delivered by nanoparticles can satisfy the needs of lowering the dose and decreasing side effects, as well as achieve the aim of combining multiple therapeutic agents.¹⁵⁰⁻¹⁵² Currently, many systems are under investigation for drug delivery and more specifically for cancer therapy. Because the potential toxicity and interaction with tissue and cells greatly depends on the actual synthetic of the nanoparticle composition, nature biological components like albumin, gelatin and phospholipids for liposomes rather than non-degradable materials like inorganic and solid metal containing nanoparticles are preferred¹⁵⁰. Instead of chemically conjugate the anti-cancer drugs to an albumin *ex vivo*, we designed a novel amphiphilic anti-cancer drug which can bind rapidly to endogenous albumin as a drug carrier to target tumor residues at the local sites.

In this chapter, we conjugated the self-delivering amphiphilic DOX and demonstrated that amphiphilic DOX can bind to endogenous albumin after systemic injection as well as *ex vivo* ligand binding study. Due to the self-assembling and membrane insertion property of amphiphilic substance, the three-way equilibrium with their biological surroundings are discussed respectively. In the presence of albumin and cells, the micellar structure is disrupted by binding to albumin (albumin hitchhiking) or inserting on plasma membrane (membrane insertion). However, albumin does not facilitate the tumor uptake *in vitro*. But *in vivo* tumor model results suggested that amphiphilic DOX increase anti-tumor efficacy via prolonging in body half-life of parental doxorubicin and enhancing tumor specific accumulation. Altogether, the novel molecular and albumin-based

self-delivery conjugate also features several favorable advantages as a cancer therapeutic option: exogenous carrier-free and fully synthetic and molecularly defined structure which has advantages in manufacturability, security and in principle, could be readily translated to the clinic for cancer chemotherapy.

Chapter 3. Amphiphilic doxorubicin specifically targets cell mitochondria.

3.1 Introduction.

3.1.1 Targeting mitochondria for cancer therapy.

Mitochondria are special subcellular components that play a key role in mediation of essential cellular metabolism including lipid metabolism, adenosine triphosphate (ATP) production and apoptosis activation¹⁵³⁻¹⁵⁴. Furthermore, the mitochondria have been assigned to produce copious quantity of reactive oxygen species (ROS) leading to DNA deconstruction and genetic flexibility¹⁵⁵⁻¹⁵⁶. Growing evidences suggest mitochondrial biochemistry energy, signaling and biosynthesis are indispensable for tumorigenesis and progression¹⁵⁴. Thus, mitochondria have been an emerging and attractive target for anticancer agent. To explore the approach to targeting mitochondria of cancer cells, two levels of specific accumulation are required: drug accumulation in the tumor site after systemic administration, and then accumulation in the mitochondria when uptake into tumor cells¹⁵⁷. Attempt to achieve this multi-level targeting has included the use of nanocarriers by which a tumor-specific ligand and a mitochondria ligand are both conjugated. Thus, in cancer chemotherapy, a successful mitochondriotropic delivery requires multi-levels of targeting: it must achieve sufficient circulating time in blood for drug exposure, and must achieve tumor tissue- and tumor cell-specific accumulation followed by mitochondria-specific accumulation.^{35, 158-164}

There are multiple functionally different molecules that can interfere with mitochondrial function currently being tested or in clinical trial.¹⁶⁵ For example, due to the mitochondria membrane potential, delocalized lipophilic cations with positive

charge (DLCs) are efficiently accumulating within mitochondria driven by electrical force.¹⁶⁶⁻¹⁷² However, the intrinsic toxicities associated with DLCs have limited their applications in clinical development.¹⁷³⁻¹⁷⁴ Other approaches to target mitochondria via synthetic amino-acid-based transporters or mitochondria derived sequence (MTS)^{160, 175-177} are reported to exhibit specific mitochondrial accumulation^{1, 178-179}. Due to the considerable molecular size, poor water solubility and lack of stability^{159, 170}, small molecular compounds such as delocalized lipophilic components or mitochondria specific peptides fail to maintain drug retention above target level and, in some cases, non-specific accumulation in brain, heart, liver, and muscle.¹⁶⁶ Mitochondria-target ligand decorated drug carriers are demonstrated to offer many advantages compared with traditional small molecular drugs alone.^{144, 146-147, 163} Unfortunately, current nanocarriers are difficult to meet all the criteria for multi-level drug targeting and increase the risk of immune disorder resulting from complex formulation. Possible stability and toxicological issues including immunogenicity also greatly restrict the nanocarrier's clinical application in the current stage.

3.1.2 Multi-drug resistance (MDR) in cancer chemotherapy.

Chemotherapy is a powerful intervention that can prevent tumor regression and recurrence and, in some cases, completely cure cancer. This therapeutic method is often used as a single-agent therapy or combined with other cancer treatments. While chemotherapy might initially be effective, it is very common for patients to develop resistance to such agents. In fact, drug resistance has emerged as a major limitation which impedes chemotherapeutic agents against the therapeutic outcomes, causing tumor recurrence and treatment failure^{133, 152, 180}.

In the past four decades, various mechanisms have been demonstrated from drug sensitive cancers cells evolving to resistant cells. Some of these theories, such as impairment of delivering anticancer drugs to tumor cells, and genetic and epigenetic alterations of cancer cells that hinder the drug sensitivity¹⁵⁰⁻¹⁵¹. In order to solve such problems, combining multiple anticancer therapeutic agents with different transportation and lethal mechanisms or various cellular targets promises the remedial effective and high cure rates. Unfortunately, cells genetically expressing evolutionary exchanges in functions confer simultaneous resistance to many different structurally and functionally distinct drugs. This phenomenon, known as multidrug resistance (MDR), is shown after generating drug resistance experimental model *in vitro*. When treated with a single drug, cells would finally express cross-resistance to other unrelated drugs. Resistance to natural hydrophobic components, sometimes known as classical MDR, generally results from over expression of adenosine triphosphate (ATP)-dependent efflux pumps¹⁸¹⁻¹⁸³.

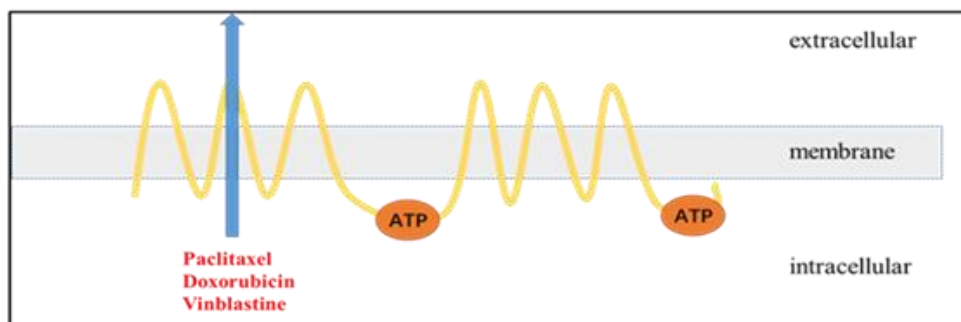


Figure 3.2.1.1. Structures and anticancer drugs as substrates of P-glycoprotein (P-gp) transporter.⁴³⁻⁴⁵

P-glycoprotein (P-gp) confers resistance against a wide variety hydrophobic natural compounds that are either neutral or positively charged drugs including paclitaxel¹⁸⁴, vinblastine¹⁸⁵ and doxorubicin ¹⁸⁶. As the firstly detected cellular surface phosphoglycoprotein involving in MRD, P-gp is composed of 12 transmembrane α -helices (in two membrane-spanning domains) and two ATP-binding sites (**Figure 3.2.1.1**)¹⁸⁷. Stimulating by the binding of substrates, a conformational change happens that the substrates are released either the outer leaflet of the membrane (from which it can diffuse into the medium) or the extracellular space¹⁸⁶. And the second ATP site is supposed to recover so that it can continuing binding and hydrolysis activity. ¹⁸⁸

3.2 Method.

3.2.1 Materials, cells and animals.

Doxorubicin hydrochloride salt was obtained from LC laboratories (Woburn, MA). 1,2-Distearoyl-sn-Glycero-3-Phosphoethanolamine (DSPE) conjugated polyethylene glycol (PEG 2000) with active succinimidyl ester (DSPE-PEG-NHS) was purchased from Biochempeg scientific Inc (Watertown, MA). Cholesterol polyethylene glycol (PEG 2000) NHS and DSPE-PEG₂₀₀₀-NHNH₂ were ordered from Nanocs Inc (New York, NY). Triethylamine (TEA), N-hydroxysuccinimide (NHS), bovine serum albumin (BSA), filipin (FLP), ethyl-isopropyl amiloride (EIPA) and sucrose were purchased from Sigma-Aldrich (St Louis, MO). Alexa Fluor 660 NHS Ester (Succinimidyl Ester), NHS-Fluorescein (5/6-carboxyfluorescein succinimidyl ester), alamarBlue reagent, MitoTracker green, Mitochondria-RFP and MITO-ID were obtained from Thermo Fisher Scientific (Waltham, MA). Cells were cultured in complete medium (RPMI1640, 10% fetal bovine serum (Greiner Bio-one), 100 U/mL penicillin G sodium and 100 µg/mL streptomycin (Pen/Strep). Mouse skin melanoma (B16F10) cell line, mouse mammary carcinoma (4T1) cell line and EG7 cell line were ordered from ATCC. Human ovarian carcinoma (OVCAR-8) cell line and its adriamycin resistant derivative (NCI/ADR-RES) cell lines were obtained from National Institutes of Health.

3.2.2 Design and conjugation of amphiphilic doxorubicin.

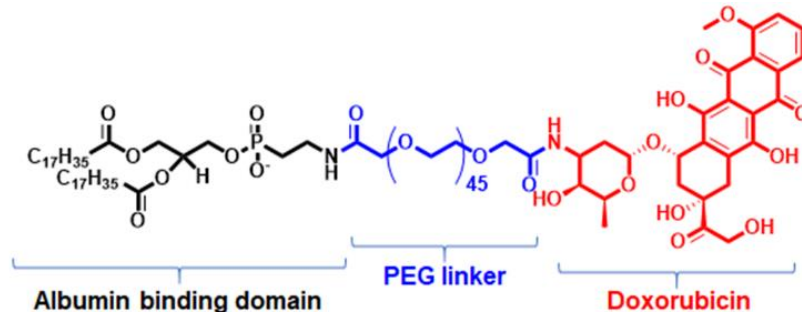


Figure 3.2.3.1 Molecular structure of amphiphilic doxorubicin (amph- DOX).⁵⁸

The molecularly defined drug conjugate can be divided into three distinct segments (**Figure 3.2.3.1**): a diacyl lipid tail as albumin-binding and membrane-anchor domain, a central repeat block containing ethylene glycol (EG) units and DOX conjugated to the end of EG. Briefly, doxorubicin hydrochloride (DOX, 5 mg, 8.6 mmol) and DSPE-PEG₂₀₀₀-NHS (38 mg, 5.7 mmol) were dissolved in dimethyl sulfoxide (DMSO) and activated with triethylamine (TEA) at room temperature for 24 hours (**Figure 2.3.1.1A**)⁵⁸. After the reaction, the solution was dried, re-dissolved in PBS and analyzed by reverse phase HPLC. Amphiphilic DOX was purified by a C4 reverse-phase HPLC column (Thermo Scientific, 250 x 4.6 mm, 5 μm). 200 μL samples were injected and separation using a solvent gradient (**Table 2.2.2.1**)⁵⁸ with methanol and triethylammonium acetate (TEAA, 0.1 M pH = 7.4) buffer. The elution and concentration of DSPE-PEG₂₀₀₀-DOX was monitored by measurement of the UV absorbance at 260 nm and 485 nm. The chromatography spectra of amphiphilic DOX was eluted at 13 min and product was collected from 12 min to 14 min. After that resulting component was dried and re-dissolved in DMSO. ¹H-NMR (Varian, 400 MHz) and Mass spectrum (Bruker Daltonics MALDI

Ultraflex Extreme TOF/TOF) were used to characterize DSPE-PEG₂₀₀₀-DOX (amphiphilic DOX).

3.2.3 Synthesis of pH sensitive amphiphilic doxorubicin.

Doxorubicin hydrochloride (DOX, 5 mg, 8.6 mmol) and DSPE-PEG₂₀₀₀-NHNH₂ (38 mg, molar ratio of DSPE-PEG₂₀₀₀-NHNH₂: DOX = 1.5: 1) were dissolved in dimethyl sulfoxide (DMSO) and activated with triethylamine (TEA) at room temperature for 24 hours (**Figure 3.3.4.2A**)⁵⁸. After the reaction, the solution was dried, re-dissolved in PBS and analyzed by reverse phase HPLC. pH sensitive amphiphilic doxorubicin (DSPE-PEG₂₀₀₀-NHNH-DOX) was purified by a C4 reverse-phase HPLC column (Thermo Scientific, 250 x 4.6 mm, 5 μm). 200 μL samples were injected and separation using a solvent gradient (**Table 2.2.2.1**)⁵⁸ with methanol and triethylammonium acetate (TEAA, 0.1 M pH = 7.4) buffer. The elution and concentration of DSPE-PEG₂₀₀₀-NHNH-DOX was monitored by measurement of the UV absorbance at 260 nm and 485 nm.

3.2.4 Preparation of doxorubicin loaded DSPE-PEG₂₀₀₀ micelles.

Doxorubicin were loaded into DSPE-PEG₂₀₀₀ micelles by the single solvent film casting method. Briefly, doxorubicin hydrochloride (2 mg, 3.5 mmol) was pre-treated with triethylamine (TEA, 7 mg, 7 mmol) at a 1:2 molar ratio in methanol for 1 h at RT, subsequently mixed with 20 mg DSPE-PEG₂₀₀₀ in chloroform. Solvent in mixture was air dried at room temperature for overnight, resulting a thin film. The dried film was then mixed with 1 mL D.I water and stirring at 60 °C for 20 min. Free un-entrapped doxorubicin existing in the supernatant were separated by centrifugation (5500 rpm, 15 min).

3.2.5 *In vitro* cytotoxicity.

The *in vitro* anti-tumor activities of the unmodified DOX and the amphiphilic DOX against B16F10, 4T1, EG7, OVCAR-8 and NCI/ADR-RES cells were assigned using AlamarBlue assay. B16F10, EG7 and 4T1 cells at the density of 5×10^4 cells per well and OVCAR-8 and NCI/ADR-RES cells at the density of 1×10^5 cells per well were seeded in 96-wells plates for overnight at 37 °C. Cells were replaced with cell culture medium with DOX or amphiphilic DOX at serial doxorubicin concentrations ranging from 0.05 to 10 μ M for 24 or 48 h, subsequently with the addition of 10% (v/v) AlamarBlue reagent for another 1 h. Cells treated with DMSO in complete medium were used as the no treatment controls. Finally, the UV/vis absorbance of the whole cell residues was measured at 570 nm with 600 nm as a reference by a microplate reader (Thermo Scientific). The cell visibility was calculated as the value of absorbance from treated cells normalized to none treated cells. Dose-response curve was interpolated using Prism Graphpad software (San Diego, CA) to determine the half maximal inhibitory concentration (IC_{50}). All the experiments were carried out in triplicate.

3.2.6 Cellular uptake studies.

The cellular uptake of unmodified DOX and amphiphilic DOX were quantified in B16F10 cells by flow cytometry (Applied Biosystems). Cells with a density of 1×10^6 cells per well were seeded to 96-wells plate for overnight. The cell medium was removed and replaced with 1.0 μ M DOX and amphiphilic DOX in cell culture medium for different time periods at 37 °C. Following washed three

times with PBS, cells were harvested in FACS and analyzed by Attune acoustic focusing cytometer. Each assay was performed in triplicate.

3.2.7 Subcellular tracking study.

To track the intracellular location after internalization of unmodified DOX and amphiphilic DOX, B16F10, NCI/ADR-RES as well as 4T1 cells at the density of 1×10^4 cells per well were seeded on a coverslip in 6-wells plates at 37 °C for 24 h to achieve adhesion. To visualize mitochondria by MitoTracker Green FM, cells were treated with 1 μ M unmodified DOX or amphiphilic DOX at 37 °C for 4 h. After treatment, the cells were washed three times with PBS, following incubating 500 nM with MitoTracker Green FM (Invitrogen) for 15 min and 200 nM DAPI (Invitrogen) for another 15min. For CellLight Mitochondria-RFP BacMam 2.0 (Invitrogen) labeling mitochondria, cells were transfected with 10 μ L CellLight reagent in whole cell culture medium at 37 °C for 24 h. Then cells treated with 1 μ M unmodified DOX or amphiphilic DOX were fixed with 3% paraformaldehyde (PFA) and cocultured with 200 nM DAPI (Invitrogen) for 10 min. Slides samples were washed with fresh PBS before imaging. Confocal microscopy images were obtained by Zeiss microscope system (LSM 780) with a 63 \times oil-immersion objective. Parameters upon exciting/emission wavelength were set as below (**Table 3.2.7.1**)⁵⁸: doxorubicin (excitation 488 nm, emission 560 nm bandpass filter), MitoTracker Green (excitation 488 nm, emission 515 nm bandpass filter), CellLight Mitochondria-RFP (excitation 561 nm, emission 585 nm bandpass filter).

Table 3.2.7.1 Confocal microscopy setting for mitochondria tracking. ⁵⁸

Reagents	Excitation wavelength	Emission bandpass filter
Doxorubicin	488nm	560nm
Amphiphilic DOX	488nm	560nm
MitoTracker Green	488nm	515nm
CellLight Mitochondria-RFP	561nm	585nm

3.2.8 *In vitro* colocalization analysis.

The level of colocalization was quantified by ImageJ (NIH, Bethesda, Maryland) with Coloc2 plugin ¹⁸⁹. The level of colocalization between unmodified DOX or amphiphilic DOX was evaluated on the account of the red to green signal intensities and that with cell nuclei were based on red to blue signal intensities. Pearson's ¹⁹⁰ and Manders' (M1/M2) coefficients were calculated from an specified cellular area of the whole view in each of the three independent experiments (total 12 fields).

3.2.9 Mitochondria and nuclei isolation.

1×10^8 per well of the B16F10 Cells were seeded in 15 mL of cell culture medium in 100-mm diameter tissue culture dishes and allowed to grow overnight. 10 μ M unmodified DOX and amphiphilic DOX were added to cells and incubated for different time periods. Following manufacturer's instructions. Intracellular compartments from drug treated or untreated cells were isolated using a mitochondria isolation kit (Thermo Fisher Scientific, Waltham, MA) and a nuclei isolation kit (Sigma- Aldrich, St. Louis, Missouri), respectively. The percent of unmodified DOX and amphiphilic DOX existing in each component were quantified

by measuring fluorescence intensity from doxorubicin after solvent extraction normalized with 10 μ M standard samples. All the experiments were carried out in triplicate.

3.2.10 Measurement of reactive oxygen species (ROS) generation.

B16F10 cells (1×10^6 cells/well) were pre-cultured in 24-wells plates for overnight. Cells were then incubated with unmodified DOX and amphiphilic DOX at a final concentration of either 1.0, 5.0 or 10.0 μ M for four hours. After treatment, cells were resuspended in PBS and incubated with 10 μ M 2',7'-dichlorodihydrofluorescein diacetate (H2DCFDA), a ROS indicator, for 30 min at 37 °C. Finally, the cells were washed and analyzed by flow cytometry (Applied Biosystems). No treatment group was used as a negative control for the quantifications of mitochondrial ROS production.

For visualizing intracellular ROS generation, 1×10^4 cells were seeded on square coverslips in 6-wells plates and treated with 10.0 μ M unmodified DOX and amphiphilic DOX for 4 h. After drug treatment, cells were resuspended in PBS and incubated with 10 μ M 2',7'-dichlorodihydrofluorescein diacetate (H2DCFDA), a ROS indicator, for 30 min at 37°C. Finally, cells were stained with 500 nM MitoTracker Green (Invitrogen) for 15 min and 200 nM DAPI (Invitrogen) with another 15min. Images were captured by Zeiss microscope system (LSM 780) with a 63 \times oil-immersion objective.

3.2.11 Tumor model and confocal microscopy images of tumor tissue.

B16F10 (5.0×10^5 cells in 100 μ L PBS) were subcutaneously inoculated into the left flank of 5-6-weeks C57BL/6 mice. When the tumor volumes reached

30 mm³ (on day 5), mice were divided into three treatment groups (n = 8). The tumor-bearing mice were intravenously injected with either 5 mg/kg doxorubicin hydrochloride, amphiphilic DOX or PBS every 72 h (on days 5, 8, and 11) in total three times. Tumor samples were isolated on the last day of experiment and fixed for 48h in formaldehyde fixation buffer. Each tissue was merged in optimal cutting temperature compound, freeze at -80 °C in the dark and slice into 10 µm-thickness tissue sections using a cryostat (Leica CM3050 S). The fixed tissue slides were incubated with 100 µL MITO-ID Red (Enzo life sciences) reagent for 30 min and 200 nM DAPI for additional 15 min.

3.2.12 Statistical analysis.

Statistical analysis the mean values of two groups were performed using unpaired Student's t tests. The statistical difference between groups were determined using a one-way analysis of variance (ANOVA) with Bonferroni post-test. All the values were expressed as means ± standard error of mean. GraphPad Prism (San Diego, CA) software was used for all the statistical analyses. ***p < 0.001, **p < 0.01, *p < 0.05. NS, not significant.

3.3 Results and discussions.

3.3.1 Amphiphilic modification increases DOX-induced antitumor effect in multiple murine cell lines.

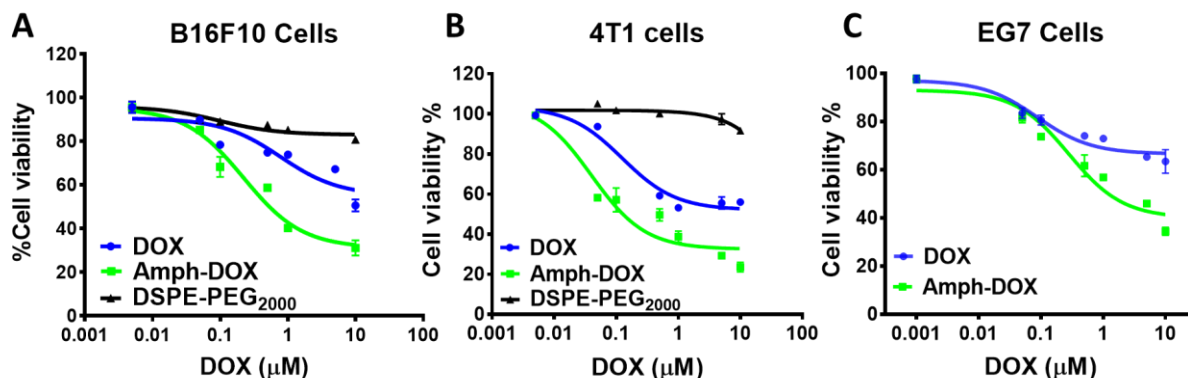


Figure 3.3.1.1 Amphiphilic DOX induced cytotoxicity in murine cell lines.⁵⁸ (A-C) *In vitro* cell viability of B16F10 (A), 4T1 (B), or EG7 (C) cells against unmodified DOX and amphiphilic DOX for 24 h after exposure.

To compare the impact of amphiphilic modification on the DOX induced antiproliferation efficacy, the cytotoxicity of several murine cancer cells, including murine melanoma B16F10, murine mammary carcinoma 4T1 and the murine thymoma EG-7 cell lines were evaluated. Data interpolation and the half maximal inhibitory concentration (IC₅₀) were calculated by Prism GraphPad (**Table 3.3.1.1**)⁵⁸. Exposure of cells to amphiphilic DOX caused a dose-dependent viability, with an IC₅₀ value of 0.2299 μM in B16F10 cells, versus 0.6152 μM in cells cultured with unmodified DOX (**Figure 3.3.1.1A**)⁵⁸. Similarly, treatment with amphiphilic DOX reduced the IC₅₀ values in 4T1 cells (0.05458 μM versus 0.1500 μM with free DOX) and the EG7 cells (0.08746 μM versus 0.2805 μM with unmodified DOX) (**Figure 3.3.1.1B, C**)⁵⁸. As the negative controls, DSPE-PEG₂₀₀₀-NHS or its hydrolyzed derivative exhibited negligible toxicity, suggesting amphiphilic DOX

induce its cytotoxic effects in a DOX-dependent manner instead of amphiphilic polymer.

Table 3.3.1.1 Amphiphilic modification increases DOX-induced antitumor effect in multiple murine cell lines.⁵⁸

Cell line	DOX IC ₅₀	Amph-DOX IC ₅₀
B16F10	0.6152 μ M	0.2299 μ M
4T1	0.1500 μ M	0.05458 μ M
EG7	0.2805 μ M	0.08746 μ M

3.3.2 Amphiphilic modification overcomes drug resistance in breast adenocarcinoma cells.

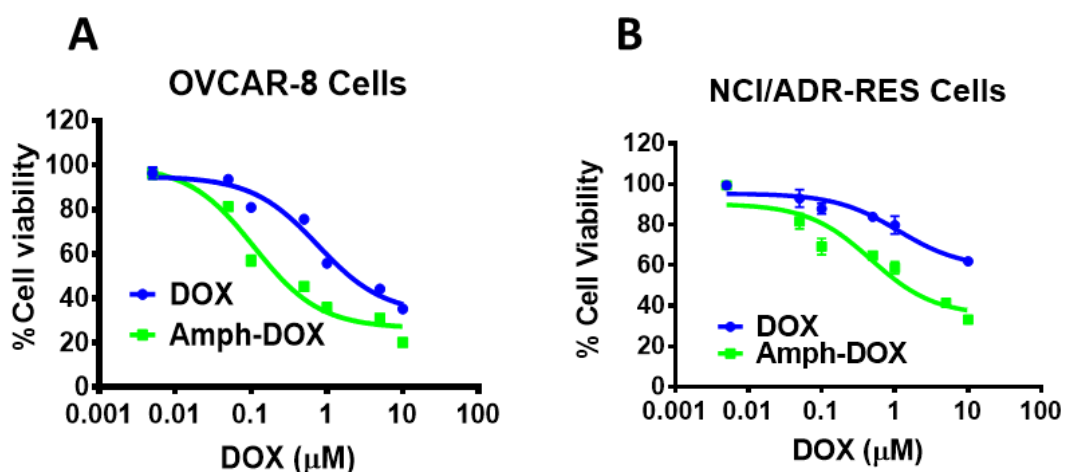


Figure 3.3.2.1 Amphiphilic DOX overcame drug resistance in breast adenocarcinoma cells.⁵⁸ (A and B) *In vitro* DOX sensitive OVCAR-8 (A) and drug resistance NCI/ADR-RES cells against unmodified DOX and amphiphilic DOX for 48 h exposure.

Chemotherapeutic agents such as anthracyclines have been shown to induce cell apoptosis by a wide variety of mechanisms and have been a major treatment modality for cancer, especially metastatic cancers. However, intrinsic or evolutionary drug resistance greatly limited the development of anthracyclines (e.g. DOX) in the clinical management of cancers. Overexpress of the drug pump

receptors such as P-glycoprotein (P-gp) receptors on the cell membrane is the major drug efflux pumps which is often associated with drug resistance. Encouraged by the favorable tumor antiproliferation property of amphiphilic DOX, we next evaluated their tumor killing efficiency in human cancer, including P-gp overexpressed drug resistance cell line. Exposure with amphiphilic DOX reduced the IC₅₀ values (**Table 3.3.2.1**)⁵⁸ in both DOX sensitive OVCAR-8 cells (0.1094 μM versus 1.12 μM with unmodified DOX) (**Figure 3.3.2.1A**)⁵⁸ and the anthracyclines resistant NCI/ADR-RES cells (0.4725 μM versus 0.7565 μM with unmodified DOX) (**Figure 3.3.2.1B**)⁵⁸. These results gave evidence that amphiphilic DOX was considerably more potent than free DOX in both drug sensitive and drug-resistant cell lines.

Table 3.3.2.1 Amphiphilic DOX overcame drug resistance in breast adenocarcinoma cells.⁵⁸

Cell line	DOX IC ₅₀	Amph-DOX IC ₅₀
OVCAR-8	0.1094 μM	1.12 μM
NCI/ADR-RES	0.7565 μM	0.4725 μM

3.3.3 Amphiphilic DOX accumulates in mitochondrial area *in vitro*.

To track the localization of amphiphilic DOX related to its parental compound after cell uptake, B16F10 melanoma tumor cells were incubated with DOX or amphiphilic DOX in the whole cell culture medium containing 10% FBS. The internalization was analyzed by confocal laser scanning microscopy (CLSM). As previously reported, unmodified DOX exhibited strong affinity to cell nuclei showing the colocalization between red (DOX) and blue (nuclei)¹⁹¹ (**Figure 3.3.3.1**)

⁵⁸. In contrast, amphiphilic DOX fluorescence exists as the light red dots and was mainly confined around the nuclear (**Figure 3.3.3.1**)⁵⁸. Through colocalization with a mitochondria-specific dye (green, MitoTracker Green FM), it was demonstrated that amphiphilic DOX was aggregating in mitochondrial area. (**Figure 3.3.3.1**, upper two panels)⁵⁸. As in our previous observation, amphiphilic oligonucleotides were mainly delivered within the endo/lysosomal compartment, the mitochondria-selective accumulation of amphiphilic DOX was unexpected.

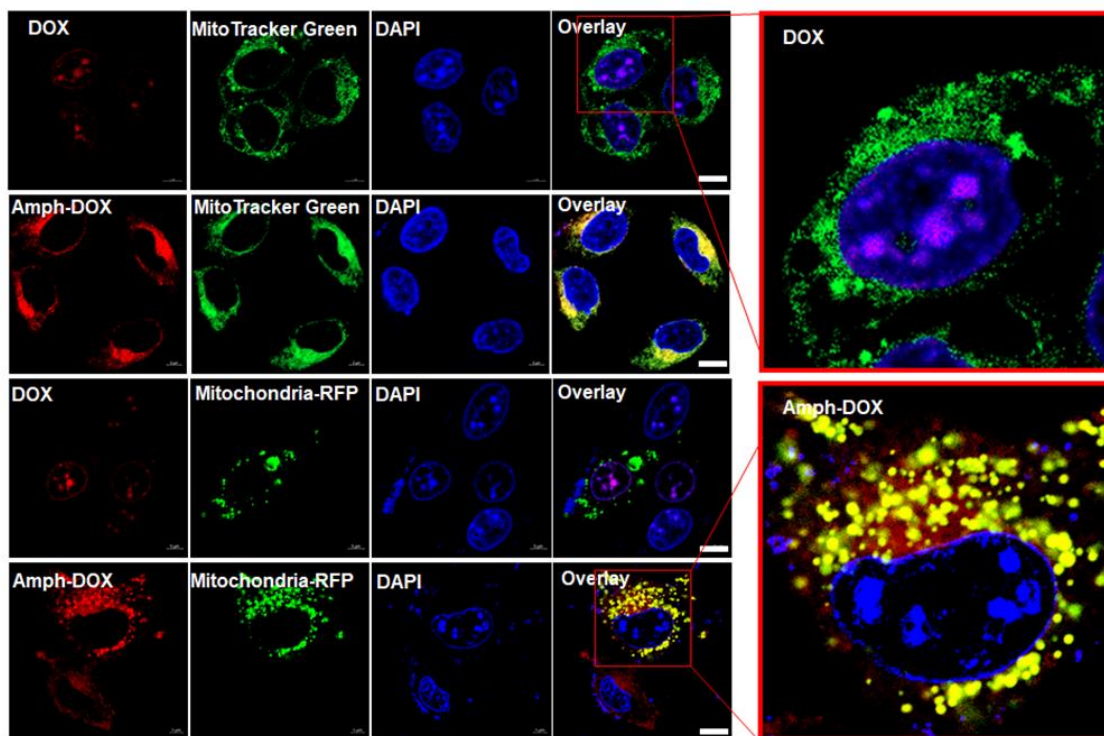


Figure 3.3.3.1 Amphiphilic DOX accumulated in B16F10 cellular mitochondrial area *in vitro*.⁵⁸ Subcellular tracking of unmodified DOX and amphiphilic DOX at the incubating concentration of 1 μ M in B16F10 cells. Cells treated with either free DOX (red, from DOX intrinsic fluorescence) or amphiphilic DOX were incubated with Mito-Tracker Green (green, upper two panels) or Mitochondria-RFP (green, lower two panels). Cell nuclei were tracking with DAPI (blue). Noting that some cells were not transfected in the Mitochondria-RFP treated group. Scale bar = 10 μ m.

Table 3.3.3.1. Pearson's Correlation Coefficients and Manders' coefficients.

58

	DOX		Amph-DOX	
	Ps	M1/M2	Ps	M1/M2
Mitochondria	-0.26	0.196/0.039	0.52	0.901/0.750
	-0.19	0.083/0.020	0.52	0.773/0.975
	-0.04	0.133/0.083	0.57	0.874/0.992
Nuclei	0.63	0.709/0.937	-0.06	0.463/0.014
	0.62	0.675/0.873	-0.01	0.517/0.004
	0.56	0.811/0.946	-0.06	0.897/0.331

To verify the mitochondria-specific accumulation, another transfection-based red fluorescent protein (RFP) was used to label the mitochondrial area (**Figure 3.3.3.1**, lower two panels). This reagent uses BackMam 2.0 technology and is effective on a wide range of mammalian cell lines. The transfection process was conducted according to manufacturer's instruction by adding CellLight reagent to cells for overnight. The cells were subsequently imaged. The transfection can be seen by the RFP fluorescence under confocal microscope. We also noticed that in our hands, not 100% of the cells were transfected (**Figure 3.3.3.1**, lower panel), which is typical for a lot of transfection reagents. This partial transfection is also a circumstantial evidence which rules out the possibility of fluorescence artifact of the images. Colocalization coefficients assigned by Coloc 2 algorithm revealed significant spatial overlapped between amphiphilic DOX with both mitochondria dyes in B16F10 cells (Ps and Manders' coefficients were shown in **Table 3.3.3.1**). For unmodified DOX, low coefficient values were obtained indicating the weak associations of the drug and the mitochondrial matrix (**Table 3.3.3.1**).

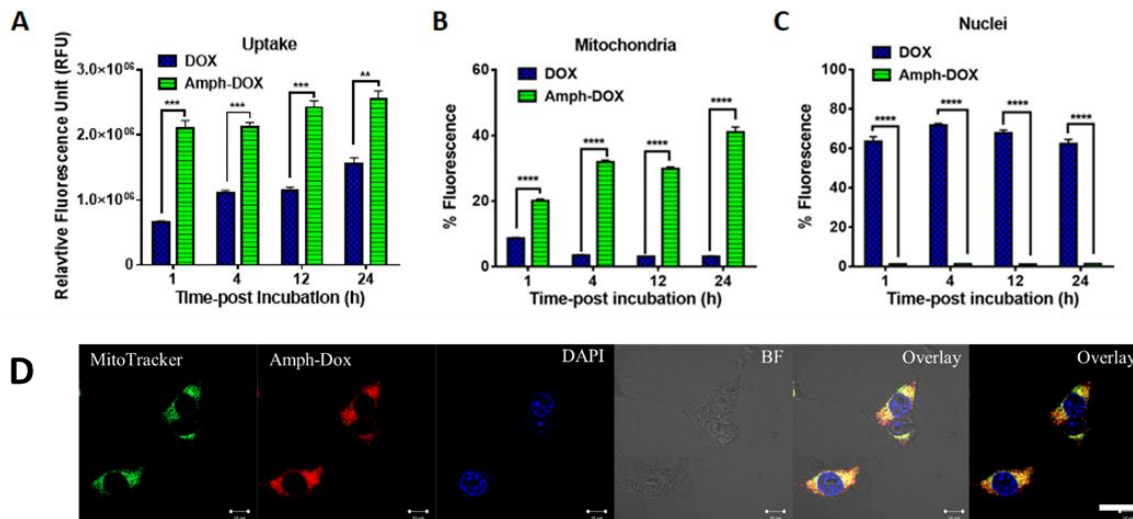


Figure 3.3.3.2 Amphiphilic DOX selectively accumulated in both B16F10 and 4T1 cellular mitochondria.⁵⁸ (A-C) Pharmacokinetic quantification of relative drug tracking total cells (A), mitochondria (B) and (C) nuclei of DOX or amphiphilic DOX treated B16F10 cells. B16F10 cells at the density of 1×10^8 per well were incubated with $10 \mu\text{M}$ DOX or amphiphilic DOX for 1, 4, 12 or 24 h. Mitochondria and nuclei compartments were isolated by commercial isolating kits. The fluorescent intensity of each drugs was quantified by fluorescence spectrophotometer after extraction. (D) CLSM images of amphiphilic DOX (concentration of $1 \mu\text{M}$) treated 4T1 cells showing the cellular uptake and intracellular distribution of free doxorubicin or amphiphilic DOX at four hours. Mitochondria tracking of 4T1 cells was employed MitoTracker Green reagent. Scale bar = $10 \mu\text{m}$.

Because DOX has intricate features intercalating to DNA, the drug concentration in subcellular compartments could directly reflect the different destination upon free DOX and amphiphilic DOX. To verify the observations on uptake and distribution, the mitochondria and the nuclei the drug treated B16F10 cells were extracted and drug concentration were quantified by fluorescence spectrophotometer. Similar to flow cytometry results (**Figure 2.3.5.1A**)⁵⁸, cells treated with free DOX reached approximately 50% (30% to 70%) of the uptake from amphiphilic DOX-treated cells at different time points (**Figure 3.3.3.2A**)⁵⁸. Consistent with CLSM colocalization analysis (**Figure 3.3.3.1**)⁵⁸, unmodified DOX

had a high affinity to nuclei, accounting for 72% of the fluorescence localized within the cells in 24 h (**Figure 3.3.3.2 B and C**)⁵⁸. By comparison, approximately 45% of the amphiphilic DOX was tracked in isolated mitochondria after 24h incubation (**Figure 3.3.3.2B and C**)⁵⁸. Although compared with free DOX, a fraction of amphiphilic DOX might be lost during organelle isolation, other portion of them were still under lipid sorting process or residue in cytosol. To investigate whether the mitochondria accumulation of amphiphilic DOX was limited to B16F10 cell, we tracked the drug location on mouse breast tumor 4T1 cells. Uniform mitochondrial accumulation observed in 4T1 cells (**Figure 3.3.3.2D**)⁵⁸ clearly demonstrated the selective mitochondria accumulation in murine tumor cells after treatment with amphiphilic DOX.

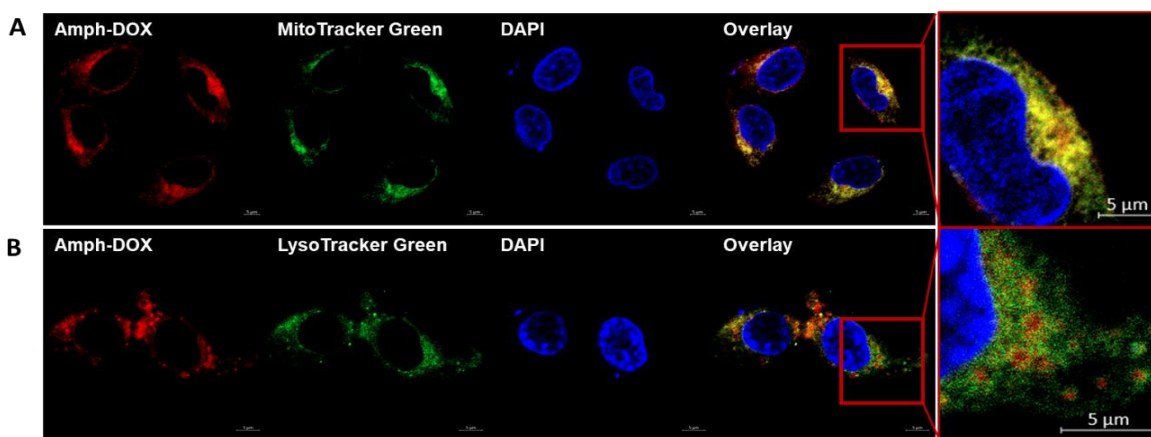


Figure 3.3.3.3. Confocal microscopy images show colocalization of amphiphilic DOX with mitochondria or lysosomes.⁵⁸ (A and B) B16F10 cells were treated with 1 µM amphiphilic DOX and tracked mitochondria by MitoTracker Green (A) or lysosome LysoTracker Green (B). Cell nuclei were stained with DAPI (blue). Scale bar = 5 µm.

In addition, amphiphilic DOX employs multiple uptake mechanisms in typical cell culture conditions which has been discussed in Chapter 2.3.5. Engulfing molecules through endocytosis mechanisms are the main pathway for. Fusion of

the lipid-based amphiphiles with the endosomal membrane is generally accepted as a possible lipid sorting process to release lipoplex into the cytoplasm. To investigate the role of lysosome/endosome in lipid sorting process as well as intracellular distribution of lipid conjugated DOX related, colocalization between amphiphilic DOX with either mitochondria or lysosomes were observed using confocal laser scanning microscopy (CLSM). Amphiphilic DOX was synthesized through DOX covalently conjugated with DSPE-PEG₂₀₀₀ which was not able to release under intracellular environment. It was hypothesized that after lipid sorting process, amphiphilic DOX was released and exposed in cytosol. Thus, we colocalized amphiphilic DOX with subcellular organelles mitochondria (**Figure 3.3.3.3.A**, green) ⁵⁸ and lysosome (**Figure 3.3.3.3.B**, green) ⁵⁸. Colocalization coefficients assigned by Coloc 2 algorithm revealed significant spatial overlap between amphiphilic DOX with both mitochondria dyes in B16F10 cells (Pearson coefficient, 0.57; Manders coefficient, 0.874/0.992), whereas colocalization of the amphiphilic DOX with lysosome (Pearson coefficient, 0.09; Manders coefficient, 0.415/0.241) showed little correlation.

3.3.4 Discussion of potential mitochondrial targeting mechanism.

Lipids spread all over the whole cell, trafficking from the cell surface to/ within the various organelle membrane where lipid metabolism happens. The increasing evidence demonstrated that internalized lipid-based amphiphiles were distributed to various subcellular organelles in a lipid-specific manner. ¹⁹²⁻¹⁹³. Structure of lipid-based amphiphiles is generally believed to govern the intracellular sorting pathways and thus determines the distribution and destination

of these components. However, few researches focused on the mitochondrial targeting property of lipid-based amphiphiles. Since the same negative charge of amphiphilic DOX (**Figure 2.3.2.2**)⁵⁸ with mitochondrial transmembrane potentials¹⁹⁴, it is unlikely amphiphilic DOX concentrating in mitochondria is driven by electrostatic force. As clarified in chapter 2 (**Figure 2.3.4.2**)⁵⁸, we assumed that amphiphilic DOX exists three status when incubating with cell and could possess multiple uptake mechanism.

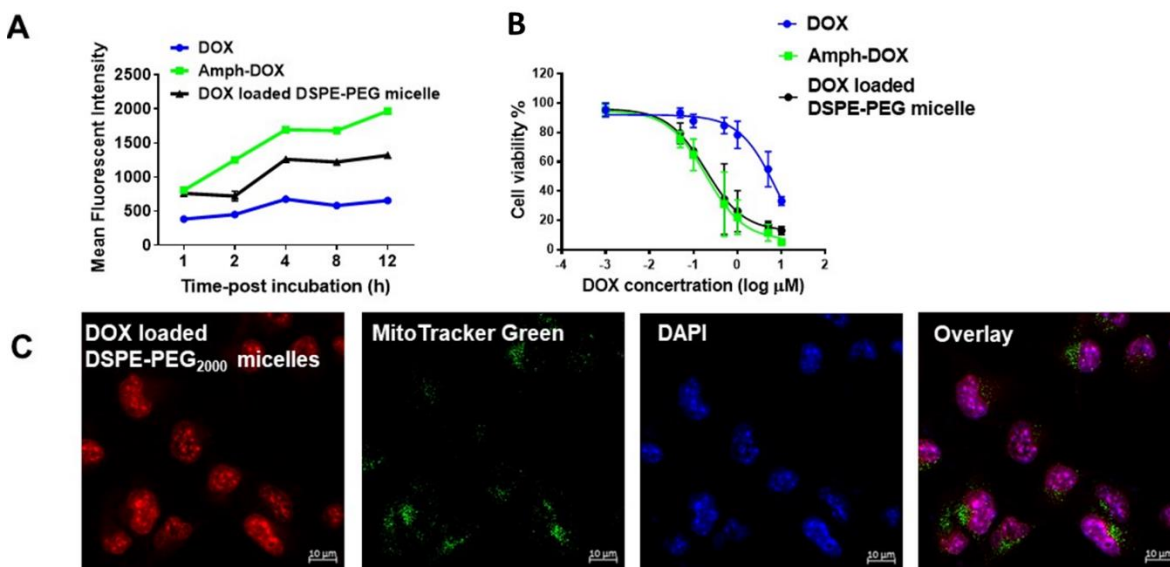


Figure 3.3.4.1 *In vitro* antitumor activity and subcellular location of DOX encapsulated DSPE-PEG₂₀₀₀ micelles.⁵⁸ (A-C) Cells internalization of DOX loaded DSPE-PEG₂₀₀₀ micelles was examined by flow cytometry (A and B) and subcellular location at 4h were analyzed by confocal microscope (C). B16F10 cells (5×10^5 cells per well) were seeded to 96-well plate at 37 °C for overnight. Cells were incubated with DOX loaded DSPE-PEG₂₀₀₀ micelles (DOX concentration of 1.0 μM) at for different time periods before flow cytometry analysis. (C) B16F10 cells at the density of 1×10^5 cells per well were seeded to 6-well plate for overnight. Cells were treated with DOX loaded DSPE-PEG₂₀₀₀ micelles and MitoTracker Green for mitochondria tracking, whereas cell nuclei were stained with DAPI (blue). Scale bar = 10 μm.

To explore the potential explanation of mitochondria target, we compared and discussed the three conditions individually. Polymeric micelles are reported to

show a rapid internalization in most of tumor cells and disassemble and release their content into cell cytosol once internalized. We firstly analyzed the intracellular accumulation of amphiphilic DOX and DOX loaded DSPE-PEG₂₀₀₀ micelles. . DOX loaded DSPE-PEG₂₀₀₀ micelles was synthesized by the film casting method. Briefly, doxorubicin hydrochloride (2 mg, 3.5 mmol) in methanol was pre-treated with triethylamine (TEA, 7 mg, 7 mmol) at a 1:2 molar ratio for one hour at RT, then mixed with 20 mg DSPE-PEG₂₀₀₀ in chloroform. The DOX loaded DSPE-PEG₂₀₀₀ micelle was obtained under a stream of air form a thin film and hydrated with D.I water. Consistent with previous reports, DOX entrapped in DSPE-PEG₂₀₀₀ micelles showed a significantly improved cytotoxicity (**Figure 3.3.4.1B**)⁵⁸, equivalent to that of amphiphilic DOX *in vitro*. The enhanced cytotoxicity correlated with enhanced uptake (**Figure 3.3.4.1A**)⁵⁸. However, after 4h incubation, the capsulated DOX were observed to be primarily accumulated in the nuclei which indicates the release of unmodified DOX(**Figure 3.3.4.1C**)⁵⁸. These results proved that the intracellular trafficking of amphiphilic DOX is not the same as DOX entrapped in polymeric micelles.

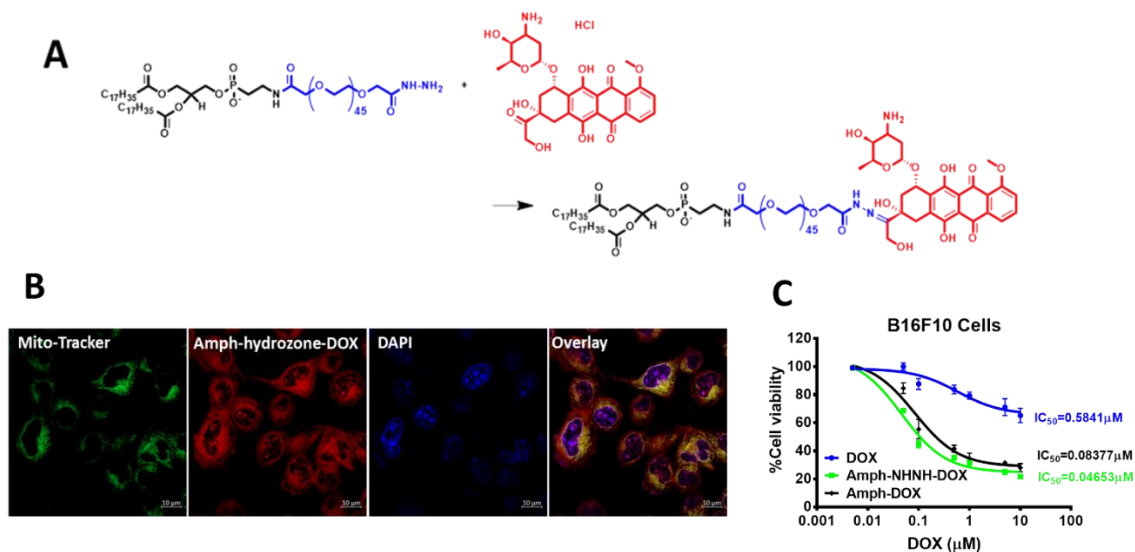


Figure 3.3.4.2 Design of pH sensitive amphiphilic DOX, and its intracellular distribution and cytotoxicity.⁵⁸ (A) Amphiphilic NHNH-DOX was synthesized by conjugating of doxorubicin hydrochloride (DOX) to DSPE-PEG₂₀₀₀-NHNH₂. (B) B16F10 cells at the density of 1×10^5 cells per well were seeded to a 6-wells plate for overnight. Cells were treated with DOX loaded DSPE-PEG₂₀₀₀ micelles and MitoTracker Green for mitochondria tracking whereas cell nuclei(blue) were stained with DAPI. Scale bar = 10 μm . (C) *In vitro* cytotoxicity of free DOX, amphiphilic DOX and amphiphilic NHNH-DOX against B16F10 cells 24 h. B16F10 cells at the density of 5×10^5 were incubated with either amphiphilic DOX or free doxorubicin with varying concentrations for 24h. Cell proliferation was evaluated by AlamarBlue assay.

The sorting of lipids is a process of central importance in cellular transportation pathways. Intracellular rearrangement of lipid has been proposed to be mediated by a physical mechanism based on the coordinating between intracellular membranal composition and cell membrane transport curvatures. To address whether the lipid sorting of diacyl lipid PEG transported DOX to mitochondria, we constructed the same amphiphilic DOX conjugation but through a pH sensitive hydrazone linkage (amphiphilic NHNH-DOX) (**Figure 3.3.4.2A**)⁵⁸. As the hydrazone linkage between the PEG units and drug (DOX) is liable to hydrolysis in low pH environment, the releasing of DOX happens in the acidic

condition of the endosomal/lysosomal intracellular compartments after the amphiphilic NHHH -DOX internalization, thereby providing a clear demonstration of the act of amphiphilic lipid motif and free doxorubicin drug (**Figure 3.3.4.2B**)⁵⁸. In this case, DOX fluorescence in nuclei as well as in mitochondria was observed. The mitochondria accumulation of this pH-sensitive amphiphilic DOX might be the incomplete cleavage of hydrazone bond under endosomal pH. Another possibility is that cargos transported via caveolae-dependent route are delivered to caveosomes instead of lysosomes. Along this route, the pH is maintained neutral and no degradative substrate is appeared. Nevertheless, the partial nuclear accumulation of amphiphilic hydrazone-DOX strongly suggest that DOX is not released in our original amphiphilic DOX (non-cleavable) design. To compare the anti-proliferation efficacy of DOX from amphiphilic DOX is released with not releasable, cell was treated with either amphiphilic DOX (amphiphilic DOX) or pH-sensitive amphiphilic DOX(amphiphilic NHHH-DOX). After 24 hours, we observed slightly enhanced cytotoxicity, indicating in our case, release free DOX promoted the cytotoxic efficacy (**Figure 3.3.4.2C**)⁵⁸. However, amphiphilic DOX selectively accumulating in mitochondria is still unique and superior in novelty and functions.

3.3.5 Albumin is not engaged as a participant of the intracellular sorting of amphiphilic DOX.

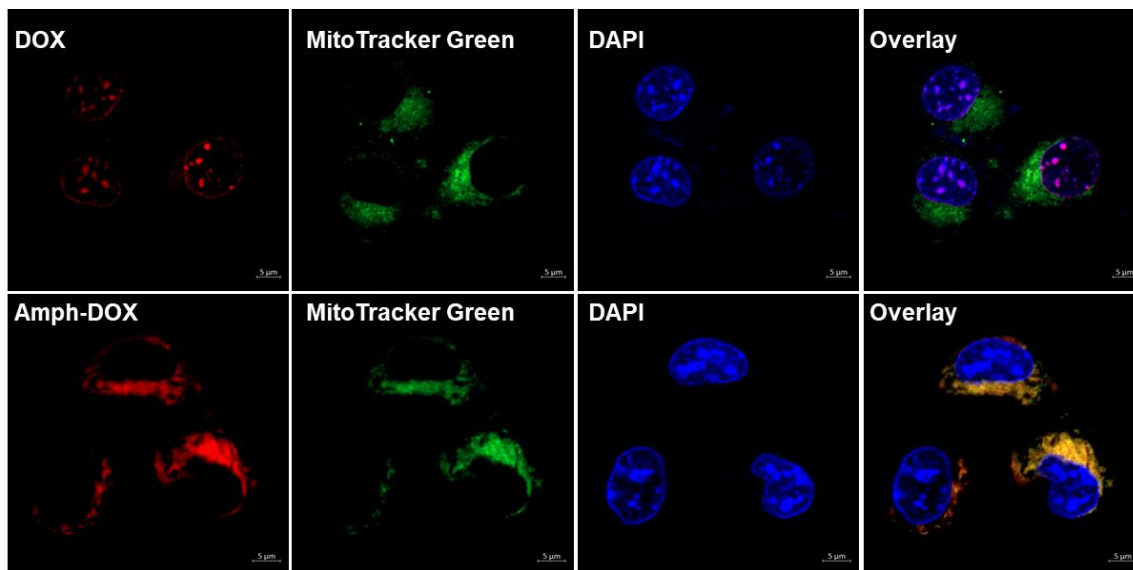


Figure 3.3.5.1 Influence of serum on amphiphilic DOX uptake and distribution.
⁵⁸ B16F10 cells at the density of 1×10^5 cells per well were seeded to a 6-wells plate at 37 °C. After overnight adhesion, cell medium was removed and replaced with 0% FBS and 10% FBS medium with DOX and amphiphilic DOX at a final concentration of 1.0 μM for 4 hours. Cells were treated with free DOX, and amphiphilic DOX. Cell nuclei and mitochondria were tracked by DAPI (blue) and MitoTracker, respectively. Scale bar = 5 μm .⁵⁸

Albumin is reported to be engulfed by cells via endocytosis pathway. Degraded in lysosomal compartment of cells is the termination of the fate of albumin. The exact mechanism is few discussed, since albumin is such a ubiquitous molecule that any experimental setting trying to mimic the mechanism of its uptake pathway is supposed to be very difficult. To explore the effect of albumin on albumin containing on intracellular accumulation and distribution *in vitro*, the B16F10 cells uptake of free DOX and amphiphilic DOX in complete cell growth medium (10% fetal bovine serum, FBS) and FBS-free medium were examined by confocal microscope (**Figure 3.3.5.1**).

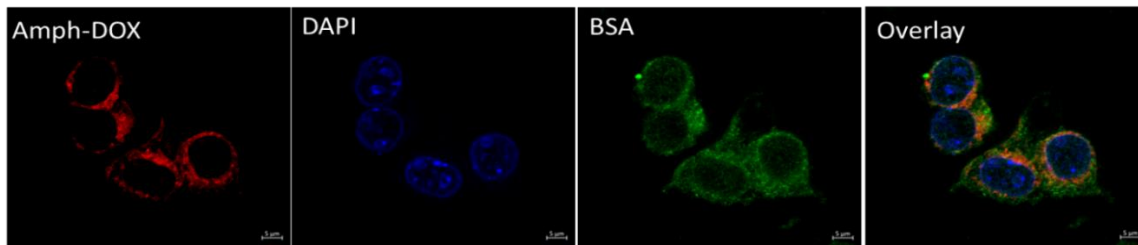


Figure 3.3.5.2 Subcellular location of amphiphilic DOX/ bovine serum albumin (BSA).⁵⁸ Bovine serum albumin-Alexa 660 (BSA-Alexa 660) were pre-incubated with amphiphilic DOX in PBS (pH 7.4) for 4 h at 37 °C. B16F10 cells seeded on the a 6-wells plated were incubated with BSA/amphiphilic DOX complex for 4 h amphiphilic DOX (1.0 μ M) in FBS free cell culture medium.

As discussed in Chapter 2, at first two hours, uptake of amphiphilic DOX showed negatively correlated with FBS content *in vitro*, reflecting the shift of equilibrium lay to the direction of cellular membrane insertion at low albumin concentrations (**Figure 2.3.5.2A and B**)⁵⁸. However, after twelve hours incubation, parity between cellular uptake and albumin binding was observed for amphiphilic DOX in the various of FBS content (the major protein in FBS is albumin) in B16F10 cells (**Figure 2.3.5.2C**)⁵⁸. At low content of albumin, amphiphilic DOX equilibrated between albumin/drug complex status and cell anchoring status (**Figure 2.3.4.2**)⁵⁸. The coexistence of these status jointly promotes intracellular uptake compared than free DOX. However, in physical environment the blood albumin concentration (35–50 g/L) is ~ 10 times higher than that in cell culture medium (<4.5 g/L), leading to albumin binding be a majority. Natheless, amphiphilic DOX retained in the mitochondria even without presence of FBS in cell culture medium (**Figure 3.3.5.1**)⁵⁸, suggesting albumin is not participate in the intracellular trafficking of amphiphilic DOX, and that the intracellular release of amphiphilic DOX from albumin/amphiphilic DOX complex in biomembranes before lipid sorting is highly possible.

To further demonstrate the albumin/drug complex is degraded before lipid sorting process and albumin is not participate in tracking of amphiphilic DOX, amphiphilic DOX/ bovine serum albumin (BSA, 1:1 in molar ratio) complex were incubated with B16F10 cells for 4 hours in FBS free cell culture medium at 37 °C. After that, cells were stained with DAPI and analyzed by CLSM. While pre-incubated with BSA, amphiphilic DOX was partially occupied by cells showing the incomplete co-localization between BSA and amphiphilic DOX (**Figure 3.3.5.1**).^{37, 68} These results demonstrated that in vitro, albumin competes with cells to amphiphilic DOX conjugation and not engage as a participant of the intracellular sorting of amphiphilic DOX.

3.3.6 Amphiphilic modification is not a universal strategy for mitochondria drug delivering.

In this study, amphiphilic modification via diacyl lipid poly(oxyethylene) is considered to the essence for mitochondria target. To investigate whether it can be a universal strategy for mitochondria-specific targeting, we modified fluorescein with the same amphiphilic groups and tracking its internalization. In B16F10 cells, the intracellular uptake of amphiphilic fluorescein was further colocalized with mitochondria tracker and investigated using confocal microscopy. Interestingly, distinct with amphiphilic DOX, no mitochondrial retention of amphiphilic fluorescein was observed (**Figure 3.3.6.1**). These results indicated that amphiphilic conjugation would not be a universal strategy for the mitochondrial targeting and need to be discussed case by case.

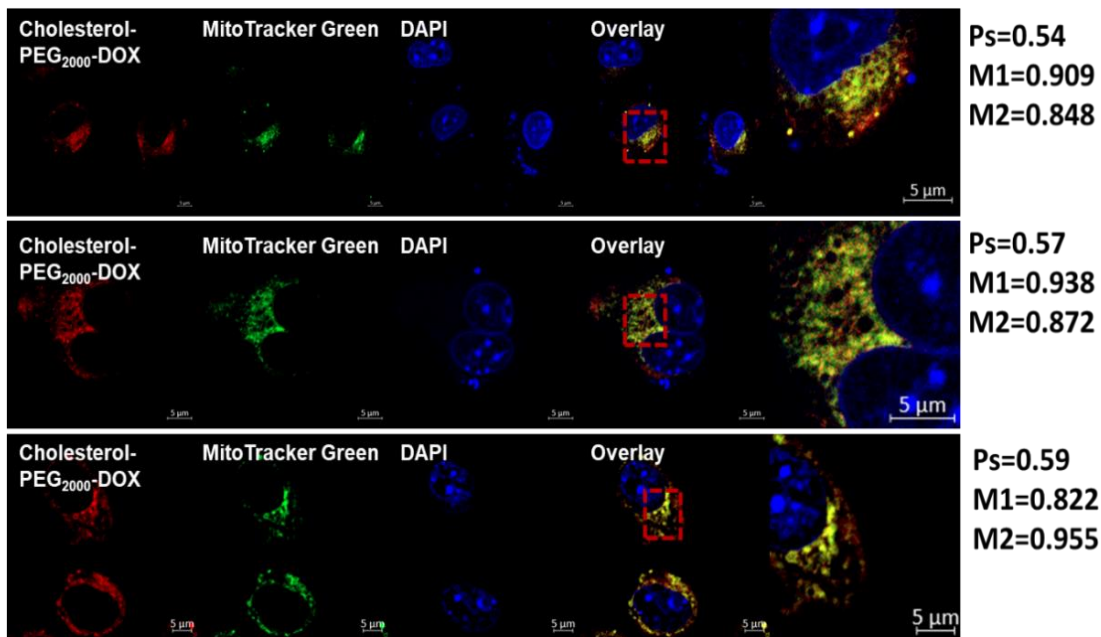


Figure 3.3.6.2 Subcellular location of Cholesterol-PEG₂₀₀₀-DOX at 4 h. ⁵⁸ B16F10 cells at the density of 1×10^5 cells per well were seeded on cover glasses in 6-wells plates for adhesion. Cells were treated with Cholesterol-PEG₂₀₀₀-DOX for 4 h. Cell nuclei and mitochondria were tracked by DAPI (blue) and Mito-Tracker, respectively. Scale bar = 5 μ m.

To determine whether DOX is an indispensable portion in the amphiphilic mitochondria targeting drug, we conjugated DOX to another lipid poly(oxyethylene), cholesterol-PEG₂₀₀₀. Unlike diacyl lipid poly(oxyethylene) which is anionic, cholesterol is in electric neutrality and more hydrophilic. CLSM images showed that, cholesterol-PEG₂₀₀₀-DOX accumulated in mitochondria (**Figure 3.3.6.2**), which was identical to amphiphilic DOX. Correlation coefficient analysis between green and red colors was performed in triplicate and showed strong colocalization (Pearson coefficient, 0.547, 0.57 and 0.59; Manders coefficient, 0.909/0.848, 0.938874/0.872 and 0.822/0.955992), which suggested similar results with amphiphilic DOX. These data indicated that amphiphilic modification on DOX played a leading role on altering its internalized destination. And the lipid structural requirement for mitochondrial accumulation can tolerate the transformation on

amphiphilic property to some extent. This observation schematized that the unique mitochondrial targeting property was under the particular combination between amphiphilic lipid and doxorubicin, resulting from its chemical and biophysical peculiarity

However, currently, we are not able to give a full explanation of the detail structure-function relationship (e.g. whether PEG plays a role). It appears the amphiphiles and DOX contributed jointly to the overall physicochemical characteristics which govern the mitochondria targeting. Perhaps amphiphilic modification alters the overall hydrophilic/hydrophobic balance of DOX and subsequently affect its permeability, diffusion, and membrane partition. Another hypothesis is that mitochondria need fatty acid as a high energy source for the cell¹⁹⁵. Together, these results clearly demonstrated that *in vitro*, amphiphilic modification on DOX enhanced the cellular uptake and selectively targeted DOX to mitochondria.

3.3.7 Amphiphilic DOX generates massive reactive oxygen species (ROS) in mitochondria.

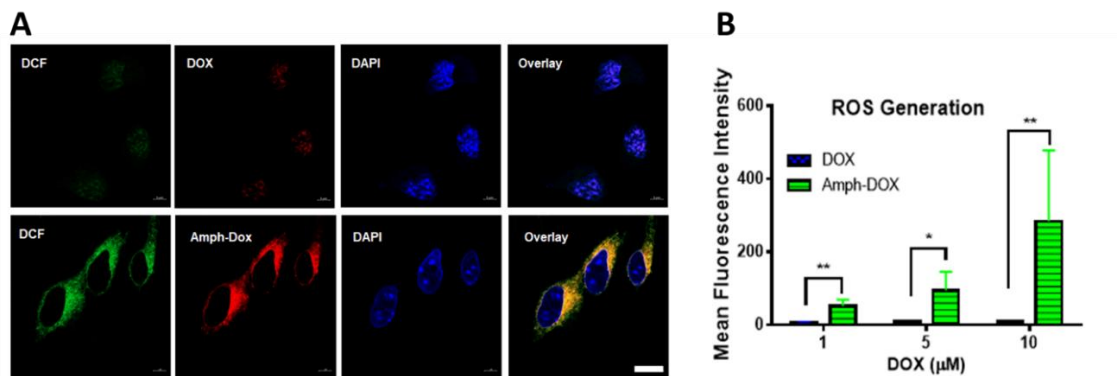


Figure 3.3.7.1 Amphiphilic DOX generated reactive oxygen species (ROS) in cellular mitochondria.⁵⁸ (A) B16F10 cells were incubated with 10 μM DOX and amphiphilic DOX for 4h. After drug treated, ROS generation was quantified by a ROS indicator, H2DCFDA (DCF, green) which was incubated with cells at a final concentration of 20 μM for 30 min. Scale bar of CLSM is 10 μm. (B) Flow cytometer quantification of ROS generation was assigned in B16F10 cells treated with DOX or amphiphilic DOX at the final concentration at 1, 5 and 10 μM.⁵⁸

The action mechanism of doxorubicin is known primarily by DNA intercalation to disrupt topoisomerase-II-mediated DNA repair¹⁹⁶. DOX-induced reactive oxygen species (ROS) generation leads to oxidative damage of mitochondria functions or endoplasmic reticulum stress via *in vitro* has been reported to be another mechanism¹⁹⁷. To address the source and potential mechanism of action of amphiphilic DOX, we analyzed the production and intracellular location of ROS using the ROS indicator (H2DCFDA, 2',7'-dichlorodihydrofluorescein diacetate probe). The kinetic and dose-dependent studies between ROS generation and drug concentration were performed (**Figure 3.3.7.1**). ROS generation was dominantly coincided with amphiphilic DOX on CLSM analysis demonstrating the amphiphilic DOX was responsible for ROS

production (**Figure 3.3.7.1A**). Flow cytometry analysis indicated that the ROS generation compliance with the presence of amphiphilic DOX in a dose-dependent manner (**Figure 3.3.7.1B**). Since the colocalization between amphiphilic DOX and ROS source, it is well-documented to deduce that ROS response in mitochondria, which locations of amphiphilic DOX, induced tumor cell damage and death. Together, these data set a certification to amphiphilic DOX as a promising chemotherapy approach, which significantly increased anti-cancer potency, through effective delivery and recruiting DOX to mitochondria and induce DOX-related cytotoxicity inside of tumor cells.

3.3.8 Amphiphilic DOX achieves tumoral -mitochondrial targeting *in vivo*.

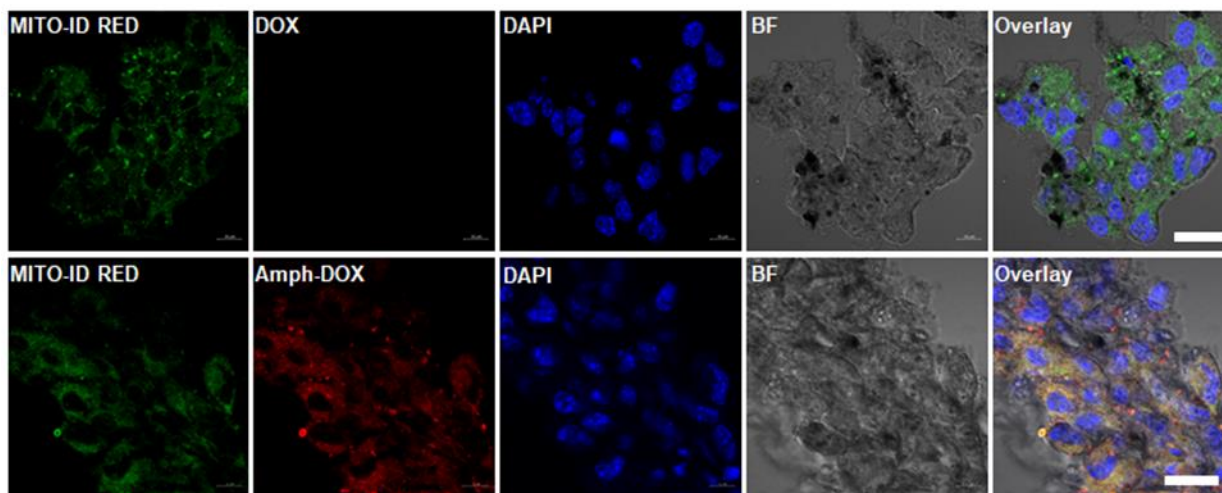


Figure 3.3.8.1 Amphiphilic DOX achieved dual target *in vivo*.⁵⁸ Melanoma tumor bearing mice were injected with doxorubicin hydrochloride, or amphiphilic DOX, or PBS. All groups (n = 8) of mice received above treatments (5 mg/kg equivalent doxorubicin, 10 μ L/g of the body weight) on days 5, 8 and 11 by intravenous injection in the lateral tail vein. At the end of experimental period, tumor tissues were isolated, frozen and sliced in to sections. Mitochondria and cell nuclei were stained with MITO-ID RED and DAPI. Scale bar = 10 μ m.

Mitochondria are special subcellular components that play a key role in mediation of essential cellular metabolism including lipid metabolism, adenosine

triphosphate (ATP) production and apoptosis activation.¹⁵³⁻¹⁵⁴ Delivery of drug to mitochondria may bypass the classical resistance pathways, however, no mitochondria-targeting pharmaceutical formulations have been approved clinically. That is because in cancer chemotherapy, a successful mitochondrial delivery requires multi-levels of targeting: it must achieve sufficient circulating time in blood for drug exposure, and must achieve tumor tissue- and tumor cell-specific accumulation followed by mitochondria-specific accumulation.^{35, 158-164} To inspect whether amphiphilic DOX could achieve such multi-level target and terminate in tumor mitochondria *in vivo*, tumor tissues were isolated at the end of experiment. After frozen, sectioned, and labeled with a mitochondria-selective dye (MITO-ID), samples were analyzed by CLSM. As displayed in **Figure 3.3.8.1**⁵⁸, delivery of amphiphilic DOX was observed in tumor tissue mitochondria showing the strong red color fluorescence coincidence with green color. In contrast, under the same conditions, fluorescence signal of free DOX in the tumor section was undetectable. These results demonstrated that amphiphilic DOX could surmount multiple physiological barriers and terminated at tumor mitochondria *in vivo*.

3.4 Conclusions.

Following the approaches and discussion in chapter 2, we investigated pharmacokinetics / pharmacodynamics of amphiphilic DOX in this chapter. *In vivo* tumor model results demonstrated that amphiphilic DOX can surmount multiple physiological barriers and terminated at tumor mitochondria. This is achieved by molecular engineering which functionalizes doxorubicin with an amphiphilic diacyl lipid connected by a PEG spacer. This functionalized modification fulfills a dual objective: first, amphiphilic DOX reaches and penetrates solid tumor by “hitchhiking” on albumin protein¹⁹⁸⁻²⁰⁰. Albumin-binding enhances the molecular size of doxorubicin and prolongs its circulating time in the blood¹⁹⁹. In addition, albumin-binding facilitate delivery of DOX drug in the tumor by the enhanced permeation and retention (EPR) effect and more importantly, by active metabolic uptake because tumors heavily use albumin as an energy and nutrient source¹⁹⁸⁻¹⁹⁹. Compared with mice treated with free DOX, injection of amphiphilic DOX accumulated heavily in tumor but not in heart. Second, amphiphilic DOX retained in mitochondria following tumor cell uptake both *in vitro* and *in vivo*. Efficient mitochondria targeting with amphiphilic DOX led to a significant increase in oxidative stress in tumor mitochondria, resulting in markedly improved antitumor efficacy. We explored the mechanism of cellular entrance as well as mitochondrial target *in vitro*. Albumin/ drug complex transported into cells via multiple pathway at the first step, following albumin degradation and drug exposure. Due to the particularly chemical and physical properties, amphiphilic DOX accumulate in mitochondria area after lipid sorting. However, the mechanism needs to be further

investigated. Thus, *in vivo*, amphiphilic functionalization improves the doxorubicin molecule's physicochemical properties, which in turn re-defines its bioavailability, organ and subcellular distributions. Amphiphilic modification represents a simple, effective, and nontoxic molecular.

Chapter 4. Enhancing Antigen Presentation and Inducing Antigen-Specific Immune Tolerance with Amphiphilic Peptides.

4.1 Introduction.

In response to an unknown trigger, autoimmune diseases proceed when the immune system begins producing responses that attack hosts' own tissues instead of fighting infections.²⁰¹ There are more than eighty types of autoimmune diseases, including type 1 diabetes (T1D), systemic lupus erythematosus (lupus), inflammatory bowel disease (IBD) and rheumatoid arthritis (RA)²⁰²⁻²⁰³. Numerous researches in developing targeted immune therapies for autoimmune disease during the past decades led to an improved range of choice for clinical treatment. However, the majority of medical treatment approved by the Food and Drug Administration (FDA) have focused on the nonspecific immune suppression of immune inflammatory activity.²⁰³ Relative side effects and occasions of global immunosuppressive of those drugs are not conducive to long-term patients survival.²⁰⁴ The aim of current researches in immune tolerance is to develop the disease-specific treatments to maintain the immune system to delete autoantigens and autoreactive immune cells without the deleterious effects of immune system. Peptide specific therapy takes advantages of other forms of therapy because without antigen process activities, it can response to the desired pathogenic epitopes, limiting the possibility for hyperactivation of immune systems. Therefore, the use of desired peptides combined with adjuvants provide a potent strategy to specifically induce tolerance or drive the immune response towards an anti-inflammatory cytokine profile.

4.1.1 Type 1 diabetes(T1D) and peptide therapy.

Type 1 diabetes (T1D) is one of the most studied chronic autoimmune disorders in the last two decades. A conventional therapy such as insulin replacement alleviates the symptoms of hyperglycemia but cannot cure the mellitus. An alternative therapy that transplanting islets cells from health donor is limited by several drawbacks such as the availability of islets cells, and the requirement for lifelong immunosuppression.^{203, 205-208}

Peptide-specific immunotherapy has emerged as a potent approach to prevent T1D and an important support in understanding of the immune tolerance.²⁰⁹⁻²¹⁵ Initiated by the presentation of self-antigens, T1D has been associated with autoreactive T cells destruction of insulin-producing beta(β)-cells within pancreatic islets. Antigen fragments or peptides triggering autoimmune disorders are generated by the degradation of self-antigen inside the by antigen-presentation cells (APCs).²¹⁶ The recognition process of autoreactive T cells depends on the presence in the APCs of major histocompatibility complex (MHC) proteins, which bind such peptides, display them on the cell surface, and present them there, along with a co-stimulatory signal, to the T cells. Indeed, the autoreactive T cells are fully activated and provided proliferative and survival signals by both the stimulation of the T-cell receptor (TCR) by MHC and co-stimulatory receptors through costimulatory molecules. There are two structurally and functionally distinct types of MHC proteins: MHC class I proteins, which present peptides to CD8 cytotoxic T cells, and MHC class II proteins, which present foreign peptides to CD4 T helper cells.^{205, 210, 212, 215}

Control antigen-specific autoreactive T cell and induction antigen-specific immune tolerance to β -cell by administration of insulin protein or insulin fragments has been reported to prevent non-obese diabetic (NOD) mice from developing T1D.²⁰⁶⁻²⁰⁷ NOD mice express rearranged diabetogenic TCR genes and spontaneously develop T1D, characterized by the autoreactive T cell mediated response of the insulinitis and eventually destruction of the pancreatic β -cells. Direct immunization of NOD mice with β -cell associated peptides causes a large percentage deletion of the autoreactive T cell. Importantly, the administration of soluble peptides treated diabetic active T cell increase the percent of T1D free NOD mice, suggesting that high-affinity peptide of autoimmune epitopes might be a potential therapeutic modulator in autoimmune disease.²¹⁷⁻²²⁰

4.1.2 Autoantigen presentation plays a key role in triggering peripheral tolerance of T1D.

In peptide immunotherapy, peptide degraded from autoantigen and presentation by MHC are essential for induction and maintenance of peripheral immune tolerance. The differentiation and proliferation of T cells in the lymphoid tissues are regulated by the antigen and co-stimulatory molecules displayed by APCs and environmental cytokines.²¹⁹ The challenges in peptide therapy of T1D are 1) soluble therapeutic peptides introduced parenterally maintain a short half-life and cannot efficiently reach LN where the antigen presentation initiated, 2) soluble therapeutic peptides possess low affinity to MHC complex leading to the poorly presenting to T cell. Low level of the antigen presentation and transitorily peptide displayed on the APCs in the lymph nodes (LNs) limit the efficacy in

regulating autoreactive T cells and activating regulatory T cells (Tregs) so that fail in restore immune tolerance.

In NOD mice, the initiating diabetogenic epitope insulin B chain 9-23 (B9-23) peptide binds weakly (with micromolar affinity and rapid dissociation rate) to IAg7²¹⁷⁻²²⁰, demonstrated by the weak simulation of diabetogenic T cells responding to wildtype insulin B9-23 peptides presented by APCs *in vitro*²²¹⁻²²³. Thus, quantitatively and qualitatively insufficient antigen presentation leads to immunological 'ignorance' to autoantigens and represents one of the major hurdles in current antigen specific immunotherapy. Several approaches are currently being tested to enhance autoantigen presentation to induce antigen-specific tolerance. For example, autoantigen delivered by nanoparticles²²⁴⁻²²⁷ or antibodies²²⁸⁻²²⁹ which target dendritic cells (DCs), the most efficient APCs, to enhance the antigen uptake, processing, and presentation. Efficient delivery of antigens to DCs in the absence of costimulatory stimuli promoted tolerance induction in murine model of T1D.²²⁵ Antigen co-delivered with small-molecular drugs which modulate the DC function is another popular approach for prophylactic and therapeutic vaccines that can drive antigenic tolerance.²²⁷ Recently, targeting DCs in the LNs and modulating DC-T cell interactions have been shown to be a viable approach to restoring T1D tolerance.⁵¹ LNs house abundant DCs/lymphocytes and are the primary anatomic sites where the inflammatory/regulatory fate of T cell polarization is determined.²³⁰ For example, intralymphatic injection of glutamic acid decarboxylase (GAD65), another major autoantigen in T1D has led to dramatically prolonged preservation of β -cell function as compared to

subcutaneous injection in clinical study, due to the enhanced antigen presentation to T cells in the LNs.⁵¹ Another intriguing approach to increase the presentation of the low-affinity antigens is to use alternative antigen ligands. For example, peptide ligands containing pathogenic epitopes obtained by post translational modifications of insulin peptide on the C-terminal (neoantigen) induced potent antigen-specific tolerance in NOD mice.²³¹ These modifications increased the stability of binding of peptide on the C-terminus MHC anchor amino acid residue.²³¹ Likewise, infusion of small amounts of insulin B₉₋₂₃ mimetope modifying the MHC anchor residue at position 9 from an arginine to a glutamic acid (R22E) completely prevented the onset of T1D in NOD mice.²²³ These important studies demonstrated that efficient antigen presentation under subimmunogenic conditions is indispensable in tolerance induction *in vivo*.

4.2 Method.

4.2.1 Materials.

Dexamethasone (DEX), methotrexate (MTX) and mycophenolic acid (Myco), 4-dimethylaminopyridine (DMAP), succinic anhydride, dicyclohexylcarbodiimide (DCC), N-hydroxysuccinimide (NHS), dimethyl sulfoxide (DMSO), chloroform, triethylamine (TEA) were purchased from Sigma-Aldrich (St. Louis, MO). 1,2-distearoyl-sn-glycero-3-phosphoethanolamine-N-[amino(polyethylene glycol)-2000] (DSPE-PEG₂₀₀₀-NH₂) and 1,2-distearoyl-sn-glycero-3-phosphoethanolamine-N-[maleimide(polyethylene glycol)-2000] (DSPE-PEG₂₀₀₀-Maleimide) were purchased from Laysan Bio Inc. (Arab, AL) HPV-16 E749-57 peptide (CRAHYNIVTE), OVA₃₂₃₋₃₃₉ Cysteine peptide (CISQAVHAAHAEINEAGR), Cysteine B₉₋₂₃(CSHLVEALALVCGERG), OVA-derived peptide SIINFEKL (CSIINFEKL) were custom synthesized by GenScript (Piscataway, NJ). Lipo-G₂-CpG were synthesized in house using an ABI 394 DNA/RNA synthesizer.²³² Murine MHC class I tetramers were obtained from MBL international Corporation (Woburn, MA). Antibodies were purchased from eBioscience (San Diego, CA) or BD Bioscience (San Jose, CA).

4.2.2 Cells and animals.

Mouse bone marrow dendritic cells (BMDCs) were generated as described by a modified protocol.²³³ Cells were cultured in complete medium (MEM, 10% fetal bovine serum (Greiner Bio-one), 100 U/mL penicillin G sodium and 100 µg/mL streptomycin (Pen/Strep). Animals were housed in the United States Department of Agriculture (USDA)-inspected Wayne State University animal facility under

federal, state, local and NIH guidelines for animal care. Female C57BL/6 mice (5-8 weeks), NOD/ShiLtJ mice (5 weeks) and OT-II mice were obtained from the Jackson Laboratory.

4.2.3 Preparation and purification of amphiphilic antagonists.

For amphiphilic dexamethasone (amphiphilic DEX), dexamethasone (1.0 g, 2.54 mmol), succinic anhydride (0.51 g, 5.10 mmol) and DMAP (0.155g, 1.27 mmol) were dissolved in acetone. After reaction for 12 hours, the solvent was evaporated under reduced pressure. The product (DEX-succinic acid) was re-dissolved in ethanol/ water mixture (0.6% v/v) and recrystallized. The white solid product (DEX-succinic acid) was further dried using oil pump. DEX-succinic acid (1.1 g, 2.23 mmol) was dissolved in 50mL acetone and activated by DCC (0.55 g, 2.67 mmol) and NHS (0.37 g, 3.21 mmol). The product (DEX-succinic-NHS) in filtrate solution was obtained by filtration after overnight reaction. DEX-succinic-NHS compound was dried under reduced pressure. Amphiphilic DEX conjugated was produced by coupling DEX-succinic-NHS (25 mg, 0.043 mmol) to the DSPE-PEG₂₀₀₀-amine (100 mg, 0.036 mmol) in DMSO (3.5 mL) and TEA (2.5 μ L). After overnight coupling, amphiphilic DEX was purified by HPLC with a reverse-phase C4 column, lyophilized and dissolve in DMSO.

For amphiphilic methotrexate (amphiphilic MTX), methotrexate (0.5 g, 1.56 mmol) was dissolved in 10 mL chloroform and activated using DCC (0.37 g, 1.87 mmol) and NHS (0.22 g, 1.87 mmol). MTX-NHS was concentrated by air dry after overnight reaction. Amphiphilic MTX conjugated was produced by reacting MTX-NHS (25 mg, 0.033 mmol) to the DSPE-PEG₂₀₀₀-amine (100 mg, 0.036 mmol) in

chloroform (2 mL) and TEA (2.5 μ L). After overnight coupling, Amphiphilic MTX was purified by HPLC with a reverse-phase C4 column, lyophilized and re-dissolved in chloroform.

For amphiphilic Mycophenolic acid (amphiphilic Myco), Mycophenolic acid (0.1 g, 0.22 mmol) was dissolved in 2 mL DMSO and activated by DCC (0.055 g, 0.27 mmol) and NHS (0.03 g, 0.26 mmol). Myco-NHS was concentrated by air dry after overnight reaction. Amphiphilic Myco conjugated was produced by coupling Myco-NHS (25 mg, 0.040 mmol) to the DSPE-PEG₂₀₀₀-amine (100 mg, 0.036 mmol) in DMSO (2 mL) and TEA (2.5 μ L). After overnight coupling, Amphiphilic Myco was purified by HPLC with a reverse-phase C4 column, lyophilized and dissolve in DMSO.

4.2.4 Preparation and purification of amphiphilic peptides.

5 mg peptides was mixed with two equivalent DSPE-PEG₂₀₀₀-Maleimide in 1 mL DMF with additional 3 μ L triethylamine (TEA). After stirred in the dark at room temperature (RT) for overnight, the DMSO solvent was removed in a stream of air for 72 h to as much as possible. The product residues were re-dissolved in 5 mL D.I water for HPLC purification. Amphiphilic peptides were purified by a C4 reverse-phase HPLC column (Thermo Scientific, 250 x 4.6 mm, 5 μ m).

4.2.5 *In vitro* characterization.

The cellular uptake of unmodified peptides and amphiphilic peptide was quantified in B16F10 cells by flow cytometry (Applied Biosystems). Cells with a density of 1×10^6 cells per well were seeded to 96-wells plates for overnight. The cell medium was removed and replaced with fluorescein labeled peptide and

amphiphilic peptide at a final concentration of 1.0 μM for 2 hours. Following washed three times with 1 \times PBS, cells were harvested in FACS and analyzed by Attune acoustic focusing cytometer. Each assay was performed in triplicate.

For characterization of subcellular location, cells (10^4 cells per well) were seeded on a coverslip in a 6-wells plate. For visualization amphiphilic peptide, cells were then incubated with fluorescein labeled peptide or amphiphilic peptide at the concentration of 1 μM at 37 $^\circ\text{C}$. After 4 hours' incubation, the cells were washed with 1 \times PBS, fixed in 3% paraformaldehyde (PFA) and washed with PBS three times. Images were captured by Zeiss confocal (LSM 780) microscope with a 63 \times oil-immersion objective.

4.2.6 Electrophoretic mobility shift assay (EMSA).

An agarose gel (0.7%) electrophoresis mobility shift assay was used to detect the interaction between albumin with lipo-peptide. The solution of fluorescein labeled free OVA₃₂₃₋₃₃₉ and lipo-OVA₃₂₃₋₃₃₉ were incubated with Fetal Bovine Serum (FBS) (estimate molar ratio 1:1) for 4 hours at 37 $^\circ\text{C}$. Samples were loaded for electrophoresis run under 75 V for 30 min. Images were recorded using a digital camera (Canon) under UV illustration for fluorescein labeled peptide, or briefly stained with Coomassie blue for protein characterization.

4.2.7 Lymph nodes draining and cellular uptake.

The study was approved by the division of laboratory animal resources (DLAR) and animals were cared in the DLAR animal facility under federal, state, local, and NIH guidelines for animal care. 3.3 nmol of fluorescein labeled free OVA₃₂₃₋₃₃₉ or amphiphilic OVA₃₂₃₋₃₃₉ were subcutaneously (s.c.) administrated in

the tail base of C57BL/6 mice (n=4 LNs/group). After 24 h drug administration, treated mice were euthanasia using carbon dioxide. Inguinal and axillary lymph nodes were next isolated and digested with 1.5 mL freshly prepared enzyme solution in RPMI-1640 medium consisted of collagenase/ dispase (0.8 mg/mL, Sigma-Aldrich) and deoxyribonuclease (DNase, 0.1 mg/mL, Sigma-Aldrich). Lymph nodes cells were extracted and stained with anti-CD11c antibody. Percentages of peptide positive cells among the CD11c positive in the lymph nodes were quantified by flow cytometry.

4.2.8 *Ex vivo* antigen presentation assay.

A round-bottom 96-wells plate were seeded with BMDCs (7 days after isolation). Cells were pulsed with different concentrations of OVA₃₂₃₋₃₃₉ or lipo-OVA₃₂₃₋₃₃₉ peptides for 2 hours. Cells were then washed and cocultured with freshly isolated OT-II CD4⁺ T cells (DC/T cell ratio 1:2) for 48 hours. Supernatant was transferred and stored at -80 °C prior to IL-2 quantification by ELISA assays. All experiments were performed in triplicate. In some cases, BMDCs were fixed with 1% PFA at room temperature for 30 min, or treated with NH₄Cl (200 µM) at 37 °C in culture medium for 45 min.

4.2.9 *In vivo* tolerization with amphiphilic peptide.

On day 0, C57BL/6 mice at the age of 6-8 weeks (n = 3) were immunized with ovalbumin protein (OVA, 10 µg) and lipo-CpG (1.24 nmol) and tolerized with OVA₃₂₃₋₃₃₉ (10 µg) or amphiphilic OVA₃₂₃₋₃₃₉ on days 7 and 17. On day 21, mice were challenged with ovalbumin (10 µg) and lipo-CpG (1.24 nmol). The antigen-specific cellular and humoral immune response were evaluated on day 28. Vaccine

injections were performed s.c. at the base of the tail with the volume of 100 μL /animal.

4.2.10 *In vivo* tolerization with amphiphilic antagonists and antigen.

On day 0, C57BL/6 mice at the age of 6-8 weeks ($n = 3$) were stimulated with ovalbumin protein (10 μg) and lipo-CpG (1.24 nmol) and tolerized with antagonists or amphiphilic antagonists (10 μg) mixed with ovalbumin (10 μg) on days 7 and 17. On day 21, mice were challenged with Ovalbumin (10 μg) and lipo-G₂-CpG (1.24 nmol). The antigen-specific cellular and humoral immune response were evaluated on day 28. Vaccine injections were performed s.c. at the base of the tail with the volume of 100 μL /animal.

4.2.11 Antigen-specificity study for amphiphilic antagonists.

On day 0 and day 14, C57BL/6 mice (6-8 weeks; $n = 4$ per group) were stimulated with ovalbumin protein (10 μg) and lipo-CpG (1.24 nmol) at the left tail side and tolerized with HPV peptide(10 μg) and antagonists or amphiphilic antagonists at the right tail side. On day 21, antigen-specific cellular immune responses were evaluated. Vaccine injections were performed s.c. at the base of the tail with the volume of 100 μL /animal.

4.2.12 Antigen-specific cytotoxic T lymphocyte (CTL) detection.

OVA-specific CD8⁺ T cells were detection by tetramer assay. Seven days after vaccinal boost, blood samples (100 μL) were collected and lysed by ACK lysing buffer twice. White blood cells were next blocked with Fc-blocker (anti-mouse CD16/CD32 monoclonal antibody). Blocked cells were further incubated with phycoerythrin (PE)-labeled SIINFEKL/K^b tetramer and (allophycocyanin) APC

labeled anti-CD8 antibody (ebioscience) for 30 minutes at room temperature. After washed and resuspended in flow cytometry staining buffer (FACS buffer, 1% w/v BSA in PBS), cells were analyzed using flow cytometer. OVA-specific CD8⁺ T cells were gated on living, APC and PE positive group.

4.2.13 Intracellular cytokine staining.

Lysed cells from blood were pulsed with peptide antigen for 6 hours at 37 °C in T-cell expansion medium (RPMI 1640, 10% v/v fetal bovine serum (FBS), 1 mM HEPES, 50 µM β-mecaptoethanol(BME), 100 U/mL Penn/Strep, 1 mM sodium pyruvate, 1x MEM non-essential amino acids solution), with additional autophagy inhibitor brefeldin A for 4 hours. After stimulation, intracellular staining for IFN-γ secreting CD4 T cells was performed according to previous protocol²³⁴. Cells were incubated with APC labeled anti-CD4 antibody and then fixed and permeabilized using fixation and permeabilization solutions (BD Biosciences). Foxp3 staining was performed according to the manufacturer's instructions (Ebioscience) for fixation and permeabilization.

4.2.14 Enzyme-linked immunosorbent assay (ELISA).

Serum or cell culture supernatant levels of antibodies and cytokines were determined by Enzyme-linked immunosorbent assay (ELISA). ELISA plates were coated with capture antibodies in PBS for overnight. On the next day, coated plates were blocked with 1% BSA solution for at least 1 h. A series of dilutions of serum samples were then added and incubate for 1h. Plates were washed with three times and horseradish peroxidase (HRP) conjugated goat anti-mouse IgG was added at 1 µg/ml for 30 min. After washed three times with PBS/1% Tween 20

solution, plates were added with 3,3',5,5'-Tetramethylbenzidine (TMB) for color developing. Finally, 1 M H₂SO₄ stop solution were added and the absorbance was read at 450 and 570 nm as the reference using a plate reader.

4.2.15 Monitoring blood glucose levels.

Blood glucose of NOD mice was monitored with glucose meters (Accu-Check III) twice a weekly during the experimental period. Diabetes was defined as two subsequent blood glucose values over 300 mg/100 mL.

4.2.16 Statistical analysis.

Statistical analysis the mean values of two groups were performed using unpaired Student's t tests. The statistical difference between groups were determined using a one-way analysis of variance²⁰ with Bonferroni post-test. All the values were expressed as means ± standard error of mean. GraphPad Prism (San Diego, CA) software was used for all the statistical analyses. ***p < 0.001, **p < 0.01, *p < 0.05. NS, not significant.

4.3 Results and discussions.

Lymph nodes (LNs) are essential for the functioning of the adaptive immune system, including initiating and resolving immune response as well as maintaining tolerance²³⁵. Antigen presenting cells (APCs) such as dendritic cells (DC) presenting antigen to T lymphocytes are initiating and maturing in LNs. Recently, we reported an 'albumin-hitchhiking' approach which self-deliver vaccine subunit to antigen presenting cells in the draining lymph nodes. The self-delivery strategy was achieved by the molecular design of amphiphilic molecules that hijack the traffic pathway of endogenous albumin in the lymphocytic interstitial fluid ²³⁵. To test whether this approach can be translated to deliver small molecular anti-agonist or peptide for immune regulation, we conjugated anti-agonists: dexamethasone (DEX), methotrexate (MTX) and mycophenolic acid (Myco) and CD4 epitope peptide OVA₃₂₃₋₃₃₉, an ovalbumin derived, MHC II restricted peptide to the amphiphilic lipid, DSPE-PEG₂₀₀₀, following our previously published procedure.

4.3.1 Synthesis of amphiphilic antagonists.

The coupling of antagonists with amphiphilic motif were performed using a primary amine/NHS ester chemistry. The schematic diagram and chemical formula of every components are shown in **Figure 4.3.1.1**. Subsequently, products were purified by reverse phase high performance liquid chromatography (HPLC). Unconjugated antagonists were separated from amphiphilic antagonists after applying the one-step gradient (0-100% of methanol) HPLC purification. The presence of products was monitored through the absorption at 260 nm.

Amphiphilic DEX, MTX and Myco were collected during 18 to 19.5 min, 19 to 20 min, and 19 to 20 min, respectively.

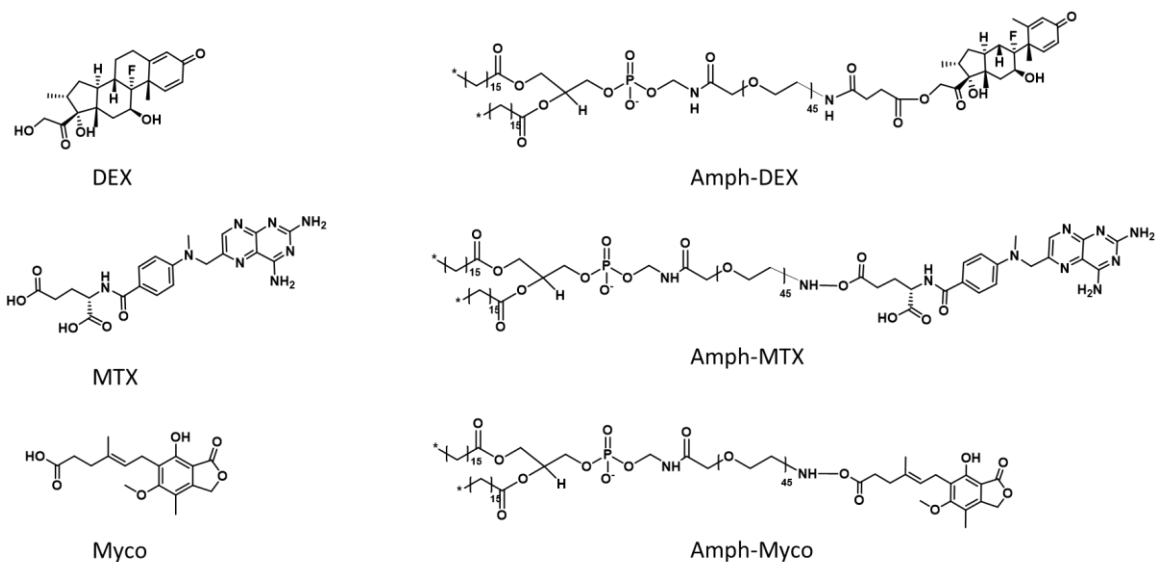


Figure 4.3.1.1 Schematic diagram and chemical formula of DEX, amphiphilic DEX, MTX, amphiphilic MTX, Myco and amphiphilic Myco. Synthesis procedures are dropped in the method part. Briefly, DEX was firstly coupled with succinic anhydride. The DEX-succinic acid was further activated by NHS and conjugated to DSPE-PEG₂₀₀₀-amine. The MTX and Myco was pre-activated with NHS and coupled to DSPE-PEG₂₀₀₀-amine directly.

4.3.2 Synthesis of amphiphilic peptides.

The schematic diagram and chemical formula of amphiphilic peptides (lipo-peptide) was shown in **Figure 4.3.2.1**, HPV-16 E7₄₉₋₅₇ peptide (CRAHYNIVTE), OVA₃₂₃₋₃₃₉ cysteine peptide (CISQAVHAAHAEINEAGR), cysteine B₉₋₂₃ (CSHLVEALALVCGERG) and OVA-derived peptide SIINF EKL (CSIINF EKL) at N-terminal.

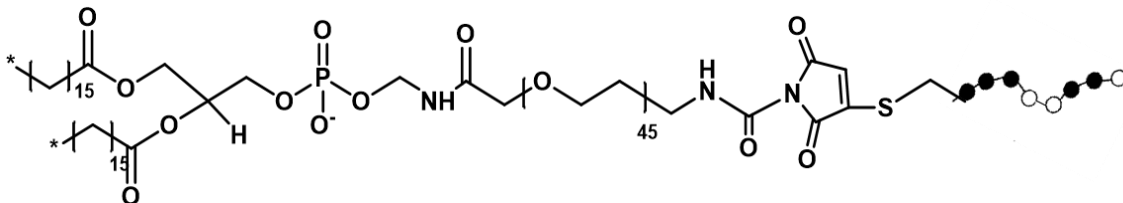


Figure 4.3.2.1 Schematic diagram of amphiphilic peptides. Synthesis procedures are dropped in the method part. Briefly, peptides with amino-terminal cysteines and DSPE-PEG₂₀₀₀-Maleimide were dissolved in dimethylformamide (DMF) and agitated at room temperature for 24 hours, following the addition of triethylamine (TEA) for their coupling.

4.3.3 Amphiphilic antagonists downregulate the expression of CD40, CD80.

Dendritic cells (DCs) in lymphocytic systems can initiate both antigen-specific adaptative immune response or tolerance.²³⁶ The administration of a stimulus for maturation switches DC function from tolerance to immunity, including the development of CD4⁺T helper cells and activation cytolytic CD8⁺ T cells. Co-stimulatory signals (for example, CD40/80) and cytokines (e.g. TNF- α) are necessary to induce a strong antigen-specific CTL response.²³⁶ To determine the efficiency of amphiphilic antagonists to inhibit DCs maturation, we stimulated murine bone marrow BMDCs from C57BL/6J mice with CpG which is the TLR9 ligand and can enhance DC maturation and induce high-level expression of CD40 and CD80. BMDCs cultured with granulocyte–macrophage colony-stimulating factor (GM-CSF) for 6 days were stimulated with CpG ODNs in the presence or absence of anti-agonists. Flow cytometry analysis indicated DC cells cultured with CpG increased the expression of CD80 and CD40. Pre-treated of 10 nM amphiphilic antagonists or free drugs resulted in inhibition of CD40 but not CD80 expression compared with only CpG-treated cells (**Figure 4.3.3.1**). Specifically, both inhibitory expression in CD40 and CD80 were observed in MTX and

amphiphilic MTX treated cells (**Figure 4.3.3.1 C, D**). However, there was no significant difference between both amphiphilic drugs and the free drugs treated groups.

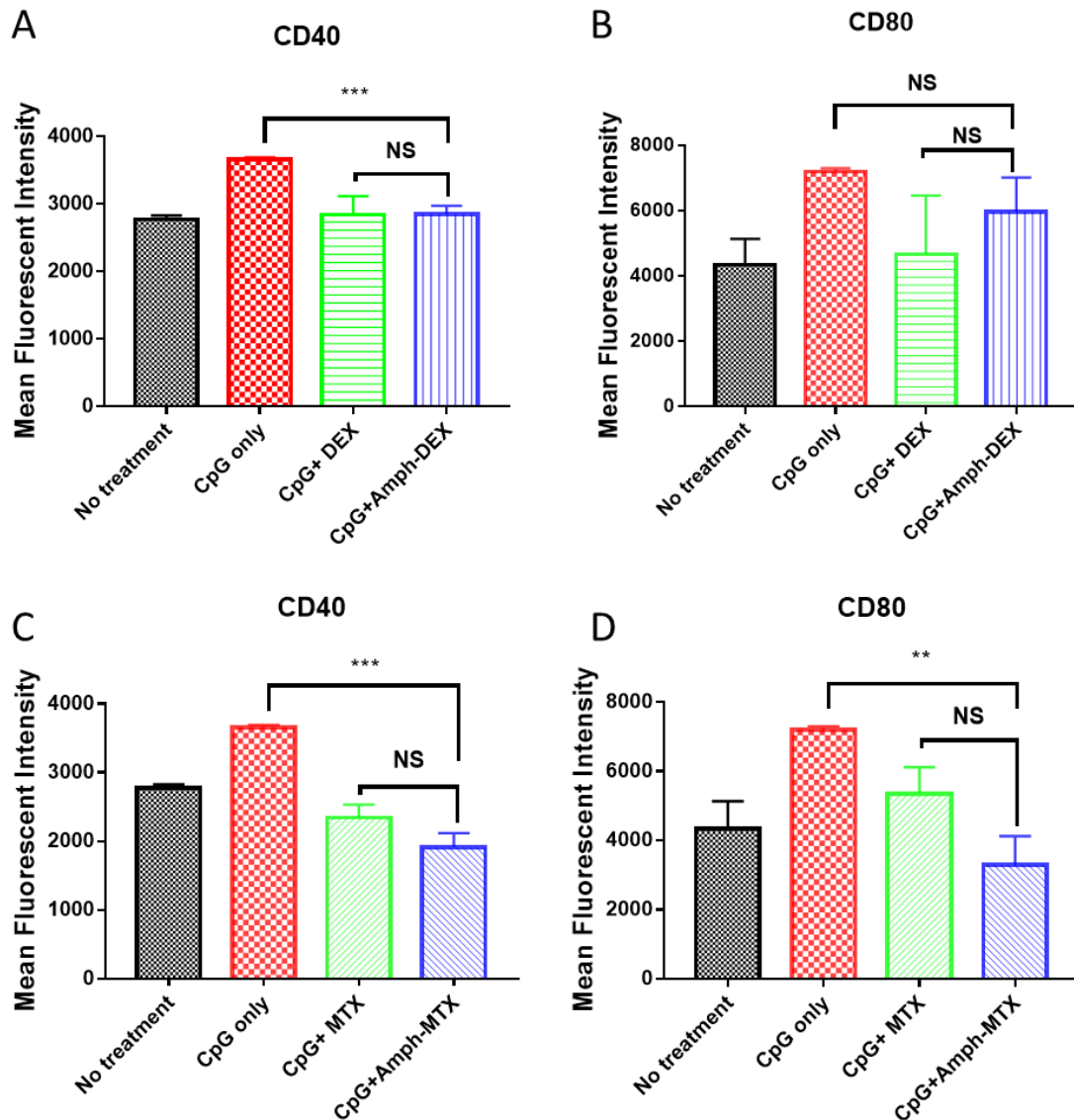


Figure 4.3.3.1 Amphiphilic antagonists downregulated the expression of CD40, CD80. ³ DCs were incubated with DEX (10 nM) and CpG (1 nM), or amphiphilic DEX (10 nM) and CpG (1 nM), or CpG (1nM) only, or medium (No treatment) alone for 24 h. Expression of the membrane markers CD80 (A and C) and CD40 (B and D) were assessed by flow cytometric analysis. Data shown the

mean values \pm SEM. *, $p < 0.05$; **, $p < 0.01$; ***, $p < 0.001$; ****, $p < 0.0001$ by one-way ANOVA with Bonferroni post-test.

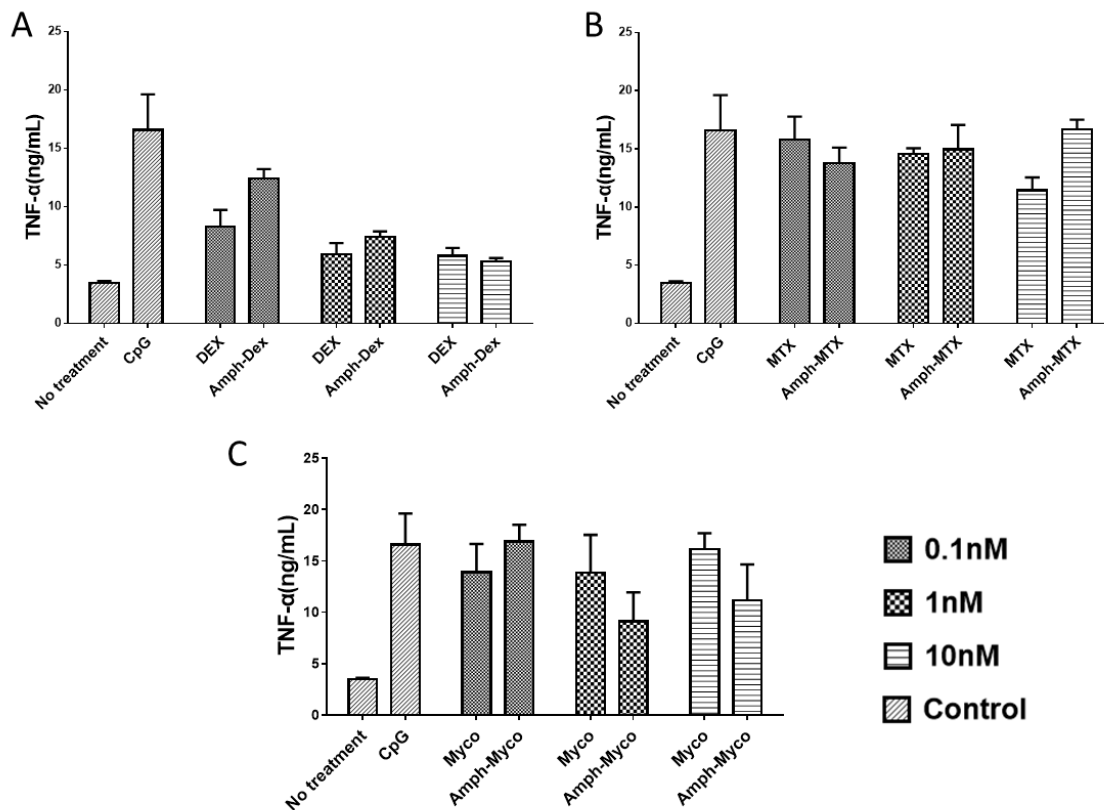


Figure 4.3.3.2 Amphiphilic antagonists inhibited TNF- α production *in vitro*. (A-C) DCs harvested on day 6 were incubated for 24 hours with various concentration of antagonists or their amphiphilic conjugation and CpG (1 nM), CpG (1 nM) only, or medium (No treatment) alone. At the end of the incubation, supernatants were analyzed by ELISA for TNF- α content.

It is reported that DC maturation with tumour necrosis factor (TNF)- α up-regulates surface MHC and costimulatory molecules.²³⁷⁻²³⁸ To determine the efficiency of amphiphilic antagonists on inhibiting maturation of DCs triggered by CpG, we assessed the production of TNF- α cytokine. The BMDC were pre-treated with varies concentration of antagonists and stimulated with CpG. Free DEX treatment resulted in inhibition of cytokine secretion and situated at 1 nM, whereas

amphiphilic DEX showed a dose-dependent inhibition of TNF- α production (**Figure 4.3.3.2A**). Free MTX exhibit inhibition only in a high drug concentration and its amphiphilic conjugation showed almost the same level with CpG only, indicating lack of inhibitory effects (**Figure 4.3.3.2B**). Although, the MTX were less effective in control the TNF- α production, regarding of downregulatory of CD40 and CD80 receptors (**Figure 4.3.3.1B**), it was still a candidate for further study. Moreover, TNF- α secreting were suppressed by low concentration of free Myco but high concentration of amphiphilic Myco. (**Figure 4.3.3.2C**).

4.3.4 Immunosuppression with amphiphilic antagonists *in vivo*.

To evaluate the efficacy of the tolerization using amphiphilic antagonists *in vivo*, we firstly quantified the OVA-specific CD8⁺ T cells after immunization. Briefly, animals were immunized subcutaneously on day 0 with premixture of 10 μ g ovalbumin (OVA) ²³⁹ protein and 1.25 nmol lipo-G₂-CpG which is a potent LN targeting adjuvant and stimulates toll-like receptor 9.³⁵ On the 7, mice randomly separated into eight groups were initially tolerized with soluble mixture of 10 μ g OVA and 10 μ g antagonists or their amphiphilic conjugation. On day 14, animals were tolerization with double dose (20 μ g OVA and 20 μ g antagonists or their amphiphilic conjugation). Mice were finally challenged on day 21 with OVA and lipo-G₂-CpG. The percentage of OVA-specific CD8⁺ T cell proliferation in peripheral blood was quantified on day 28 to determine the cellular immunity. As we reported before, lipo-G₂-CpG adjuvant induced relatively robust antigen-specific CD8⁺ T cell responses, showing more than 25% OVA-specific CD8⁺ T cells in blood³⁵ (**Figure 4.3.4.1B, C, D**). Decreased percent of antigen-specific T

cell were observed by antagonists or OVA treatment (**Figure 4.3.4.1B, C, D**), showing a reduced percent of OVA specific CD8⁺ T cells and, therefore indicating induction antigen-specific immunosuppressive. Unexpectedly, the opposite trends were observed in groups whose mice treated with an antagonists or amphiphilic antagonists admixed with OVA protein. Mice administration with mixture of antagonists or their amphiphilic conjugation with OVA antigen did not showed a synergistic immunosuppressive effect, even compensated the inhibitory contribution from OVA protein (**Figure 4.3.4.1B, C, D**).

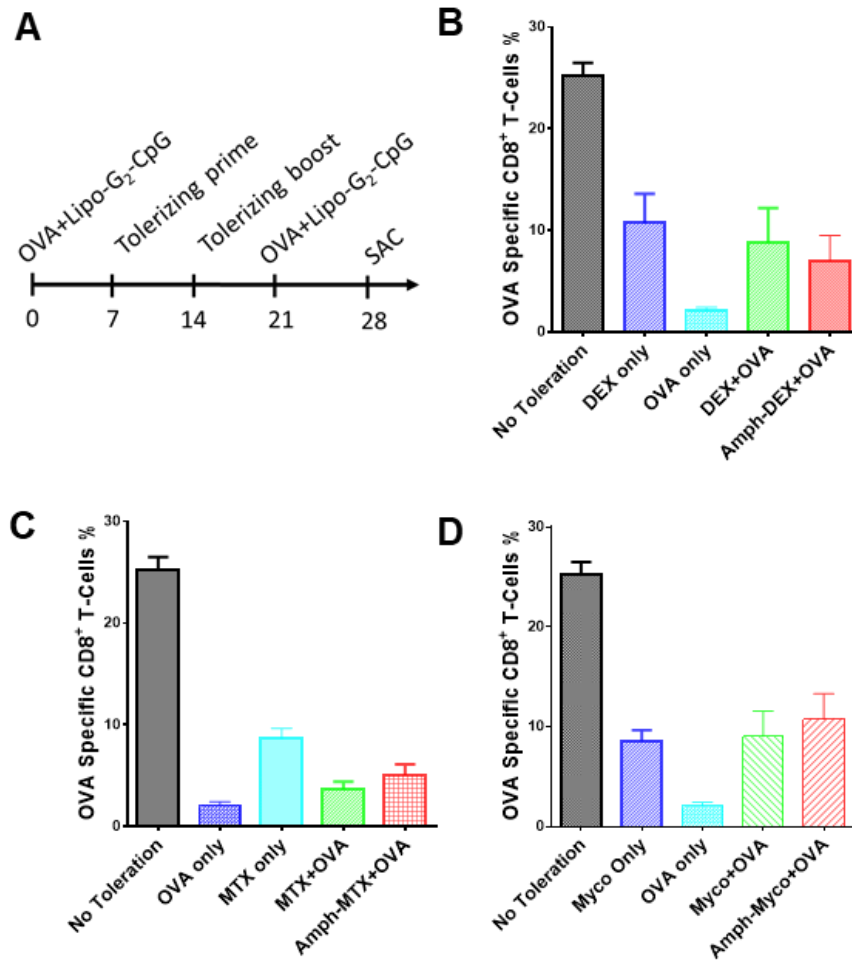


Figure 4.3.4.1 Amphiphilic antagonists or antigen alone induced immunosuppression in the cytotoxicity T cell response. (A) Mice were immunized with 10ug OVA protein and 1.25nmol lipo-G₂-CpG at day 0. Mice were received s.c. immunizations with 10 µg OVA and 10ug free antagonists or amphiphilic conjugation on day 7 and double dose on day 14. (B-D) Mice were sacrificed (SAC) and blood was collected 7 days post challenge and assayed for cytotoxicity OVA-specific CD8⁺ T cell.

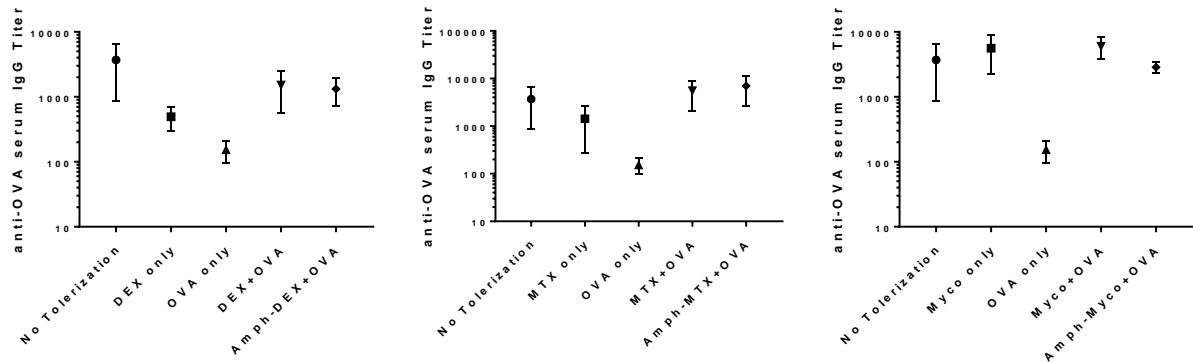


Figure 4.3.4.2 Amphiphilic antagonists or antigen alone induced immunosuppression in humoral response. Blood was collected 7 days post challenge and assayed for ELISA. The IgG titers were defined as the half maximal effective dose (EC₅₀) of a 4-parameter logistic (4PL) curve fit curve.

Peripheral antibody response gives insight into the humoral immunity.²⁴⁰ To investigate the capacity of amphiphilic antagonists on development humoral immune tolerance, the level of OVA-specific IgG tolerization with amphiphilic antagonists were evaluated. Animals were immunized subcutaneously with an admix of lipo-G₂-CpG and OVA on day 0 and successive two tolerization with amphiphilic antagonists or their free drugs with or without OVA protein. Seven days after stimulating with OVA and lipo-G₂-CpG on day 20, sera were isolated from mice for antibody response analysis. Mice without treatment showed a crescent antibody response with mounting anti-OVA titers. Compared with no treatment, the group treated with OVA protein showed suppressive the anti-OVA antigen response (**Figure 4.3.4.2**). However, the inhibitory effect on humoral response was weakened by the antagonists, as providing all the co-administration groups had enhanced anti-OVA IgG titers comparing with OVA group (**Figure 4.3.4.2**). These results suggested that administration of amphiphilic antagonists

and their parental drugs induced the activation of T-cell and humoral immunity and pre-mix of antigen and adjuvants are critical.

4.3.5 Study of antigen-specific immune tolerance

To test whether the specificity of the immunosuppressive effects of antagonists is broad and systemic, animals were injected (subcutaneously) with mixture of amphiphilic human papillomaviridae (HPV-16 E7₄₉₋₅₇) peptide, antagonists or amphiphilic antagonists and lipo-G₂-CpG were injected in the left limb and OVA protein plus lipo-G₂-CpG were administered in the right limbs (**Figure. 4.3.5.1A**). Mice immunized with amphiphilic HPV only did not broadly induce OVA specific CD8⁺ T-cell responses indicating the antigen specificity. Mixing amphiphilic HPV peptide with DEX and amphiphilic DEX completely blocked the development of HPV specific CD8⁺ T-cell responses. At the same time, amphiphilic DEX had no effect on the OVA-specific response initiated in the contralateral limb, whereas the inhibitory effect was observed in the free DEX group (**Figure. 4.3.5.1B and C**). Injection of either MTX or Myco or their amphiphilic conjugation had no significant effect on the response to either HPV or OVA epitope (**Figure. 4.3.5.1B and C**). As a summary, co-immunization amphiphilic HPV peptide with antagonists did not show a universal immunosuppressive effect (**Figure. 4.3.5.1 B, C**) and the mode of action and pathway of every antagonists need to be addressed. On the other hand, these results encouraged us to explore amphiphilic peptides instead of amphiphilic antagonists as a vaccine to induce immune tolerance.

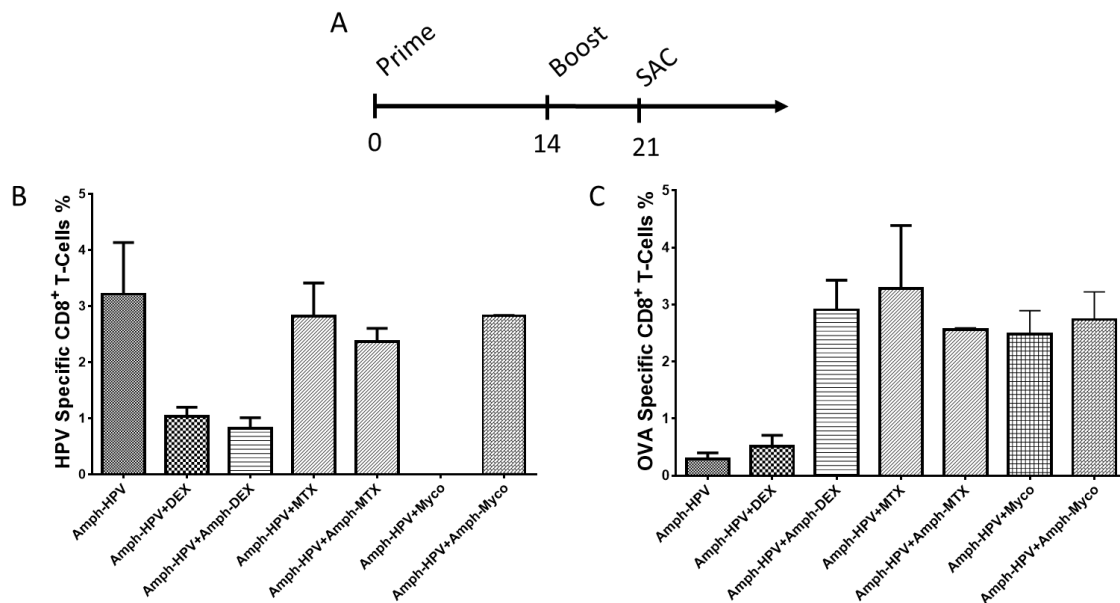


Figure 4.3.5.1 Treatment with amphiphilic antagonists did not result in broad immunosuppression. (A) Mice were immunized with OVA and lipo-G₂-CpG in the right limbs and with anti-agonists or amphiphilic antagonists with amphiphilic HPV peptide and lipo-G₂-CpG in the left limbs twice on day 0 and day 14. (B and C) HPV-specific CD8⁺ T cells (B) and OVA-specific CD8⁺ T cells (C) were isolated from blood seven-days post the vaccination boost.

4.3.6 Immunosuppression with amphiphilic peptides.

IFN- γ secreting from T helper cells was a critical cytokine for T cell proliferation and an important activator of APCs.²⁴¹ To investigate whether amphiphilic peptides can inhibit T-cell activation under inflammatory conditions, animals were immunized with OVA protein combined with lipo-G₂-CpG on day 0. Mice were tolerized twice with 10 μ g MHC class II-restricted OVA₃₂₃₋₃₃₉ peptide and its amphiphilic conjugation (on N-terminal) on day 7 and day 14. The final challenge with OVA protein and lipo-G₂-CpG was performed on day 21 (**Figure 4.3.6.1A**).

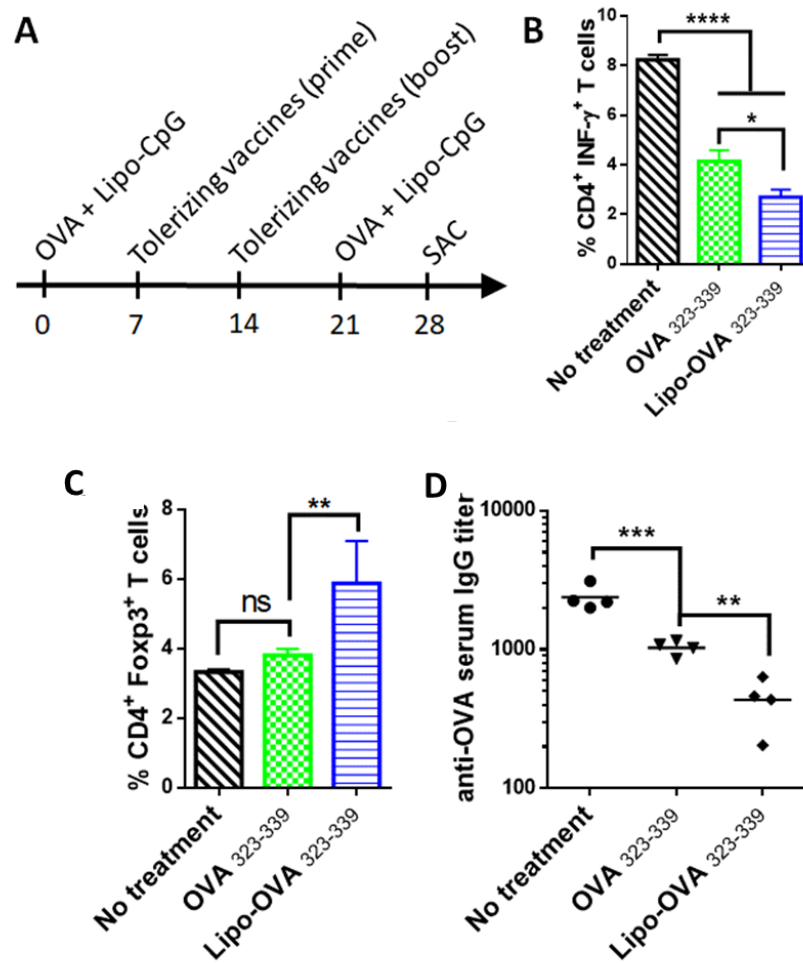


Figure 4.3.6.1 Amphiphilic peptides induction antigen-specific immunological tolerance. (A) One week after immunized with OVA protein mixed with lipo-G₂-CpG, animals were separated into two subgroups and tolerized with 10 μ g dominant MHC-II peptide (OVA₃₂₃₋₃₃₉) vaccine, or lipo-OVA₃₂₃₋₃₃₉, respectively. (B-D) Blood was collected 7 days post immunological challenge and assayed for IFN- γ secreting CD4⁺ T cell (B), CD4⁺ CD25⁺ Foxp3⁺ Treg cells (C) and anti-OVA IgG responses (D).

Both free OVA₃₂₃₋₃₃₉ peptide and amphiphilic OVA₃₂₃₋₃₃₉ peptide reduced the frequency of peripheral IFN- γ producing CD4⁺ T cell (**Figure 4.3.6.1B**). Moreover, a significantly inhibition of CD4⁺ IFN- γ ⁺ T cell was observed in mice treated with lipo-OVA₃₂₃₋₃₃₉, as compared to those with soluble OVA₃₂₃₋₃₃₉ (**Figure 4.3.6.1B**). Mice tolerization with amphiphilic OVA₃₂₃₋₃₃₉ also substantially attenuated antigen responses against OVA showing decreasing anti-OVA IgG titers compared with non-tolerized treatment group as well as free peptide group (**Figure 4.3.6.1D**). Regulatory T cells (Tregs) are a subset of immunosuppressive T cell that have a major role in mediating the activity of self-reactive cells.^{3, 242} To investigate if the amphiphilic peptides can restore autoreactive regulatory mechanism, the CD4⁺ CD25⁺ Foxp3⁺ from mice blood were quantified on day 28. An enhancement in the percentage of CD4⁺ CD25⁺ Foxp3⁺ T cells in the blood was distinct after lipo-OVA₃₂₃₋₃₃₉ treatment (**Figure 4.3.6.1C**), indicating induction of T regulatory cells.

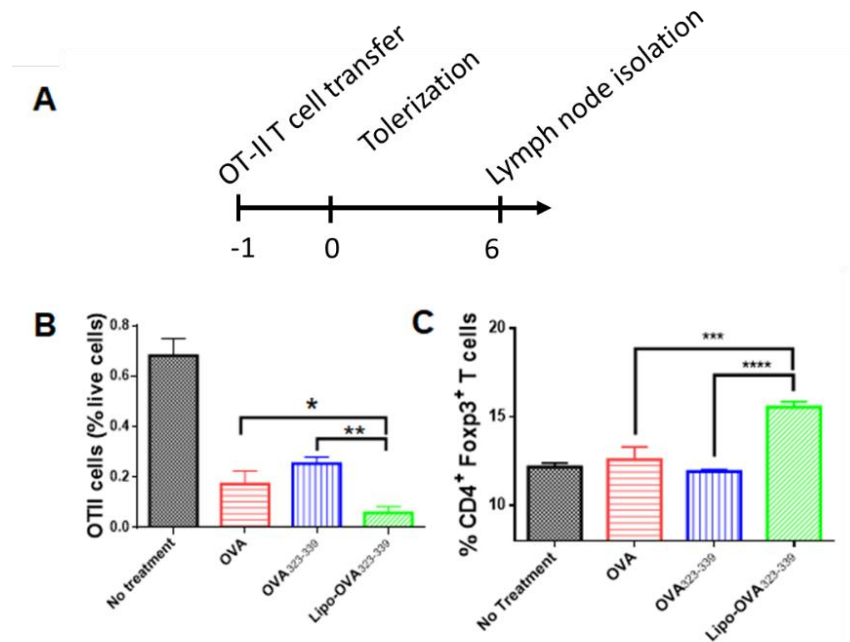


Figure 4.3.6.2 Immunization with lipo-OVA₃₂₃₋₃₃₉ deleted OT-II T cells and promoted the induction of regulatory T cells. (A-C) CD4⁺ OT-II T cells labeled with CFSE and were i.v. transferred into C57BL/6 mice on day -1. At day 0, animal received s.c. immunizations with PBS (no treatment), ovalbumin protein (OVA, 10 µg), OVA₃₂₃₋₃₃₉ peptide (10 µg), or amphiphilic OVA₃₂₃₋₃₃₉ (equal amount peptide). Six days later, inguinal nodes were harvested and the frequencies of OT-II T cells (B) as well as the percentage of Foxp3⁺CD25⁺CD4⁺ T cells were quantified(C) (n = 3 per group).

Animals from **Figure 4.3.6.1** immunized with amphiphilic peptide conjugation that had shown a long-lasting inhibition of T helper cells and anti-OVA responses with promoting regulatory T cells. To further demonstrate the lipo-OVA₃₂₃₋₃₃₉ can efficiently promote T reg and restore immune tolerance, the carboxyfluorescein succinimidyl ester (CFSE)-labeled OTII CD4⁺ T cells (CD45.1⁺) were adoptively transferred into CD45.2⁺ mice. Six days after administration of 10 µg of OVA or OVA₃₂₃₋₃₃₉ or lipo-OVA₃₂₃₋₃₃₉ peptide, the proliferation of the OTII CD4⁺ Foxp3⁺ T cells were measured using flow cytometry (**Figure 4.3.6.2A**). Lymphocytic and splenic OTII T-cell proliferation, determined by dilution of the

fluorophore CFSE as measured by flow cytometry (**Figure 4.3.6.2B**) were decreased in mice treated with amphiphilic OVA₃₂₃₋₃₃₀ compared with OVA protein or peptide. OTII CD4⁺ Foxp3⁺ T cells were markedly enhanced in mice administrated lipo-OVA₃₂₃₋₃₃₀ (**Figure 4.3.6.2C**) demonstrating that amphiphilic conjugation increased antigen-specific Treg priming compared with the soluble antigen.

4.3.7 Amphiphilic peptide antigen binds albumin, accumulates in the antigen presenting cells in the draining lymph nodes.

To determine whether this approach can bind with albumin, fluorescein labeled free peptide and lipo-OVA₃₂₃₋₃₃₉ were developed. We firstly validated lipo-OVA₃₂₃₋₃₃₉ binding to fetal bovine serum (FBS) and the interaction between lipo-peptide and albumin was visualized by electrophoretic mobility shift assay.²⁴³ FBS showed a major albumin band visible after Coomassie staining (**Figure 4.3.7.1A**, lane 5). OVA₃₂₃₋₃₃₉ peptides (**Figure 4.3.7.1A**, lane 1) and its amphiphilic conjugation (**Figure 4.3.7.1A**, lane 3) were analyzed by native gel electrophoresis. FBS showed a major albumin band visible after Coomassie staining (**Figure 4.3.7.1A**, lane 5). The avidity of lipo-OVA₃₂₃₋₃₃₉ to albumin was confirmed by (**Figure 4.3.7.1A**, lane 3-5), showing a short-haul fluorescent band visible under UV co-migrated with pure albumin as compared with lipo-OVA₃₂₃₋₃₃₉. In contrast, OVA₃₂₃₋₃₃₉ incubated with FBS showed no changes in relative mobility (**Figure 4.3.7.1A**, lane 1 and 2), indicating a lack of interaction with albumin.

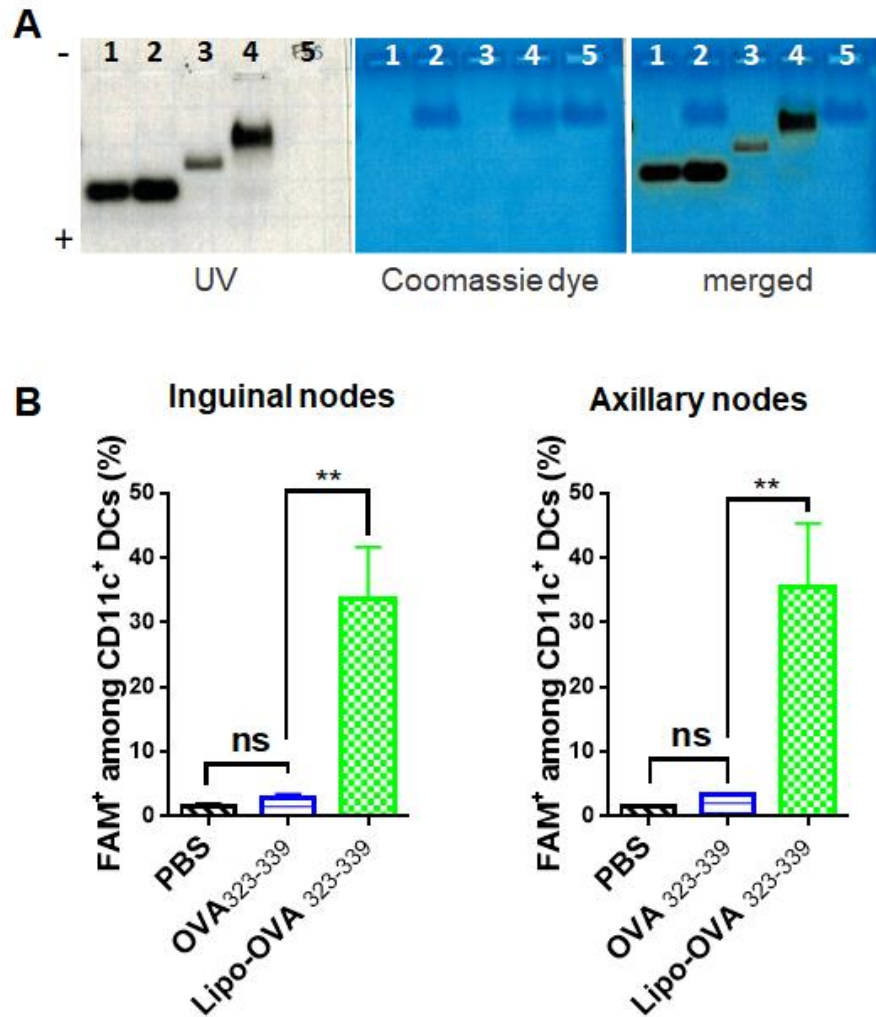


Figure 4.3.7.1 Albumin-binding lipo-peptide remarkably increased LNs drainage and DCs uptake. (A) Fluorescein labeled lipo-OVA₃₂₃₋₃₃₉, or OVA₃₂₃₋₃₃₉ were incubated with FBS at 37 °C for 4 hours and analyzed by native gel electrophoresis (0.8% agarose). The peptide bands were visualized by photograph under UV; protein bands were stained with Coomassie blue. (B) Fluorescein labeled peptides were injected s.c. at the tail base (n = 4 LNs/group), inguinal and axillary nodes were isolated 24 h after injection and analyzed by flow cytometry.

Next, we validated lipo-OVA₃₂₃₋₃₃₉ uptake in LNs following subcutaneously administration into animals at tail base (n = 4 LNs per group). Inguinal and axillary LNs were excised 24h following injection of either OVA₃₂₃₋₃₃₉-FAM or lipo-OVA₃₂₃₋₃₃₉-FAM confirmed the mounting LNs accumulation. As shown in **Figure 4.3.7.1B**,

albumin-binding lipo-OVA₃₂₃₋₃₃₉ exhibited dramatically increased accumulation in DCs in both inguinal nodes and axillary nodes. By contrast, negligible amount of unmodified OVA₃₂₃₋₃₃₉ was detected in DCs in the lymph nodes.

4.3.8 Amphiphilic peptide antigen anchors on cell membrane and increase the interaction between peptide and major histocompatibility complex (MHC) complex.

Animals from **Figure 4.3.7.1** had shown an inhibition of anti-OVA responses and CD4 T helper cells were immunized and boosted with lipo-OVA₃₂₃₋₃₃₉. Major histocompatibility complex (MHC) binds protein fragments derived from infectious microorganism or agents and displays them for recognition by the miscellaneous T cells.⁴¹⁻⁴³ Antigen specific CD4⁺ T cells are reported to compete for access to the peptide-MHC class II complex on the APCs. OVA₃₂₃₋₃₃₉ peptide can be directly displayed by MHC II complex and present to CD4⁺ T cells by APCs.²⁴⁴⁻²⁴⁷ In this study, we hypothesized that lipo-OVA₃₂₃₋₃₃₉ interacts with MHC II by a hetero-bivalent interaction: the peptide moiety binds to MHC-II while the lipid tail anchors the peptide on DC membrane (**Figure 4.3.8.1C**). We firstly investigated the uptake and biodistribution *in vitro* of amphiphilic peptide on bone marrow dendritic cells (BMDCs) which containing unmaturred APCs. CLSM results showed amphiphilic peptide colocalization to the cell membrane equatorial periphery (**Figure 4.3.8.1A**), indicating a significant portion of the peptide anchored on the membrane surface. Compared with unmodified peptide, flow cytometric analysis of lipo-OVA₃₂₃₋₃₃₉ treated cells exhibited a 10-fold increase in DC uptake (**Figure 4.3.8.1B**) and demonstrated binding to be in a high affinity.

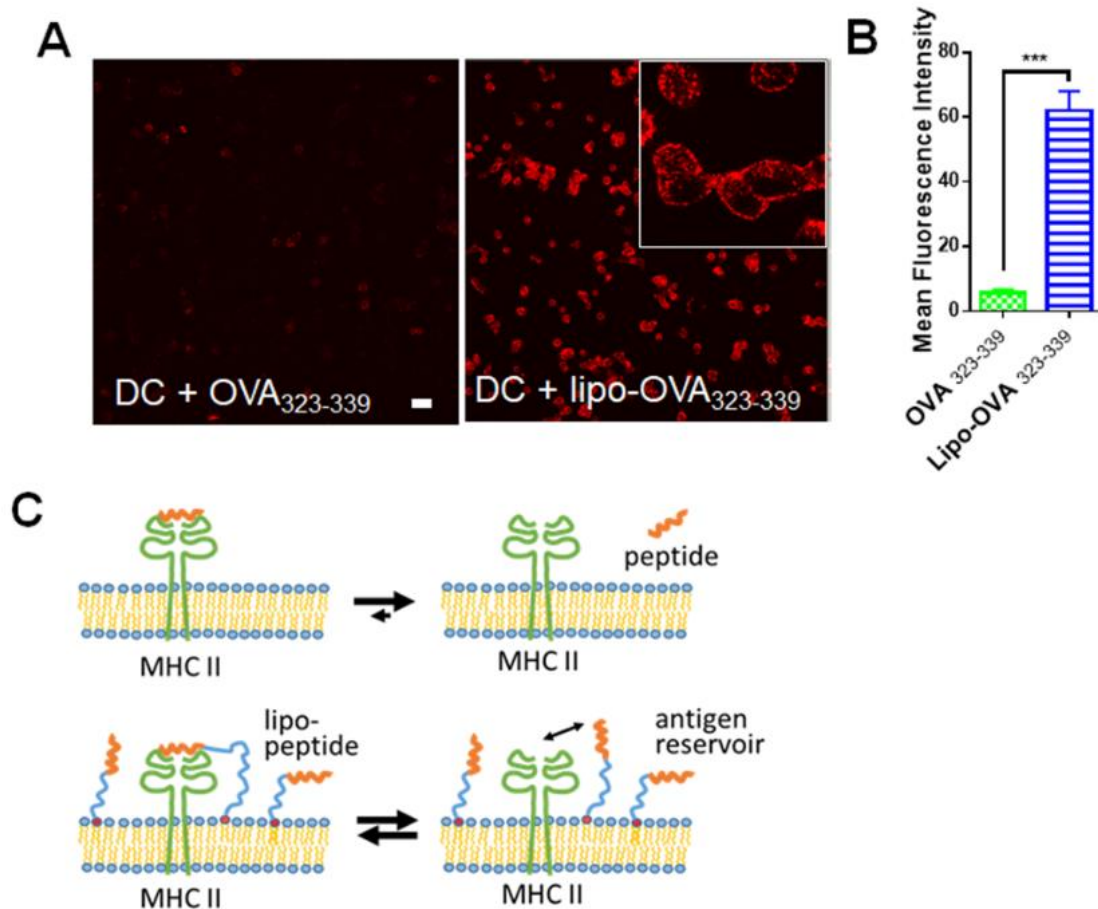


Figure 4.3.8.1 Enhanced interaction of peptide to MHC complex expressed on cell surface of DCs. (A and B) Confocal images (A) and uptake quantifications (B) of BMDCs after 1h incubation with fluorescence dye labeled OVA₃₂₃₋₃₃₉ (A, left) or lipo-OVA₃₂₃₋₃₃₉ (A, right) showing red color on cell membrane equatorial periphery. (C) Schematic illustration showing CD4 lipo-peptide anchors on the cell surface and directly loads onto MHC-II. Unmodified peptide displays transient interaction (low affinity and short half-live) with MHC, resulting in insufficient presentation to T cells (upper panel). In contrast, membrane anchored peptide acts as an antigen reservoir, enhancing the binding and presentation via an additional association with cell membrane. Membrane-anchor enables rebind as peptide and MHC disengage (lower panel). Scale bar = 20 μ m.

4.3.9 Membrane anchored amphiphilic peptide enhances the antigen presentation.

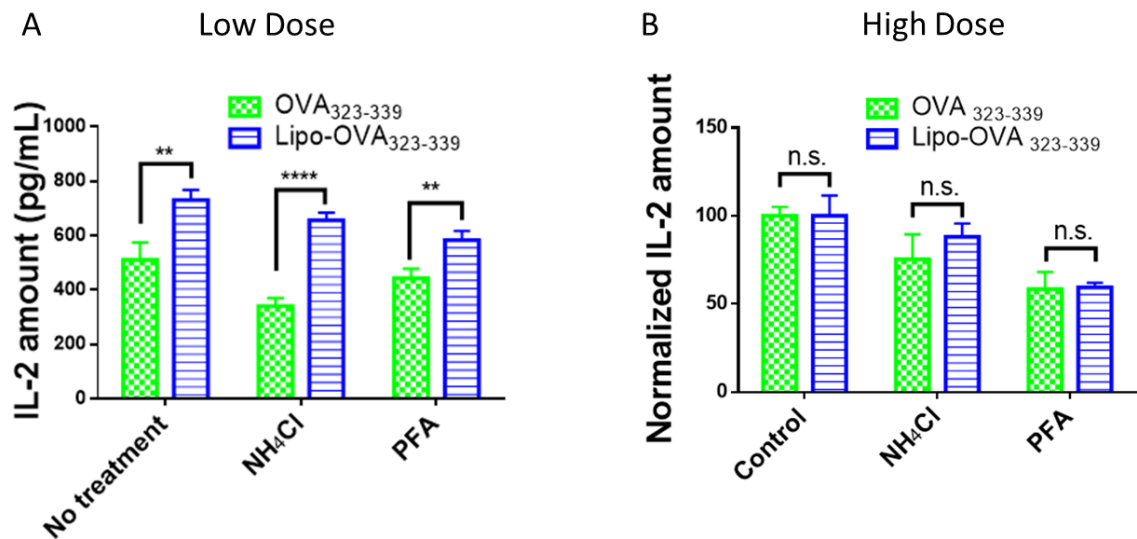


Figure 4.3.9.1 Amphiphilic OVA₃₂₃₋₃₃₉ peptide recognized CD4 epitope and can be presented to T cells without antigen processing. (A and B) BMDCs pre-treated with NH₄Cl, or fixed with paraformaldehyde (PFA), were pulsed with low dose of 2 µg/mL (A) or high dose of 10 µg/mL lipo-OVA₃₂₃₋₃₃₉ (B) or unmodified OVA₃₂₃₋₃₃₉ for 2 h. OT-II T cells were then added and co-cultured for 48 h. IL-2 production were quantified by ELISA measurement of IL-2 production. Data show the mean values ± SEM. *, p < 0.05; **, p < 0.01; ***, p < 0.001; ****, p < 0.0001 by unpaired student's t-test.

Next, we explored the ability of lipo-OVA₃₂₃₋₃₃₉ vaccine to enhance MHC class II antigen presentation by *ex vivo* antigen presentation assay.²⁴⁸⁻²⁴⁹ To suppress the interference, BMDCs were pre-treated with NH₄Cl, or fixed with paraformaldehyde (PFA) for 30 min, washed, and pulsed with (2 µg/mL or 10 µg/mL) lipo-OVA₃₂₃₋₃₃₉ or the same amount of unmodified OVA₃₂₃₋₃₃₉ for another 2 h. Interleukin-2 (IL-2) has a key role in immune system function as promoters of effector T cells and memory T cells when the initial T cell is stimulated.²⁵⁰⁻²⁵² To investigate the capacity of lipo-OVA₃₂₃₋₃₃₉ bound DCs to stimulate OVA-specific naive CD4⁺ T cells, IL-2 production was quantified by enzyme-linked

immunosorbent assay (ELISA) measurement. As shown in **Figure 4.3.9.1A**, with low concentration (2 $\mu\text{g/mL}$, unsaturated) GM-CSF induced BMDCs loaded with lipo-OVA₃₂₃₋₃₃₉ exhibited significantly enhanced activation of OT-II T cells compared with unmodified OVA₃₂₃₋₃₃₉. At higher peptide concentration (10 $\mu\text{g/mL}$) (**Figure 4.3.9.1B**), IL-2 secreting induced by both lipo-OVA₃₂₃₋₃₃₉ and unmodified OVA₃₂₃₋₃₃₉ activated OT-II T cells at similar level indicating the saturated binding capacity. Resulting above suggested that amphiphilic modification did not disrupt the bioactivity of the peptide, including binding epitopes and antigen presentation.

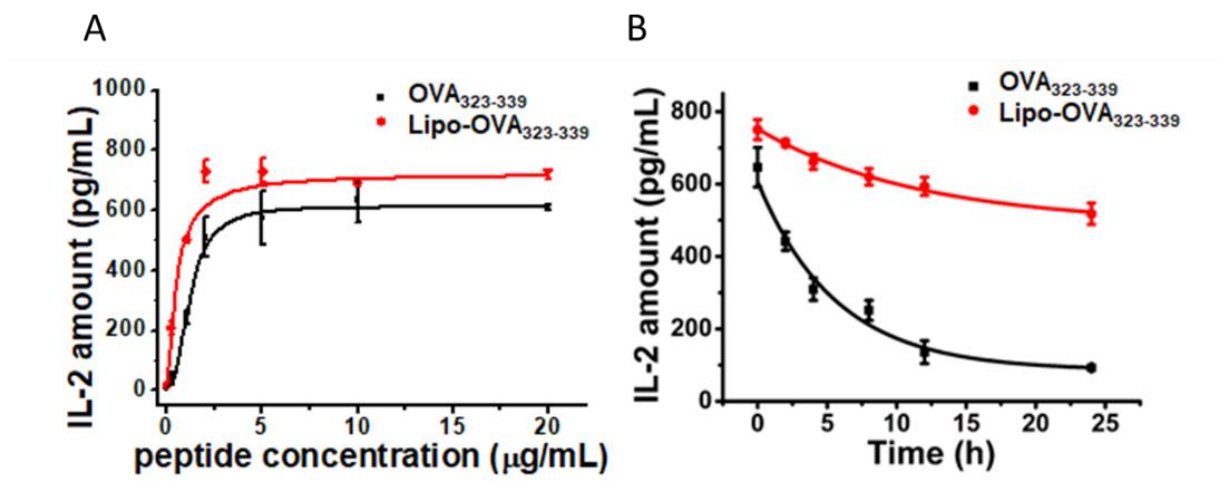


Figure 4.3.9.2 Amphiphilic OVA₃₂₃₋₃₃₉ peptide enhanced antigen presentation to T cells. (A) BMDCs were incubated with different concentrations of lipo-OVA₃₂₃₋₃₃₉, or unmodified OVA₃₂₃₋₃₃₉, washed and co-cultured with OT-II T cells. IL-2 was measured at 48 h. (B) BMDCs were pulsed with 10 $\mu\text{g/mL}$ lipid-OVA₃₂₃₋₃₃₉ or unmodified OVA₃₂₃₋₃₃₉ for 2 h, washed, and cultured for the indicated times to allow peptide/MHC to decay. OT-II T cells were then added and co-cultured for another 48 h. T cell responses to DCs loaded with CD4 epitope were quantified by ELISA measurement of IL-2 productions.

Lack of stability and ability on peptide interaction to MHC class II limited antigen presentation and T cell differentiation.²⁴⁶⁻²⁴⁷ One of the critical challenges on the peptides/ MHC II molecules interaction is that empty molecules quickly lose the affinity to such peptides. Dosage, potency, and stability of peptide/MHC

complex define a cumulative quantity of T cell receptor (TCR) stimulation that governs the initial induction and persistence of peripheral T cell tolerance.^{230, 253-254} To assess the efficacy of membrane-anchored amphiphilic peptide on the potency and duration of peptide presentation, BMDCs were pulsed with low concentrations of lipo-OVA₃₂₃₋₃₃₉, or soluble OVA₃₂₃₋₃₃₉, washed and incubated with OT-II T cells. Cell culture medium were collected at the different time point for IL-2 measurement. Cells treated with lipo-OVA₃₂₃₋₃₃₉ yielded an EC₅₀ at 0.5µg/mL which was 3-fold lower than that of unmodified OVA₃₂₃₋₃₃₉ (1.5 µg/mL) (**Figure 4.3.9.2A**). The potency of peptide stimulation was significantly promoted by lipo-OVA₃₂₃₋₃₃₉.

To test whether membrane-anchored lipo-OVA₃₂₃₋₃₃₉ can prolong the antigen presentation, BMDCs were treated with 10 µg/mL (saturated) lipo-OVA₃₂₃₋₃₃₉ or equivalent amounts of free OVA₃₂₃₋₃₃₉. Cell culture medium were then removed and replace with fresh medium for various time periods during 24 h. OT-II T cells were then added, and antigen presentation was determined by quantification of IL-2 secretion following 48 h co-culture. Displaying of OVA₃₂₃₋₃₃₉ peptide ($t_{1/2} = 37$ h) were sustainable showing 7-fold half-life extension in T-cell stimulation, as compared to DCs pulsed with unmodified OVA₃₂₃₋₃₃₉ ($t_{1/2} = 5$ h) in equal amounts (**Figure 4.3.9.2B**). Due to the transit associating with MHC II, free OVA₃₂₃₋₃₃₉ resulted to 50% less IL-2 release by 5 h and lost >95% a day post peptide incubating. These results indicated that treatment with amphiphilic peptide can enhance peptide presentation to T cells through concentrating antigen displayed on DCs as well as providing a unique hetero-bivalent interaction with

MHC-II: the peptide moiety binds to MHC-II while the lipid tail anchors the peptide on DC membrane.

4.3.10 Albumin-hitchhiking amphiphilic vaccines in animal models of Type 1 Diabetes (T1D).

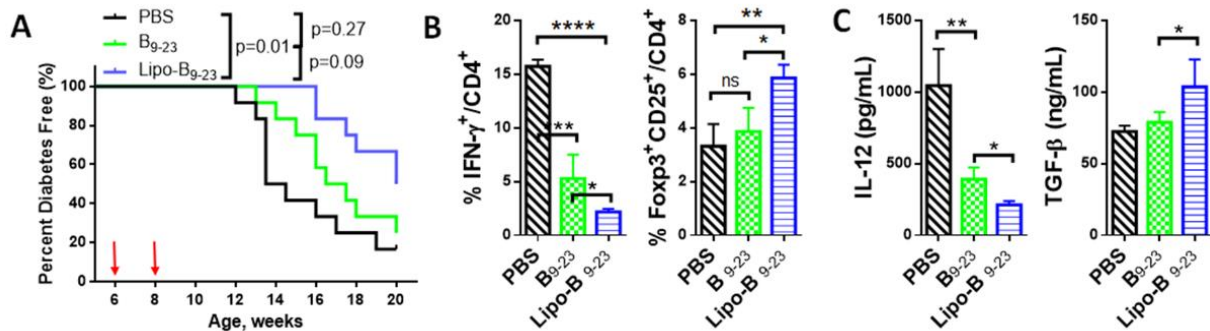


Figure 4.3.10.1 Amphiphilic peptide vaccine protected mice from T-cell induced autoimmune type 1 diabetes at the early period. (A-C) NOD mice were treated with two (on week 6 and 8) s.c. injections of 20 μg B₉₋₂₃ peptide, LN-targeting B₉₋₂₃ peptide (lipo- B₉₋₂₃) or PBS, blood glucose concentrations were monitored. (A) Percentage of diabetic mice (n = 12 for each group, p values were shown by log-rank test). (B) At the age of week 10, percentage of IFN-γ secreting CD4⁺ T cells and Foxp3⁺ CD25⁺ CD4⁺ T cells in blood. (C) At week 10, serum cytokine levels were measured by ELISA.

Among the insulin epitopes recognized by non-obese diabetic (NOD) islet-infiltrating T cells, insulin B chain amino acids 9 to 23 (insulin B: 9–23) is an immunodominant T-cell target peptide that plays a central role in the disease initiation.²⁵⁵⁻²⁵⁶ Subcutaneous injections of B₉₋₂₃ peptide to NOD mice substantially increased the threshold and reduced the incidence of diabetes, by controlling B₉₋₂₃-specific Th1 inflammation responses (i.e., IFN-γ-producing) and inducing Th2 cellular responses.^{2, 257-258} To explore albumin-binding peptide-based deletion of pathogenic T cells in an autoimmune model, we tested the ability of lipo-peptide vaccine to prevent type 1 diabetes using non-obese diabetic mice model.

Amphiphilic insulin B₉₋₂₃ peptide was engineered implementation of our concept. Tolerization with two dosing of free B₉₋₂₃ or lipo-B₉₋₂₃ at the week 6 and 8 of age, the glucose level of mice was performed a long time tracking (>20 weeks) to allow the vaccine to induce autoimmune diabetes. The occurrence of T1D of NOD mice were developed spontaneously at week 12 and shared many symptomatic and pathophysiological features of T1D. Mice treated with either B₉₋₂₃ peptide or amphiphilic B₉₋₂₃ peptide postponed the onset to week 13 and 16, respectively. Flow cytometry analysis on blood lymphocyte at 10 weeks of age indicated that treatment with lipo- B₉₋₂₃ significantly reduced the percentage of B₉₋₂₃ reactive CD4⁺ IFN- γ ⁺ T lymphocytes after B₉₋₂₃ peptide re-stimulation *ex vivo* and increased the frequency of Foxp3 expressing regulatory T cells (**Figure 4.3.10.1B**). These results suggested the lipo-B₉₋₂₃ lowered the incidence of type 1 diabetes through restoring immune tolerance and inhibiting auto-reactive T cell.

Cytokines are crucial mediators of the immune system and necessary for process of the immune response. Interleukin 12 (IL-12) family ^{239, 259} are key cytokines in the promotion of T cell responses which are required for the induction of IFN- γ production and development of Th1 cells. On the contrary, transforming growth factor-beta (TGF- β) is an immunosuppressive cytokine which regulates immune response ²⁶⁰⁻²⁶². To further address the regulatory function and demonstrate our hypothesis, IL-12 and TGF- β in peripheral blood serum were quantified at the age of week 10 of NOD mice. ELISA analysis of blood cytokine showed that following treatment with lipo- B₉₋₂₃, inflammatory IL-12 production was significantly reduced, whereas production of TGF- β was elevated (**Figure**

4.3.10.1C), as compared to animals treated with PBS or unmodified B₉₋₂₃ peptide. These results demonstrated that target peptide autoantigen to DCs in the draining LNs via 'albumin-hitchhiking' supported the induction of tolerogenic mechanisms, delaying the onset and reducing the incidence of T1D in NOD mice.

4.4 Conclusions.

Herein, we have discussed several approaches to restore immune tolerance to prevention autoimmunity: 1) antagonists and its amphiphilic conjugation treatment inhibited activation and proliferation of CTL and induce a global immune tolerance. However, this inhibitory effect was compensated by combination with antigen. 2) Lipid functionalization targets peptide antigen to DCs in the LN by binding and trafficking with endogenous albumin after subcutaneous injection. More importantly, lipid functionalization markedly enhanced peptide presentation by a unique bivalent interaction with MHC II molecules on cell surface. This approach might be applicable for diseases other than T1D, where efficient antigen presentation is needed.

Chapter 5. Conclusions and Future Perspectives.

Self-delivery drug amphiphiles represent a simple yet effective approach designed to overcome the various biological barriers for drug delivery without the need for exogenous carriers. The ability to program the molecular structures and the physicochemical properties, which controls the interactions between the drug amphiphiles and their biological surroundings has attracted significant research interests. In fact, several of the drug amphiphiles have been approved by FDA and more have reached the clinical testing stage. Despite tremendous progress made in the field, many challenges remain. The delivery challenges include: 1) lack of mechanisms for active targeting. Instead of ligand-receptor mediated targeting, the drug amphiphiles accumulate in tumor or inflammatory tissues by passive targeting (EPR effect)^c, such passive targeting approach is limited due to the heterogeneous nature of the diseases. The overall delivery efficiency of nanoparticle cancer drugs (by EPR effect) is low—only a median of 0.7% of the injected dose retained in the tumor. 2) lack of chemistry to precisely control the drug release. The linker design must integrate the pharmaceutical performance, systemic stability, and overall drug physicochemical properties. However, designing an ideal linker with all above key attributes remains difficult, in many cases where the drugs need to be released, premature or over-delayed release profiles are often observed. Additionally, the structure and functional impacts of non-cleavable modification cannot be overlooked; 3), lack of design mechanisms to guide the intracellular trafficking and retention. Although lipids are constantly sorted and transported within the cells, the exact trafficking mechanisms and specific organelle accumulation remains largely

unknown. Drug conjugation further complicates the process because of the intracellular protein binding and trafficking of drug molecule.

As we gain more knowledge toward the fundamental aspect of diseases, new drug amphiphiles and novel design principles will emerge in the future. Next generation drug amphiphiles are expected to overcome these challenges, enabling structure-based rational design and optimization.

References

- (1) Maiti, K. K.; Lee, W. S.; Takeuchi, T.; Watkins, C.; Fretz, M.; Kim, D. C.; Futaki, S.; Jones, A.; Kim, K. T.; Chung, S. K. Guanidine-Containing Molecular Transporters: Sorbitol-Based Transporters Show High Intracellular Selectivity toward Mitochondria. *Angewandte Chemie* **2007**, *119* (31), 5984-5988.
- (2) Shoda, L. K.; Young, D. L.; Ramanujan, S.; Whiting, C. C.; Atkinson, M. A.; Bluestone, J. A.; Eisenbarth, G. S.; Mathis, D.; Rossini, A. A.; Campbell, S. E.; Kahn, R.; Kreuwel, H. T. A comprehensive review of interventions in the NOD mouse and implications for translation. *Immunity* **2005**, *23* (2), 115-26, DOI: 10.1016/j.immuni.2005.08.002.
- (3) Nedoszytko, B.; Sokolowska-Wojdylo, M.; Renke, J.; Lange, M.; Trzonkowski, P.; Sobjanek, M.; Szczerkowska-Dobosz, A.; Niedozytko, M.; Gorska, A.; Romantowski, J.; Skokowski, J.; Kalinowski, L.; Nowicki, R. J. The role of regulatory T cells and genes involved in their differentiation in pathogenesis of selected inflammatory and neoplastic skin diseases. Part III: Polymorphisms of genes involved in Tregs' activation and function. *Postepy Dermatol Alergol* **2017**, *34* (6), 517-525, DOI: 10.5114/pdia.2017.67053.
- (4) Zacche, M. M.; Srikrishna, S.; Cardozo, L. Novel targeted bladder drug-delivery systems: a review. *Res Rep Urol* **2015**, *7*, 169-78, DOI: 10.2147/RRU.S56168.
- (5) Jeschek, D.; Lhota, G.; Wallner, J.; Vorauer-Uhl, K. A versatile, quantitative analytical method for pharmaceutical relevant lipids in drug delivery systems. *J Pharm Biomed Anal* **2016**, *119*, 37-44, DOI: 10.1016/j.jpba.2015.11.020.

- (6) Odeberg, J. M.; Kaufmann, P.; Kroon, K. G.; Hoglund, P. Lipid drug delivery and rational formulation design for lipophilic drugs with low oral bioavailability, applied to cyclosporine. *Eur J Pharm Sci* **2003**, *20* (4-5), 375-82.
- (7) Misra, A.; Ganesh, S.; Shahiwala, A.; Shah, S. P. Drug delivery to the central nervous system: a review. *J Pharm Pharm Sci* **2003**, *6* (2), 252-73.
- (8) Yeom, D. W.; Son, H. Y.; Kim, J. H.; Kim, S. R.; Lee, S. G.; Song, S. H.; Chae, B. R.; Choi, Y. W. Development of a solidified self-microemulsifying drug delivery system (S-SMEDDS) for atorvastatin calcium with improved dissolution and bioavailability. *Int J Pharm* **2016**, *506* (1-2), 302-11, DOI: 10.1016/j.ijpharm.2016.04.059.
- (9) Yoo, J.; Baskaran, R.; Yoo, B. K. Self-nanoemulsifying drug delivery system of lutein: physicochemical properties and effect on bioavailability of warfarin. *Biomol Ther (Seoul)* **2013**, *21* (2), 173-9, DOI: 10.4062/biomolther.2013.011.
- (10) Zhu, J. X.; Tang, D.; Feng, L.; Zheng, Z. G.; Wang, R. S.; Wu, A. G.; Duan, T. T.; He, B.; Zhu, Q. Development of self-microemulsifying drug delivery system for oral bioavailability enhancement of berberine hydrochloride. *Drug Dev Ind Pharm* **2013**, *39* (3), 499-506, DOI: 10.3109/03639045.2012.683875.
- (11) Datta, S.; Jutkova, A.; Sramkova, P.; Lenkavska, L.; Huntosova, V.; Chorvat, D.; Miskovsky, P.; Jancura, D.; Kronek, J. Unravelling the Excellent Chemical Stability and Bioavailability of Solvent Responsive Curcumin-Loaded 2-Ethyl-2-oxazoline-graft-2-(4-dodecyloxyphenyl)-2-oxazoline Copolymer Nanoparticles for Drug Delivery. *Biomacromolecules* **2018**, *19* (7), 2459-2471, DOI: 10.1021/acs.biomac.8b00057.

- (12) Elgart, A.; Cherniakov, I.; Aldouby, Y.; Domb, A. J.; Hoffman, A. Improved oral bioavailability of BCS class 2 compounds by self nano-emulsifying drug delivery systems (SNEDDS): the underlying mechanisms for amiodarone and talinolol. *Pharm Res* **2013**, *30* (12), 3029-44, DOI: 10.1007/s11095-013-1063-y.
- (13) Ghaderi, S.; Ramesh, B.; Seifalian, A. M. Fluorescence nanoparticles "quantum dots" as drug delivery system and their toxicity: a review. *J Drug Target* **2011**, *19* (7), 475-86, DOI: 10.3109/1061186X.2010.526227.
- (14) Arias, J. L. Liposomes in drug delivery: a patent review (2007 - present). *Expert Opin Ther Pat* **2013**, *23* (11), 1399-414, DOI: 10.1517/13543776.2013.828035.
- (15) Accardo, A.; Morelli, G. Review peptide-targeted liposomes for selective drug delivery: Advantages and problematic issues. *Biopolymers* **2015**, *104* (5), 462-79, DOI: 10.1002/bip.22678.
- (16) Matteucci, M. L.; Thrall, D. E. The role of liposomes in drug delivery and diagnostic imaging: a review. *Vet Radiol Ultrasound* **2000**, *41* (2), 100-7.
- (17) Zhang, S.; Guan, J.; Sun, M.; Zhang, D.; Zhang, H.; Sun, B.; Guo, W.; Lin, B.; Wang, Y.; He, Z.; Luo, C.; Sun, J. Self-delivering prodrug-nanoassemblies fabricated by disulfide bond bridged oleate prodrug of docetaxel for breast cancer therapy. *Drug Deliv* **2017**, *24* (1), 1460-1469, DOI: 10.1080/10717544.2017.1381201.
- (18) Janesirisakule, S.; Sinthusake, T.; Wanichwecharungruang, S. Nanocarrier with self-antioxidative property for stabilizing and delivering ascorbyl palmitate into skin. *J Pharm Sci* **2013**, *102* (8), 2770-9, DOI: 10.1002/jps.23641.

(19) Janjic, J. M.; Srinivas, M.; Kadayakkara, D. K.; Ahrens, E. T. Self-delivering nanoemulsions for dual fluorine-19 MRI and fluorescence detection. *J Am Chem Soc* **2008**, *130* (9), 2832-41, DOI: 10.1021/ja077388j.

(20) Odland, J. O.; Nieboer, E.; Romanova, N.; Thomassen, Y.; Brox, J.; Lund, E. Self-reported ethnic status of delivering women, newborn body mass index, blood or urine concentrations of toxic metals, and essential elements in sera of Norwegian and Russian Arctic populations. *Int J Circumpolar Health* **1999**, *58* (1), 4-13.

(21) Li, Y.; Li, Y.; Ji, W.; Lu, Z.; Liu, L.; Shi, Y.; Ma, G.; Zhang, X. Positively Charged Polyprodrug Amphiphiles with Enhanced Drug Loading and Reactive Oxygen Species-Responsive Release Ability for Traceable Synergistic Therapy. *J Am Chem Soc* **2018**, *140* (11), 4164-4171, DOI: 10.1021/jacs.8b01641.

(22) Huang, Z.; Zhao, D. M.; Deng, X.; Zhang, J.; Zhang, Y. M.; Yu, X. Q. Functionalized Asymmetric Bola-Type Amphiphiles for Efficient Gene and Drug Delivery. *Nanomaterials (Basel)* **2018**, *8* (2), DOI: 10.3390/nano8020115.

(23) Shi, Y.; Li, H.; Cheng, J.; Luan, T.; Liu, D.; Cao, Y.; Zhang, X.; Wei, H.; Liu, Y.; Zhao, G. Entirely oligosaccharide-based supramolecular amphiphiles constructed via host-guest interactions as efficient drug delivery platforms. *Chem Commun (Camb)* **2017**, *53* (91), 12302-12305, DOI: 10.1039/c7cc06553a.

(24) Ludvigsson, J.; Wahlberg, J.; Casas, R. Intralymphatic injection of autoantigen in type 1 diabetes. *New England Journal of Medicine* **2017**, *376* (7), 697-699.

(25) Kinoshita, R.; Ishima, Y.; Chuang, V. T. G.; Nakamura, H.; Fang, J.; Watanabe, H.; Shimizu, T.; Okuhira, K.; Ishida, T.; Maeda, H.; Otagiri, M.; Maruyama, T.

Improved anticancer effects of albumin-bound paclitaxel nanoparticle via augmentation of EPR effect and albumin-protein interactions using S-nitrosated human serum albumin dimer. *Biomaterials* **2017**, *140*, 162-169, DOI: 10.1016/j.biomaterials.2017.06.021.

(26) Ishima, Y.; Chen, D.; Fang, J.; Maeda, H.; Minomo, A.; Kragh-Hansen, U.; Kai, T.; Maruyama, T.; Otagiri, M. S-Nitrosated human serum albumin dimer is not only a novel anti-tumor drug but also a potentiator for anti-tumor drugs with augmented EPR effects. *Bioconjug Chem* **2012**, *23* (2), 264-71, DOI: 10.1021/bc2005363.

(27) Gallez, B.; De Keyser, J. L.; Debuyst, R.; Dejehet, F.; Neuvens, L.; Dumont, P. The effects of pasteurisation on albumin: an EPR binding assay for polymeric albumin. *J Pharm Biomed Anal* **1995**, *13* (12), 1449-52, DOI: 10.1016/0731-7085(95)01586-8.

(28) Alexander, P.; Kucera, G.; Pardee, T. S. Improving nucleoside analogs via lipid conjugation: Is fatter any better? *Critical reviews in oncology/hematology* **2016**, *100*, 46-56, DOI: 10.1016/j.critrevonc.2016.01.015.

(29) Stephanopoulos, N.; Francis, M. B. Choosing an effective protein bioconjugation strategy. *Nature chemical biology* **2011**, *7* (12), 876-84, DOI: 10.1038/nchembio.720.

(30) Tsuchikama, K.; An, Z. Antibody-drug conjugates: recent advances in conjugation and linker chemistries. *Protein & cell* **2018**, *9* (1), 33-46, DOI: 10.1007/s13238-016-0323-0.

- (31) Taresco, V.; Alexander, C.; Singh, N.; Pearce, A. K. Stimuli-Responsive Prodrug Chemistries for Drug Delivery. *Advanced Therapeutics* **2018**, *1* (4), 1800030, DOI: 10.1002/adtp.201800030.
- (32) Mura, S.; Nicolas, J.; Couvreur, P. Stimuli-responsive nanocarriers for drug delivery. *Nature Materials* **2013**, *12*, 991, DOI: 10.1038/nmat3776.
- (33) Pearson D, L. H. Conjugates toward medicines. *J Pharmacol Med Chem* **2007**, *1* (1), 32-39.
- (34) Liu, H.; Zhu, Z.; Kang, H.; Wu, Y.; Sefan, K.; Tan, W. DNA-based micelles: synthesis, micellar properties and size-dependent cell permeability. *Chemistry (Weinheim an der Bergstrasse, Germany)* **2010**, *16* (12), 3791-7, DOI: 10.1002/chem.200901546.
- (35) Liu, H.; Moynihan, K. D.; Zheng, Y.; Szeto, G. L.; Li, A. V.; Huang, B.; Van Egeren, D. S.; Park, C.; Irvine, D. J. Structure-based programming of lymph-node targeting in molecular vaccines. *Nature* **2014**, *507* (7493), 519-22, DOI: 10.1038/nature12978.
- (36) Xiong, X.; Liu, H.; Zhao, Z.; Altman, M. B.; Lopez-Colon, D.; Yang, C. J.; Chang, L. J.; Liu, C.; Tan, W. DNA aptamer-mediated cell targeting. *Angewandte Chemie (International ed. in English)* **2013**, *52* (5), 1472-6, DOI: 10.1002/anie.201207063.
- (37) Liu, H.; Kwong, B.; Irvine, D. J. Membrane Anchored Immunostimulatory Oligonucleotides for In Vivo Cell Modification and Localized Immunotherapy. **2011**, *50* (31), 7052-7055, DOI: 10.1002/anie.201101266.

- (38) Choi, H. S.; Liu, W.; Misra, P.; Tanaka, E.; Zimmer, J. P.; Iyiti Ipe, B.; Bawendi, M. G.; Frangioni, J. V. Renal clearance of quantum dots. *Nature biotechnology* **2007**, *25* (10), 1165-70, DOI: 10.1038/nbt1340.
- (39) Strober, W.; Mogielnicki, R. P.; Waldmann, T. A. The role of the kidney in the metabolism of serum proteins. *Ciba Foundation symposium* **1972**, *9*, 25-45.
- (40) Lorber, B.; Fischer, F.; Bailly, M.; Roy, H.; Kern, D. Protein analysis by dynamic light scattering: Methods and techniques for students. **2012**, *40* (6), 372-382, DOI: 10.1002/bmb.20644.
- (41) Poulsen, H. L. Interstitial fluid concentrations of albumin and immunoglobulin G in normal men. *Scandinavian journal of clinical and laboratory investigation* **1974**, *34* (2), 119-22.
- (42) Chaudhury, C.; Mehnaz, S.; Robinson, J. M.; Hayton, W. L.; Pearl, D. K.; Roopenian, D. C.; Anderson, C. L. The major histocompatibility complex-related Fc receptor for IgG (FcRn) binds albumin and prolongs its lifespan. *The Journal of experimental medicine* **2003**, *197* (3), 315-22.
- (43) Prabhakar, U.; Maeda, H.; Jain, R. K.; Sevick-Muraca, E. M.; Zamboni, W.; Farokhzad, O. C.; Barry, S. T.; Gabizon, A.; Grodzinski, P.; Blakey, D. C. Challenges and key considerations of the enhanced permeability and retention effect for nanomedicine drug delivery in oncology. *Cancer research* **2013**, *73* (8), 2412-7, DOI: 10.1158/0008-5472.Can-12-4561.
- (44) Wunder, A.; Muller-Ladner, U.; Stelzer, E. H.; Funk, J.; Neumann, E.; Stehle, G.; Pap, T.; Sinn, H.; Gay, S.; Fiehn, C. Albumin-based drug delivery as novel

therapeutic approach for rheumatoid arthritis. *Journal of immunology (Baltimore, Md. : 1950)* **2003**, 170 (9), 4793-801.

(45) Date, T.; Paul, K.; Singh, N.; Jain, S. Drug-Lipid Conjugates for Enhanced Oral Drug Delivery. *AAPS PharmSciTech* **2019**, 20 (2), 41, DOI: 10.1208/s12249-018-1272-0.

(46) Taylor, M. D. Improved passive oral drug delivery via prodrugs. *Advanced Drug Delivery Reviews* **1996**, 19 (2), 131-148, DOI: [https://doi.org/10.1016/0169-409X\(95\)00104-F](https://doi.org/10.1016/0169-409X(95)00104-F).

(47) Guimaraes, M.; Stelova, M.; Holm, R.; Reppas, C.; Symillides, M.; Vertzoni, M.; Fotaki, N. Biopharmaceutical considerations in paediatrics with a view to the evaluation of orally administered drug products - a PEARRL review. *J Pharm Pharmacol* **2019**, 71 (4), 603-642, DOI: 10.1111/jphp.12955.

(48) Kakkar, V.; Verma, M. K.; Saini, K.; Kaur, I. P. Nano Drug Delivery in Treatment of Oral Cancer, A Review of the Literature. *Curr Drug Targets* **2019**, 20 (10), 1008-1017, DOI: 10.2174/1389450120666190319125734.

(49) Sarma, H.; Jahan, T.; Sharma, H. K. Progress in Drug and Formulation Development for the Chemoprevention of Oral Squamous Cell Carcinoma: A Review. *Recent Pat Drug Deliv Formul* **2019**, 13 (1), 16-36, DOI: 10.2174/1872211313666190222182824.

(50) Yáñez, J.; Wang, S.; W Knemeyer, I.; A Wirth, M.; Alton, K. *Intestinal lymphatic transport for drug delivery*, 2011; Vol. 63, p 923-42.

(51) Trevaskis, N. L.; Kaminskas, L. M.; Porter, C. J. From sewer to saviour - targeting the lymphatic system to promote drug exposure and activity. *Nat Rev Drug Discov* **2015**, *14* (11), 781-803, DOI: 10.1038/nrd4608.

(52) Meng, Y.; Pople, C. B.; Lea-Banks, H.; Abrahao, A.; Davidson, B.; Suppiah, S.; Vecchio, L. M.; Samuel, N.; Mahmud, F.; Hynynen, K.; Hamani, C.; Lipsman, N. Safety and efficacy of focused ultrasound induced blood-brain barrier opening, an integrative review of animal and human studies. *J Control Release* **2019**, *309*, 25-36, DOI: 10.1016/j.jconrel.2019.07.023.

(53) Thrippleton, M. J.; Backes, W. H.; Sourbron, S.; Ingrisch, M.; van Osch, M. J. P.; Dichgans, M.; Fazekas, F.; Ropele, S.; Frayne, R.; van Oostenbrugge, R. J.; Smith, E. E.; Wardlaw, J. M. Quantifying blood-brain barrier leakage in small vessel disease: Review and consensus recommendations. *Alzheimers Dement* **2019**, *15* (6), 840-858, DOI: 10.1016/j.jalz.2019.01.013.

(54) Cervos-Navarro, J.; Kannuki, S.; Nakagawa, Y. Blood-brain barrier (BBB). Review from morphological aspect. *Histol Histopathol* **1988**, *3* (2), 203-13.

(55) Zhang, R.; Qin, X.; Kong, F.; Chen, P.; Pan, G. Improving cellular uptake of therapeutic entities through interaction with components of cell membrane. *Drug Deliv* **2019**, *26* (1), 328-342, DOI: 10.1080/10717544.2019.1582730.

(56) Perlikowska, R.; Janecka, A. Bioavailability of endomorphins and the blood-brain barrier--a review. *Med Chem* **2014**, *10* (1), 2-17.

(57) Borodinov, N.; Gil, D.; Savchak, M.; Gross, C. E.; Yadavalli, N. S.; Ma, R.; Tsukruk, V. V.; Minko, S.; Vertegel, A.; Luzinov, I. En Route to Practicality of the Polymer Grafting Technology: One-Step Interfacial Modification with Amphiphilic

Molecular Brushes. *ACS Appl Mater Interfaces* **2018**, *10* (16), 13941-13952, DOI: 10.1021/acsami.7b19815.

(58) Dubes, A.; Moudrakovski, I. L.; Shahgaldian, P.; Coleman, A. W.; Ratcliffe, C. I.; Ripmeester, J. A. Distribution and modification of sorption sites in amphiphilic calixarene-based solid lipid nanoparticles from hyperpolarized ^{129}Xe NMR spectroscopy. *J Am Chem Soc* **2004**, *126* (20), 6236-7, DOI: 10.1021/ja038653d.

(59) Fang, W.; Linder, M. B.; Laaksonen, P. Modification of carbon nanotubes by amphiphilic glycosylated proteins. *J Colloid Interface Sci* **2018**, *512*, 318-324, DOI: 10.1016/j.jcis.2017.10.034.

(60) Gao, L.; Tang, Y.; Wang, C.; Yao, L.; Zhang, J.; Gao, R.; Tang, X.; Chong, T.; Zhang, H. Highly-efficient amphiphilic magnetic nanocomposites based on a simple sol-gel modification for adsorption of phthalate esters. *J Colloid Interface Sci* **2019**, *552*, 142-152, DOI: 10.1016/j.jcis.2019.05.031.

(61) Torchilin, V. P.; Levchenko, T. S.; Whiteman, K. R.; Yaroslavov, A. A.; Tsatsakis, A. M.; Rizos, A. K.; Michailova, E. V.; Shtilman, M. I. Amphiphilic poly-N-vinylpyrrolidones: synthesis, properties and liposome surface modification. *Biomaterials* **2001**, *22* (22), 3035-44, DOI: 10.1016/s0142-9612(01)00050-3.

(62) Zheng, G.; Zhang, Q.; Cha, J. J.; Yang, Y.; Li, W.; Seh, Z. W.; Cui, Y. Amphiphilic surface modification of hollow carbon nanofibers for improved cycle life of lithium sulfur batteries. *Nano Lett* **2013**, *13* (3), 1265-70, DOI: 10.1021/nl304795g.

(63) Nuttall, M. E.; Lee, J. C.; Murdock, P. R.; Badger, A. M.; Wang, F. L.; Laydon, J. T.; Hofmann, G. A.; Pettman, G. R.; Lee, J. A.; Parihar, A.; Van Wagenen, B. C.;

Fox, J.; Gowen, M.; Johnson, R. K.; Mattern, M. R. Amphibian Melanophore Technology as a Functional Screen for Antagonists of G-Protein Coupled 7-Transmembrane Receptors. *J Biomol Screen* **1999**, *4* (5), 269-278, DOI: 10.1177/108705719900400508.

(64) Pardo, L.; Ballesteros, J. A.; Osman, R.; Weinstein, H. On the use of the transmembrane domain of bacteriorhodopsin as a template for modeling the three-dimensional structure of guanine nucleotide-binding regulatory protein-coupled receptors. *Proc Natl Acad Sci U S A* **1992**, *89* (9), 4009-12, DOI: 10.1073/pnas.89.9.4009.

(65) Kong, H.; Boulter, J.; Weber, J. L.; Lai, C.; Chao, M. V. An evolutionarily conserved transmembrane protein that is a novel downstream target of neurotrophin and ephrin receptors. *J Neurosci* **2001**, *21* (1), 176-85.

(66) Rajendran, L.; Knölker, H.-J.; Simons, K. Subcellular targeting strategies for drug design and delivery. *Nat Rev Drug Discov* **2010**, *9*, 29, DOI: 10.1038/nrd2897.

(67) Soutschek, J.; Akinc, A.; Bramlage, B.; Charisse, K.; Constien, R.; Donoghue, M.; Elbashir, S.; Geick, A.; Hadwiger, P.; Harborth, J.; John, M.; Kesavan, V.; Lavine, G.; Pandey, R. K.; Racie, T.; Rajeev, K. G.; Rohl, I.; Toudjarska, I.; Wang, G.; Wuschko, S.; Bumcrot, D.; Koteliansky, V.; Limmer, S.; Manoharan, M.; Vornlocher, H. P. Therapeutic silencing of an endogenous gene by systemic administration of modified siRNAs. *Nature* **2004**, *432* (7014), 173-8, DOI: 10.1038/nature03121.

(68) Akinc, A.; Zumbuehl, A.; Goldberg, M.; Leshchiner, E. S.; Busini, V.; Hossain, N.; Bacallado, S. A.; Nguyen, D. N.; Fuller, J.; Alvarez, R.; Borodovsky, A.; Borland,

T.; Constien, R.; de Fougerolles, A.; Dorkin, J. R.; Narayanannair Jayaprakash, K.; Jayaraman, M.; John, M.; Koteliansky, V.; Manoharan, M.; Nechev, L.; Qin, J.; Racie, T.; Raitcheva, D.; Rajeev, K. G.; Sah, D. W.; Soutschek, J.; Toudjarska, I.; Vornlocher, H. P.; Zimmermann, T. S.; Langer, R.; Anderson, D. G. A combinatorial library of lipid-like materials for delivery of RNAi therapeutics. *Nature biotechnology* **2008**, 26 (5), 561-9, DOI: 10.1038/nbt1402.

(69) Selvam, C.; Mutisya, D.; Prakash, S.; Ranganna, K.; Thilagavathi, R. Therapeutic potential of chemically modified siRNA: Recent trends. *Chemical biology & drug design* **2017**, 90 (5), 665-678, DOI: 10.1111/cbdd.12993.

(70) Ding, Y.; Wang, Y.; Zhou, J.; Gu, X.; Wang, W.; Liu, C.; Bao, X.; Wang, C.; Li, Y.; Zhang, Q. Direct cytosolic siRNA delivery by reconstituted high density lipoprotein for target-specific therapy of tumor angiogenesis. *Biomaterials* **2014**, 35 (25), 7214-27, DOI: 10.1016/j.biomaterials.2014.05.009.

(71) Alexander, R. L.; Greene, B. T.; Torti, S. V.; Kucera, G. L. A novel phospholipid gemcitabine conjugate is able to bypass three drug-resistance mechanisms. *Cancer chemotherapy and pharmacology* **2005**, 56 (1), 15-21, DOI: 10.1007/s00280-004-0949-0.

(72) Chhikara, B. S.; Mandal, D.; Parang, K. Synthesis, anticancer activities, and cellular uptake studies of lipophilic derivatives of doxorubicin succinate. *Journal of medicinal chemistry* **2012**, 55 (4), 1500-10, DOI: 10.1021/jm201653u.

(73) Xi, J.; Li, M.; Jing, B.; An, M.; Yu, C.; Pinnock, C. B.; Zhu, Y.; Lam, M. T.; Liu, H. Long-Circulating Amphiphilic Doxorubicin for Tumor Mitochondria-Specific

Targeting. *ACS Applied Materials & Interfaces* **2018**, *10* (50), 43482-43492, DOI: 10.1021/acsami.8b17399.

(74) xi, J.; Li, M.; Jing, B.; An, M.; Yu, C.; B. Pinnock, C.; Zhu, Y.; T. Lam, M.; Liu, H. *Long-Circulating Amphiphilic Doxorubicin for Tumor Mitochondria-Specific Targeting*, 2018; Vol. 10.

(75) Irby, D.; Du, C.; Li, F. Lipid-Drug Conjugate for Enhancing Drug Delivery. *Molecular pharmaceuticals* **2017**, *14* (5), 1325-1338, DOI: 10.1021/acs.molpharmaceut.6b01027.

(76) Yu, C.; An, M.; Li, M.; Liu, H. Immunostimulatory Properties of Lipid Modified CpG Oligonucleotides. *Mol Pharm* **2017**, *14* (8), 2815-2823, DOI: 10.1021/acs.molpharmaceut.7b00335.

(77) Yu, C.; An, M.; Jones, E.; Liu, H. Targeting Suppressive Oligonucleotide to Lymph Nodes Inhibits Toll-like Receptor-9-Mediated Activation of Adaptive Immunity. *Pharmaceutical research* **2018**, *35* (3), 56, DOI: 10.1007/s11095-018-2344-2.

(78) Hendricks, M. P.; Sato, K.; Palmer, L. C.; Stupp, S. I. J. A. o. c. r. Supramolecular assembly of peptide amphiphiles. **2017**, *50* (10), 2440-2448.

(79) Hamley, I. W. J. C. c. Lipopeptides: from self-assembly to bioactivity. **2015**, *51* (41), 8574-8583.

(80) Cui, H.; Webber, M. J.; Stupp, S. I. Self-assembly of peptide amphiphiles: from molecules to nanostructures to biomaterials. *Biopolymers* **2010**, *94* (1), 1-18, DOI: 10.1002/bip.21328.

- (81) Hutchinson, J. A.; Burholt, S.; Hamley, I. W. Peptide hormones and lipopeptides: from self-assembly to therapeutic applications. *Journal of peptide science : an official publication of the European Peptide Society* **2017**, *23* (2), 82-94, DOI: 10.1002/psc.2954.
- (82) Raaijmakers, J. M.; De Bruijn, I.; Nybroe, O.; Ongena, M. J. F. m. r. Natural functions of lipopeptides from *Bacillus* and *Pseudomonas*: more than surfactants and antibiotics. **2010**, *34* (6), 1037-1062.
- (83) Humphries, R. M.; Pollett, S.; Sakoulas, G. J. C. m. r. A current perspective on daptomycin for the clinical microbiologist. **2013**, *26* (4), 759-780.
- (84) Taylor, S. D.; Palmer, M. The action mechanism of daptomycin. *Bioorganic & medicinal chemistry* **2016**, *24* (24), 6253-6268, DOI: 10.1016/j.bmc.2016.05.052.
- (85) Kirkham, S.; Castelletto, V.; Hamley, I. W.; Inoue, K.; Rambo, R.; Reza, M.; Ruokolainen, J. Self-Assembly of the Cyclic Lipopeptide Daptomycin: Spherical Micelle Formation Does Not Depend on the Presence of Calcium Chloride. *Chemphyschem : a European journal of chemical physics and physical chemistry* **2016**, *17* (14), 2118-22, DOI: 10.1002/cphc.201600308.
- (86) Dvorchik, B. H.; Brazier, D.; DeBruin, M. F.; Arbeit, R. D. J. A. a.; chemotherapy. Daptomycin pharmacokinetics and safety following administration of escalating doses once daily to healthy subjects. **2003**, *47* (4), 1318-1323.
- (87) Benvenuto, M.; Benziger, D. P.; Yankelev, S.; Vigliani, G. J. A. a.; chemotherapy. Pharmacokinetics and tolerability of daptomycin at doses up to 12 milligrams per kilogram of body weight once daily in healthy volunteers. **2006**, *50* (10), 3245-3249.

- (88) Cafini, F.; Aguilar, L.; Gonzalez, N.; Gimenez, M.; Torrico, M.; Alou, L.; Sevellano, D.; Vallejo, P.; Prieto, J. J. J. o. a. c. In vitro effect of the presence of human albumin or human serum on the bactericidal activity of daptomycin against strains with the main resistance phenotypes in Gram-positives. **2007**, *59* (6), 1185-1189.
- (89) Spreghini, E.; Orlando, F.; Sanguinetti, M.; Posteraro, B.; Giannini, D.; Manso, E.; Barchiesi, F. Comparative effects of micafungin, caspofungin, and anidulafungin against a difficult-to-treat fungal opportunistic pathogen, *Candida glabrata*. *Antimicrobial agents and chemotherapy* **2012**, *56* (3), 1215-22, DOI: 10.1128/aac.05872-11.
- (90) Ingallinella, P.; Bianchi, E.; Ladwa, N. A.; Wang, Y. J.; Hrin, R.; Veneziano, M.; Bonelli, F.; Ketas, T. J.; Moore, J. P.; Miller, M. D.; Pessi, A. Addition of a cholesterol group to an HIV-1 peptide fusion inhibitor dramatically increases its antiviral potency. *Proc Natl Acad Sci U S A* **2009**, *106* (14), 5801-6, DOI: 10.1073/pnas.0901007106.
- (91) Hollmann, A.; Matos, P. M.; Augusto, M. T.; Castanho, M. A.; Santos, N. C. Conjugation of cholesterol to HIV-1 fusion inhibitor C34 increases peptide-membrane interactions potentiating its action. *PLoS One* **2013**, *8* (4), e60302, DOI: 10.1371/journal.pone.0060302.
- (92) Chong, H.; Xue, J.; Xiong, S.; Cong, Z.; Ding, X.; Zhu, Y.; Liu, Z.; Chen, T.; Feng, Y.; He, L.; Guo, Y.; Wei, Q.; Zhou, Y.; Qin, C.; He, Y. A Lipopeptide HIV-1/2 Fusion Inhibitor with Highly Potent *In Vitro*, *Ex Vivo*, and

In Vivo Antiviral Activity. **2017**, *91* (11), e00288-17, DOI: 10.1128/JVI.00288-17 %J Journal of Virology.

(93) Liu, H.; Irvine, D. J. Guiding principles in the design of molecular bioconjugates for vaccine applications. *Bioconjug Chem* **2015**, *26* (5), 791-801, DOI: 10.1021/acs.bioconjchem.5b00103.

(94) Barrett, J. C.; Tirrell, M. V. Peptide Amphiphile Micelles for Vaccine Delivery. *Methods in molecular biology (Clifton, N.J.)* **2018**, *1798*, 277-292, DOI: 10.1007/978-1-4939-7893-9_21.

(95) Bachmann, M. F.; Jennings, G. T. J. N. R. I. Vaccine delivery: a matter of size, geometry, kinetics and molecular patterns. **2010**, *10* (11), 787.

(96) Hopp, T. P. J. M. i. Immunogenicity of a synthetic HBsAg peptide: enhancement by conjugation to a fatty acid carrier. **1984**, *21* (1), 13-16.

(97) Black, M.; Trent, A.; Kostenko, Y.; Lee, J. S.; Olive, C.; Tirrell, M. Self-assembled peptide amphiphile micelles containing a cytotoxic T-cell epitope promote a protective immune response in vivo. *Advanced materials (Deerfield Beach, Fla.)* **2012**, *24* (28), 3845-9, DOI: 10.1002/adma.201200209.

(98) Trent, A.; Ulery, B. D.; Black, M. J.; Barrett, J. C.; Liang, S.; Kostenko, Y.; David, N. A.; Tirrell, M. V. Peptide amphiphile micelles self-adjuvant group A streptococcal vaccination. *The AAPS journal* **2015**, *17* (2), 380-8, DOI: 10.1208/s12248-014-9707-3.

(99) Plank, J.; Bodenlenz, M.; Sinner, F.; Magnes, C.; Görzer, E.; Regittnig, W.; Endahl, L. A.; Draeger, E.; Zdravkovic, M.; Pieber, T. R. J. D. c. A double-blind, randomized, dose-response study investigating the pharmacodynamic and

pharmacokinetic properties of the long-acting insulin analog detemir. **2005**, *28* (5), 1107-1112.

(100) Jonassen, I.; Havelund, S.; Ribel, U.; Hoeg-Jensen, T.; Steensgaard, D. B.; Johansen, T.; Haahr, H.; Nishimura, E.; Kurtzhals, P. In *Insulin degludec is a new generation ultra-long acting basal insulin with a unique mechanism of protraction based on multi-hexamer formation*, Diabetes, AMER DIABETES ASSOC 1701 N BEAUREGARD ST, ALEXANDRIA, VA 22311-1717 USA: 2010; pp A11-A11.

(101) Knudsen, L. B.; Lau, J. The Discovery and Development of Liraglutide and Semaglutide. *Frontiers in endocrinology* **2019**, *10*, 155, DOI: 10.3389/fendo.2019.00155.

(102) Zaman, M.; Toth, I. Immunostimulation by synthetic lipopeptide-based vaccine candidates: structure-activity relationships. *Front Immunol* **2013**, *4*, 318, DOI: 10.3389/fimmu.2013.00318.

(103) Nigrovic, L. E.; Thompson, K. M. The Lyme vaccine: a cautionary tale. *Epidemiology and infection* **2007**, *135* (1), 1-8, DOI: 10.1017/s0950268806007096.

(104) Xie, J.; Zhang, X.; Teng, M.; Yu, B.; Yang, S.; Lee, R. J.; Teng, L. Synthesis, characterization, and evaluation of mPEG-SN38 and mPEG-PLA-SN38 micelles for cancer therapy. *International journal of nanomedicine* **2016**, *11*, 1677-86, DOI: 10.2147/ijn.S103110.

(105) Shen, Y.; Jin, E.; Zhang, B.; Murphy, C. J.; Sui, M.; Zhao, J.; Wang, J.; Tang, J.; Fan, M.; Van Kirk, E.; Murdoch, W. J. Prodrugs forming high drug loading multifunctional nanocapsules for intracellular cancer drug delivery. *Journal of the American Chemical Society* **2010**, *132* (12), 4259-65, DOI: 10.1021/ja909475m.

- (106) Cheetham, A. G.; Lin, Y. A.; Lin, R.; Cui, H. Molecular design and synthesis of self-assembling camptothecin drug amphiphiles. *Acta pharmacologica Sinica* **2017**, *38* (6), 874-884, DOI: 10.1038/aps.2016.151.
- (107) Maksimenko, A.; Dosio, F.; Mouglin, J.; Ferrero, A.; Wack, S.; Reddy, L. H.; Weyn, A. A.; Lepeltier, E.; Bourgaux, C.; Stella, B.; Cattel, L.; Couvreur, P. A unique squalenoylated and nonpegylated doxorubicin nanomedicine with systemic long-circulating properties and anticancer activity. *Proc Natl Acad Sci U S A* **2014**, *111* (2), E217-26, DOI: 10.1073/pnas.1313459110.
- (108) Huang, P.; Wang, D.; Su, Y.; Huang, W.; Zhou, Y.; Cui, D.; Zhu, X.; Yan, D. Combination of small molecule prodrug and nanodrug delivery: amphiphilic drug-drug conjugate for cancer therapy. *Journal of the American Chemical Society* **2014**, *136* (33), 11748-56, DOI: 10.1021/ja505212y.
- (109) Qin, S.-Y.; Zhang, A.-Q.; Cheng, S.-X.; Rong, L.; Zhang, X.-Z. J. B. Drug self-delivery systems for cancer therapy. **2017**, *112*, 234-247.
- (110) Koivusalo, M.; Jansen, M.; Somerharju, P.; Ikonen, E. Endocytic trafficking of sphingomyelin depends on its acyl chain length. *Molecular biology of the cell* **2007**, *18* (12), 5113-23, DOI: 10.1091/mbc.e07-04-0330.
- (111) Rajendran, L.; Udayar, V.; Goodger, Z. V. Lipid-anchored drugs for delivery into subcellular compartments. *Trends Pharmacol Sci* **2012**, *33* (4), 215-222, DOI: 10.1016/j.tips.2012.01.006.
- (112) Titov, V. N. [Functional properties of low density lipoprotein receptor family. Disturbance of cellular uptake of saturated fatty acids mediated by receptors (literature review)]. *Klin Lab Diagn* **2004**, (2), 8-15.

- (113) Curry, S. Lessons from the crystallographic analysis of small molecule binding to human serum albumin. *Drug Metab Pharmacokinet* **2009**, *24* (4), 342-57.
- (114) Bhattacharya, A. A.; Curry, S.; Franks, N. P. Binding of the general anesthetics propofol and halothane to human serum albumin. High resolution crystal structures. *J Biol Chem* **2000**, *275* (49), 38731-8, DOI: 10.1074/jbc.M005460200.
- (115) Simard, J. R.; Zunszain, P. A.; Hamilton, J. A.; Curry, S. Location of high and low affinity fatty acid binding sites on human serum albumin revealed by NMR drug-competition analysis. *J Mol Biol* **2006**, *361* (2), 336-51, DOI: 10.1016/j.jmb.2006.06.028.
- (116) Ghuman, J.; Zunszain, P. A.; Petitpas, I.; Bhattacharya, A. A.; Otagiri, M.; Curry, S. Structural basis of the drug-binding specificity of human serum albumin. *J Mol Biol* **2005**, *353* (1), 38-52, DOI: 10.1016/j.jmb.2005.07.075.
- (117) Petitpas, I.; Bhattacharya, A. A.; Twine, S.; East, M.; Curry, S. Crystal structure analysis of warfarin binding to human serum albumin: anatomy of drug site I. *J Biol Chem* **2001**, *276* (25), 22804-9, DOI: 10.1074/jbc.M100575200.
- (118) Bhattacharya, A. A.; Grune, T.; Curry, S. Crystallographic analysis reveals common modes of binding of medium and long-chain fatty acids to human serum albumin. *J Mol Biol* **2000**, *303* (5), 721-32, DOI: 10.1006/jmbi.2000.4158.
- (119) Fasano, M.; Curry, S.; Terreno, E.; Galliano, M.; Fanali, G.; Narciso, P.; Notari, S.; Ascenzi, P. The extraordinary ligand binding properties of human serum albumin. *IUBMB Life* **2005**, *57* (12), 787-96, DOI: 10.1080/15216540500404093.

- (120) Cao, H.; Liu, X.; Ulrich, N. P.; Sengupta, P. K.; Xiao, J. Plasma protein binding of dietary polyphenols to human serum albumin: A high performance affinity chromatography approach. *Food Chem* **2019**, *270*, 257-263, DOI: 10.1016/j.foodchem.2018.07.111.
- (121) Bista, S. R.; Haywood, A.; Hardy, J.; Lobb, M.; Tapuni, A.; Norris, R. Protein binding of fentanyl and its metabolite nor-fentanyl in human plasma, albumin and alpha-1 acid glycoprotein. *Xenobiotica* **2015**, *45* (3), 207-12, DOI: 10.3109/00498254.2014.971093.
- (122) Mirow, N.; Zimmermann, B.; Maleszka, A.; Knobl, H.; Tenderich, G.; Koerfer, R.; Herberg, F. W. Plasma protein binding properties to immobilized heparin and heparin-albumin conjugate. *Artif Organs* **2007**, *31* (6), 466-71, DOI: 10.1111/j.1525-1594.2007.00386.x.
- (123) Matsumura, Y.; Maeda, H. A new concept for macromolecular therapeutics in cancer chemotherapy: mechanism of tumoritropic accumulation of proteins and the antitumor agent smancs. *Cancer Res* **1986**, *46* (12 Pt 1), 6387-92.
- (124) Hobbs, S. K.; Monsky, W. L.; Yuan, F.; Roberts, W. G.; Griffith, L.; Torchilin, V. P.; Jain, R. K. Regulation of transport pathways in tumor vessels: role of tumor type and microenvironment. *Proc Natl Acad Sci U S A* **1998**, *95* (8), 4607-12, DOI: 10.1073/pnas.95.8.4607.
- (125) Maeda, H.; Wu, J.; Sawa, T.; Matsumura, Y.; Hori, K. Tumor vascular permeability and the EPR effect in macromolecular therapeutics: a review. *J Control Release* **2000**, *65* (1-2), 271-84.

- (126) Yuan, F.; Dellian, M.; Fukumura, D.; Leunig, M.; Berk, D. A.; Torchilin, V. P.; Jain, R. K. Vascular permeability in a human tumor xenograft: molecular size dependence and cutoff size. *Cancer Res* **1995**, *55* (17), 3752-6.
- (127) Burger, A. M.; Hartung, G.; Stehle, G.; Sinn, H.; Fiebig, H. H. Pre-clinical evaluation of a methotrexate-albumin conjugate (MTX-HSA) in human tumor xenografts in vivo. *Int J Cancer* **2001**, *92* (5), 718-24, DOI: 10.1002/1097-0215(20010601)92:5<718::aid-ijc1257>3.0.co;2-d.
- (128) Stehle, G.; Wunder, A.; Schrenk, H. H.; Hartung, G.; Heene, D. L.; Sinn, H. Methotrexate-albumin conjugate causes tumor growth delay in Dunning R3327 HI prostate cancer-bearing rats. *Anticancer Drugs* **1999**, *10* (4), 405-11.
- (129) Steinmann, A.; Friedrich, E.; Rath, U. A novel methotrexate-albumin (mtx-rsa)-conjugate causes significant growth delay of o-342 ovarian-carcinoma in-vivo. *Oncol Rep* **1995**, *2* (1), 107-9, DOI: 10.3892/or.2.1.107.
- (130) Vis, A. N.; van der Gaast, A.; van Rhijn, B. W.; Catsburg, T. K.; Schmidt, C.; Mickisch, G. H. A phase II trial of methotrexate-human serum albumin (MTX-HSA) in patients with metastatic renal cell carcinoma who progressed under immunotherapy. *Cancer Chemother Pharmacol* **2002**, *49* (4), 342-5, DOI: 10.1007/s00280-001-0417-z.
- (131) Bolling, C.; Graefe, T.; Lubbing, C.; Jankevicius, F.; Uktveris, S.; Cesas, A.; Meyer-Moldenhauer, W. H.; Starkmann, H.; Weigel, M.; Burk, K.; Hanauske, A. R. Phase II study of MTX-HSA in combination with cisplatin as first line treatment in patients with advanced or metastatic transitional cell carcinoma. *Invest New Drugs* **2006**, *24* (6), 521-7, DOI: 10.1007/s10637-006-8221-6.

(132) Kratz, F.; Roth, T.; Fichiner, I.; Schumacher, P.; Fiebig, H. H.; Unger, C. In vitro and in vivo efficacy of acid-sensitive transferrin and albumin doxorubicin conjugates in a human xenograft panel and in the MDA-MB-435 mamma carcinoma model. *J Drug Target* **2000**, *8* (5), 305-18, DOI: 10.3109/10611860008997908.

(133) Kratz, F.; Muller-Driver, R.; Hofmann, I.; Dreves, J.; Unger, C. A novel macromolecular prodrug concept exploiting endogenous serum albumin as a drug carrier for cancer chemotherapy. *J Med Chem* **2000**, *43* (7), 1253-6, DOI: 10.1021/jm9905864.

(134) Kratz, F.; Warnecke, A.; Scheuermann, K.; Stockmar, C.; Schwab, J.; Lazar, P.; Druckes, P.; Esser, N.; Dreves, J.; Rognan, D.; Bissantz, C.; Hinderling, C.; Folkers, G.; Fichtner, I.; Unger, C. Probing the cysteine-34 position of endogenous serum albumin with thiol-binding doxorubicin derivatives. Improved efficacy of an acid-sensitive doxorubicin derivative with specific albumin-binding properties compared to that of the parent compound. *J Med Chem* **2002**, *45* (25), 5523-33, DOI: 10.1021/jm020276c.

(135) Kastantin, M.; Missirlis, D.; Black, M.; Ananthanarayanan, B.; Peters, D.; Tirrell, M. Thermodynamic and kinetic stability of DSPE-PEG(2000) micelles in the presence of bovine serum albumin. *J Phys Chem B* **2010**, *114* (39), 12632-40, DOI: 10.1021/jp1001786.

(136) Hwang, T.; Han, H. D.; Song, C. K.; Seong, H.; Kim, J. H.; Chen, X.; Shin, B. C. Anticancer Drug-Phospholipid Conjugate for Enhancement of Intracellular Drug

Delivery. *Macromol Symp* **2007**, 249-250 (1), 109-115, DOI: 10.1002/masy.200750318.

(137) Marczak, A.; Kowalczyk, A.; Wrzesien-Kus, A.; Robak, T.; Jozwiak, Z. Interaction of doxorubicin and idarubicin with red blood cells from acute myeloid leukaemia patients. *Cell Biol Int* **2006**, 30 (2), 127-32, DOI: 10.1016/j.cellbi.2005.09.001.

(138) Arancia, G.; Molinari, A.; Crateri, P.; Calcabrini, A.; Silvestri, L.; Isacchi, G. Adriamycin-plasma membrane interaction in human erythrocytes. *Eur J Cell Biol* **1988**, 47 (2), 379-87.

(139) Wang, J.; Xing, X.; Fang, X.; Zhou, C.; Huang, F.; Wu, Z.; Lou, J.; Liang, W. Cationic amphiphilic drugs self-assemble to the core-shell interface of PEGylated phospholipid micelles and stabilize micellar structure. *Philos Trans A Math Phys Eng Sci* **2013**, 371 (2000), 20120309, DOI: 10.1098/rsta.2012.0309.

(140) Suwalsky, M.; Hernandez, P.; Villena, F.; Aguilar, F.; Sotomayor, C. P. The anticancer drug adriamycin interacts with the human erythrocyte membrane. *Z Naturforsch C* **1999**, 54 (3-4), 271-7.

(141) Wang, J.; Xing, X. Q.; Fang, X. C.; Zhou, C.; Huang, F.; Wu, Z. H.; Lou, J. Z.; Liang, W. Cationic amphiphilic drugs self-assemble to the core-shell interface of PEGylated phospholipid micelles and stabilize micellar structure. *Philos T R Soc A* **2013**, 371 (2000), DOI: ARTN 20120309

10.1098/rsta.2012.0309.

- (142) Awasthi, S.; Sharma, R.; Awasthi, Y. C.; Belli, J. A.; Frenkel, E. P. The relationship of doxorubicin binding to membrane lipids with drug resistance. *Cancer Lett* **1992**, *63* (2), 109-16.
- (143) Shikinaka, K.; Aizawa, K.; Fujii, N.; Osada, Y.; Tokita, M.; Watanabe, J.; Shigehara, K. Flexible, transparent nanocomposite film with a large clay component and ordered structure obtained by a simple solution-casting method. *Langmuir* **2010**, *26* (15), 12493-5, DOI: 10.1021/la101496b.
- (144) Weissig, V. DQAsomes as the prototype of mitochondria-targeted pharmaceutical nanocarriers: Preparation, characterization, and use. In *Mitochondrial medicine*; Springer: 2015; pp 1-11.
- (145) Anselmo, A. C.; Mitragotri, S. Nanoparticles in the clinic. *Bioeng Transl Med* **2016**, *1* (1), 10-29, DOI: 10.1002/btm2.10003.
- (146) Pathak, R. K.; Kolishetti, N.; Dhar, S. Targeted nanoparticles in mitochondrial medicine. *Wiley Interdiscip Rev Nanomed Nanobiotechnol* **2015**, *7* (3), 315-29, DOI: 10.1002/wnan.1305.
- (147) Patel, N. R.; Hatziantoniou, S.; Georgopoulos, A.; Demetzos, C.; Torchilin, V. P.; Weissig, V.; D'Souza, G. G. Mitochondria-targeted liposomes improve the apoptotic and cytotoxic action of sclareol. *J Liposome Res* **2010**, *20* (3), 244-9, DOI: 10.3109/08982100903347931.
- (148) Moon, S. Y.; Choi, Y. S.; Cho, J. K.; Yu, M.; Lee, E.; Huh, K. M.; Lee, D. H.; Kim, J. H.; Kang, H. C. Intracellular thiol-responsive nanosized drug carriers self-assembled by poly(ethylene glycol)-b-poly(epsilon-caprolactone)-b-poly(ethylene

glycol) having multiple bioreducible disulfide linkages in hydrophobic blocks. *Rsc Adv* **2016**, *6* (19), 15558-15576, DOI: 10.1039/c5ra25319e.

(149) Liu, X.; Zhang, S.; An, L.; Wu, J.; Hu, X.; Lai, S.; Mazhar, H.; Zou, Y.; He, L.; Zhu, H. Loss of Rubicon ameliorates doxorubicin-induced cardiotoxicity through enhancement of mitochondrial quality. *Int J Cardiol* **2019**, DOI: 10.1016/j.ijcard.2019.07.074.

(150) Holohan, C.; Van Schaeybroeck, S.; Longley, D. B.; Johnston, P. G. Cancer drug resistance: an evolving paradigm. *Nat Rev Cancer* **2013**, *13* (10), 714-26, DOI: 10.1038/nrc3599.

(151) DeVita, V. T., Jr.; Chu, E. A history of cancer chemotherapy. *Cancer Res* **2008**, *68* (21), 8643-53, DOI: 10.1158/0008-5472.CAN-07-6611.

(152) Chabner, B. A.; Roberts, T. G., Jr. Timeline: Chemotherapy and the war on cancer. *Nat Rev Cancer* **2005**, *5* (1), 65-72, DOI: 10.1038/nrc1529.

(153) Santos, N. A.; Bezerra, C. S.; Martins, N. M.; Curti, C.; Bianchi, M. L.; Santos, A. C. Hydroxyl radical scavenger ameliorates cisplatin-induced nephrotoxicity by preventing oxidative stress, redox state unbalance, impairment of energetic metabolism and apoptosis in rat kidney mitochondria. *Cancer Chemother Pharmacol* **2008**, *61* (1), 145-55, DOI: 10.1007/s00280-007-0459-y.

(154) Scatena, R. Mitochondria and cancer: a growing role in apoptosis, cancer cell metabolism and dedifferentiation. *Adv Exp Med Biol* **2012**, *942*, 287-308, DOI: 10.1007/978-94-007-2869-1_13.

(155) Borodkina, A.; Shatrova, A.; Abushik, P.; Nikolsky, N.; Burova, E. Interaction between ROS dependent DNA damage, mitochondria and p38 MAPK underlies

senescence of human adult stem cells. *Aging (Albany NY)* **2014**, 6 (6), 481-95, DOI: 10.18632/aging.100673.

(156) Indo, H. P.; Davidson, M.; Yen, H. C.; Suenaga, S.; Tomita, K.; Nishii, T.; Higuchi, M.; Koga, Y.; Ozawa, T.; Majima, H. J. Evidence of ROS generation by mitochondria in cells with impaired electron transport chain and mitochondrial DNA damage. *Mitochondrion* **2007**, 7 (1-2), 106-18, DOI: 10.1016/j.mito.2006.11.026.

(157) D'Souza, G. G.; Wagle, M. A.; Saxena, V.; Shah, A. Approaches for targeting mitochondria in cancer therapy. *Biochim Biophys Acta* **2011**, 1807 (6), 689-96, DOI: 10.1016/j.bbabbio.2010.08.008.

(158) Fulda, S.; Galluzzi, L.; Kroemer, G. Targeting mitochondria for cancer therapy. *Nat Rev Drug Discov* **2010**, 9 (6), 447-464, DOI: 10.1038/nrd3137.

(159) Chamberlain, G. R.; Tulumello, D. V.; Kelley, S. O. Targeted delivery of doxorubicin to mitochondria. *ACS Chem Biol* **2013**, 8 (7), 1389-95, DOI: 10.1021/cb400095v.

(160) Buondonno, I.; Gazzano, E.; Jean, S. R.; Audrito, V.; Kopecka, J.; Fanelli, M.; Salaroglio, I. C.; Costamagna, C.; Roato, I.; Mungo, E.; Hattinger, C. M.; Deaglio, S.; Kelley, S. O.; Serra, M.; Riganti, C. Mitochondria-Targeted Doxorubicin: A New Therapeutic Strategy against Doxorubicin-Resistant Osteosarcoma. *Mol Cancer Ther* **2016**, 15 (11), 2640-2652, DOI: 10.1158/1535-7163.MCT-16-0048.

(161) Riganti, C.; Rolando, B.; Kopecka, J.; Campia, I.; Chegaev, K.; Lazzarato, L.; Federico, A.; Fruttero, R.; Ghigo, D. Mitochondrial-targeting nitrooxy-

doxorubicin: a new approach to overcome drug resistance. *Mol Pharm* **2013**, *10* (1), 161-74, DOI: 10.1021/mp300311b.

(162) Modica-Napolitano, J. S.; Weissig, V. Treatment Strategies that Enhance the Efficacy and Selectivity of Mitochondria-Targeted Anticancer Agents. *Int J Mol Sci* **2015**, *16* (8), 17394-17421, DOI: 10.3390/ijms160817394.

(163) Jung, K.; Reszka, R. Mitochondria as subcellular targets for clinically useful anthracyclines. *Adv Drug Deliver Rev* **2001**, *49* (1-2), 87-105, DOI: Doi 10.1016/S0169-409x(01)00128-4.

(164) Lu, P.; Bruno, B. J.; Rabenau, M.; Lim, C. S. Delivery of drugs and macromolecules to the mitochondria for cancer therapy. *J Control Release* **2016**, *240*, 38-51, DOI: 10.1016/j.jconrel.2015.10.023.

(165) Pathania, D.; Millard, M.; Neamati, N. Opportunities in discovery and delivery of anticancer drugs targeting mitochondria and cancer cell metabolism. *Adv Drug Deliv Rev* **2009**, *61* (14), 1250-75, DOI: 10.1016/j.addr.2009.05.010.

(166) Smith, R. A.; Porteous, C. M.; Gane, A. M.; Murphy, M. P. Delivery of bioactive molecules to mitochondria in vivo. *Proc Natl Acad Sci U S A* **2003**, *100* (9), 5407-12, DOI: 10.1073/pnas.0931245100.

(167) Modica-Napolitano, J. S.; Aprille, J. R. Delocalized lipophilic cations selectively target the mitochondria of carcinoma cells. *Adv Drug Deliv Rev* **2001**, *49* (1-2), 63-70.

(168) Murphy, M. P. Selective targeting of bioactive compounds to mitochondria. *Trends Biotechnol* **1997**, *15* (8), 326-30, DOI: 10.1016/S0167-7799(97)01068-8.

- (169) Galluzzi, L.; Zamzami, N.; de La Motte Rouge, T.; Lemaire, C.; Brenner, C.; Kroemer, G. Methods for the assessment of mitochondrial membrane permeabilization in apoptosis. *Apoptosis* **2007**, *12* (5), 803-13, DOI: 10.1007/s10495-007-0720-1.
- (170) Yousif, L. F.; Stewart, K. M.; Kelley, S. O. Targeting mitochondria with organelle-specific compounds: strategies and applications. *Chembiochem* **2009**, *10* (12), 1939-50, DOI: 10.1002/cbic.200900185.
- (171) Millard, M.; Pathania, D.; Shabaik, Y.; Taheri, L.; Deng, J.; Neamati, N. Preclinical evaluation of novel triphenylphosphonium salts with broad-spectrum activity. *PLoS One* **2010**, *5* (10), DOI: 10.1371/journal.pone.0013131.
- (172) Porteous, C. M.; Logan, A.; Evans, C.; Ledgerwood, E. C.; Menon, D. K.; Aigbirhio, F.; Smith, R. A.; Murphy, M. P. Rapid uptake of lipophilic triphenylphosphonium cations by mitochondria in vivo following intravenous injection: implications for mitochondria-specific therapies and probes. *Biochim Biophys Acta* **2010**, *1800* (9), 1009-17, DOI: 10.1016/j.bbagen.2010.06.001.
- (173) Propper, D. J.; Braybrooke, J. P.; Taylor, D. J.; Lodi, R.; Styles, P.; Cramer, J. A.; Collins, W. C. J.; Levitt, N. C.; Talbot, D. C.; Ganesan, T. S.; Harris, A. L. Phase I trial of the selective mitochondrial toxin MKT 077 in chemo-resistant solid tumours. *Ann Oncol* **1999**, *10* (8), 923-927, DOI: Doi 10.1023/A:1008336904585.
- (174) Kelso, G. F.; Porteous, C. M.; Coulter, C. V.; Hughes, G.; Porteous, W. K.; Ledgerwood, E. C.; Smith, R. A. J.; Murphy, M. P. Selective targeting of a redox-active ubiquinone to mitochondria within cells - Antioxidant and antiapoptotic

properties. *J Biol Chem* **2001**, 276 (7), 4588-4596, DOI: DOI 10.1074/jbc.M009093200.

(175) Yousif, L. F.; Stewart, K. M.; Horton, K. L.; Kelley, S. O. Mitochondria-penetrating peptides: sequence effects and model cargo transport. *Chembiochem* **2009**, 10 (12), 2081-8, DOI: 10.1002/cbic.200900017.

(176) Neupert, W.; Herrmann, J. M. Translocation of proteins into mitochondria. *Annu Rev Biochem* **2007**, 76, 723-749, DOI: 10.1146/annurev.biochem.76.052705.163409.

(177) Vestweber, D.; Schatz, G. DNA-Protein Conjugates Can Enter Mitochondria Via the Protein Import Pathway. *Nature* **1989**, 338 (6211), 170-172, DOI: DOI 10.1038/338170a0.

(178) Horton, K. L.; Stewart, K. M.; Fonseca, S. B.; Guo, Q.; Kelley, S. O. Mitochondria-penetrating peptides. *Chem Biol* **2008**, 15 (4), 375-382, DOI: 10.1016/j.chembiol.2008.03.015.

(179) Marrache, S.; Dhar, S. Engineering of blended nanoparticle platform for delivery of mitochondria-acting therapeutics. *P Natl Acad Sci USA* **2012**, 109 (40), 16288-16293, DOI: 10.1073/pnas.1210096109.

(180) Singh, K.; Bhor, M.; Kasu, Y. A.; Bhat, G.; Marar, T. Antioxidants as precision weapons in war against cancer chemotherapy induced toxicity - Exploring the armoury of obscurity. *Saudi Pharm J* **2018**, 26 (2), 177-190, DOI: 10.1016/j.jsps.2017.12.013.

- (181) Adamczyk-Cioch, M. B.; Dmoszynska-Giannopoulou, A. [Multidrug resistance (MDR) to cytostatics in proliferative diseases of the hematopoietic system]. *Pol Arch Med Wewn* **1992**, *87* (3), 183-90.
- (182) Chiappetta, G.; Bevilacqua, A. M.; Picone, A.; Riccio, G.; Botti, G. Assessment of multidrug resistance (MDR) by immunohistochemistry in breast carcinoma. Correlation with tumor size and regional node status. *J Nucl Med Allied Sci* **1990**, *34* (4 Suppl), 217-9.
- (183) Shustik, C.; Groulx, N.; Gros, P. Analysis of multidrug resistance (MDR-1) gene expression in chronic lymphocytic leukaemia (CLL). *Br J Haematol* **1991**, *79* (1), 50-6, DOI: 10.1111/j.1365-2141.1991.tb08006.x.
- (184) Chen, C. J.; Chin, J. E.; Ueda, K.; Clark, D. P.; Pastan, I.; Gottesman, M. M.; Roninson, I. B. Internal duplication and homology with bacterial transport proteins in the *mdr1* (P-glycoprotein) gene from multidrug-resistant human cells. *Cell* **1986**, *47* (3), 381-9, DOI: 10.1016/0092-8674(86)90595-7.
- (185) Gottesman, M. M.; Fojo, T.; Bates, S. E. Multidrug resistance in cancer: role of ATP-dependent transporters. *Nat Rev Cancer* **2002**, *2* (1), 48-58, DOI: 10.1038/nrc706.
- (186) Wu, Q.; Yang, Z.; Nie, Y.; Shi, Y.; Fan, D. Multi-drug resistance in cancer chemotherapeutics: mechanisms and lab approaches. *Cancer Lett* **2014**, *347* (2), 159-66, DOI: 10.1016/j.canlet.2014.03.013.
- (187) Jain, R. K. Delivery of molecular and cellular medicine to solid tumors. *Adv Drug Deliv Rev* **2001**, *46* (1-3), 149-68.

- (188) Qin, Z.; Zhang, B.; Yang, J.; Li, S.; Xu, J.; Yao, Z.; Zhang, X.; Gonzalez, F. J.; Yao, X. The Efflux Mechanism of Fraxetin-O-Glucuronides in UGT1A9-Transfected HeLa Cells: Identification of Multidrug Resistance-Associated Proteins 3 and 4 (MRP3/4) as the Important Contributors. *Front Pharmacol* **2019**, *10*, 496, DOI: 10.3389/fphar.2019.00496.
- (189) Simovski, B.; Kanduri, C.; Gundersen, S.; Titov, D.; Domanska, D.; Bock, C.; Bossini-Castillo, L.; Chikina, M.; Favorov, A.; Layer, R. M.; Mironov, A. A.; Quinlan, A. R.; Sheffield, N. C.; Trynka, G.; Sandve, G. K. Coloc-stats: a unified web interface to perform colocalization analysis of genomic features. *Nucleic Acids Res* **2018**, *46* (W1), W186-W193, DOI: 10.1093/nar/gky474.
- (190) Tomai, M. A.; Miller, R. L.; Lipson, K. E.; Kieper, W. C.; Zarraga, I. E.; Vasilakos, J. P. Resiquimod and other immune response modifiers as vaccine adjuvants. *Expert review of vaccines* **2007**, *6* (5), 835-47, DOI: 10.1586/14760584.6.5.835.
- (191) Pradere, J. P.; Dapito, D. H.; Schwabe, R. F. The Yin and Yang of Toll-like receptors in cancer. *Oncogene* **2014**, *33* (27), 3485-95, DOI: 10.1038/onc.2013.302.
- (192) Ohara, M.; Ohyama, Y. Delivery and application of dietary polyphenols to target organs, tissues and intracellular organelles. *Curr Drug Metab* **2014**, *15* (1), 37-47.
- (193) Yang, Z.; Zhang, Y.; Yang, Y.; Sun, L.; Han, D.; Li, H.; Wang, C. Pharmacological and toxicological target organelles and safe use of single-walled

carbon nanotubes as drug carriers in treating Alzheimer disease. *Nanomedicine* **2010**, *6* (3), 427-41, DOI: 10.1016/j.nano.2009.11.007.

(194) Samynathan, Y. M.; Bondy, S. C. Inhibition of plasma membrane and mitochondrial transmembrane potentials by ethanol. *Neurochem Res* **1995**, *20* (2), 171-6, DOI: 10.1007/bf00970541.

(195) Purdie, L.; Alexander, C.; Spain, S. G.; Magnusson, J. P. Alkyl-Modified Oligonucleotides as Intercalating Vehicles for Doxorubicin Uptake via Albumin Binding. *Mol Pharm* **2018**, *15* (2), 437-446, DOI: 10.1021/acs.molpharmaceut.7b00805.

(196) Kovar, L.; Strohalm, J.; Chytil, P.; Mrkvan, T.; Kovar, M.; Hovorka, O.; Ulbrich, K.; Rihova, B. The same drug but a different mechanism of action: comparison of free doxorubicin with two different N-(2-hydroxypropyl)methacrylamide copolymer-bound doxorubicin conjugates in EL-4 cancer cell line. *Bioconjug Chem* **2007**, *18* (3), 894-902, DOI: 10.1021/bc060246e.

(197) Zhou, F.; Zheng, B.; Zhang, Y.; Wu, Y.; Wang, H.; Chang, J. Construction of near-infrared light-triggered reactive oxygen species-sensitive (UCN/SiO₂-RB + DOX)@PPADT nanoparticles for simultaneous chemotherapy and photodynamic therapy. *Nanotechnology* **2016**, *27* (23), 235601, DOI: 10.1088/0957-4484/27/23/235601.

(198) Kratz, F. Albumin as a drug carrier: design of prodrugs, drug conjugates and nanoparticles. *Journal of controlled release* **2008**, *132* (3), 171-183.

- (199) Larsen, M. T.; Kuhlmann, M.; Hvam, M. L.; Howard, K. A. Albumin-based drug delivery: harnessing nature to cure disease. *Molecular and cellular therapies* **2016**, *4* (1), 3.
- (200) Liu, H.; Moynihan, K. D.; Zheng, Y.; Szeto, G. L.; Li, A. V.; Huang, B.; Van Egeren, D. S.; Park, C.; Irvine, D. J. Structure-based programming of lymph node targeting in molecular vaccines. *Nature* **2014**, *507* (7493), 519.
- (201) Berrios-Torres, S. I.; Umscheid, C. A.; Bratzler, D. W.; Leas, B.; Stone, E. C.; Kelz, R. R.; Reinke, C. E.; Morgan, S.; Solomkin, J. S.; Mazuski, J. E.; Dellinger, E. P.; Itani, K. M. F.; Berbari, E. F.; Segreti, J.; Parvizi, J.; Blanchard, J.; Allen, G.; Kluytmans, J.; Donlan, R.; Schechter, W. P.; Healthcare Infection Control Practices Advisory, C. Centers for Disease Control and Prevention Guideline for the Prevention of Surgical Site Infection, 2017. *JAMA Surg* **2017**, *152* (8), 784-791, DOI: 10.1001/jamasurg.2017.0904.
- (202) Luo, X.; Herold, K. C.; Miller, S. D. Immunotherapy of type 1 diabetes: where are we and where should we be going? *Immunity* **2010**, *32* (4), 488-99, DOI: 10.1016/j.immuni.2010.04.002.
- (203) van Belle, T. L.; Coppieters, K. T.; von Herrath, M. G. Type 1 diabetes: etiology, immunology, and therapeutic strategies. *Physiol Rev* **2011**, *91* (1), 79-118, DOI: 10.1152/physrev.00003.2010.
- (204) Hatziavramidis, D. T.; Karatzas, T. M.; Chrousos, G. P. Pancreatic islet cell transplantation: an update. *Ann Biomed Eng* **2013**, *41* (3), 469-76, DOI: 10.1007/s10439-012-0676-3.

(205) Miller, S. D.; Turley, D. M.; Podojil, J. R. Antigen-specific tolerance strategies for the prevention and treatment of autoimmune disease. *Nat Rev Immunol* **2007**, *7* (9), 665-77, DOI: 10.1038/nri2153.

(206) Peakman, M.; von Herrath, M. Antigen-specific immunotherapy for type 1 diabetes: maximizing the potential. *Diabetes* **2010**, *59* (9), 2087-93, DOI: 10.2337/db10-0630.

(207) Wan, X.; Zaghouani, H. Antigen-specific therapy against type 1 diabetes: mechanisms and perspectives. *Immunotherapy* **2014**, *6* (2), 155-64, DOI: 10.2217/imt.13.172.

(208) Weigmann, B.; Franke, R. K.; Daniel, C. Immunotherapy in autoimmune type 1 diabetes. *Rev Diabet Stud* **2012**, *9* (2-3), 68-81, DOI: 10.1900/RDS.2012.9.68.

(209) Hopp, A. K.; Rupp, A.; Lukacs-Kornek, V. Self-antigen presentation by dendritic cells in autoimmunity. *Front Immunol* **2014**, *5*, 55, DOI: 10.3389/fimmu.2014.00055.

(210) Kurts, C.; Sutherland, R. M.; Davey, G.; Li, M.; Lew, A. M.; Blanas, E.; Carbone, F. R.; Miller, J. F.; Heath, W. R. CD8 T cell ignorance or tolerance to islet antigens depends on antigen dose. *Proc Natl Acad Sci U S A* **1999**, *96* (22), 12703-7, DOI: 10.1073/pnas.96.22.12703.

(211) Zinkernagel, R. M. Localization dose and time of antigens determine immune reactivity. *Semin Immunol* **2000**, *12* (3), 163-71; discussion 257-344, DOI: 10.1006/smim.2000.0253.

(212) Perera, J.; Liu, X.; Zhou, Y.; Joseph, N. E.; Meng, L.; Turner, J. R.; Huang, H. Insufficient autoantigen presentation and failure of tolerance in a mouse model

of rheumatoid arthritis. *Arthritis Rheum* **2013**, *65* (11), 2847-56, DOI: 10.1002/art.38085.

(213) Thompson, A. G.; Thomas, R. Induction of immune tolerance by dendritic cells: implications for preventative and therapeutic immunotherapy of autoimmune disease. *Immunol Cell Biol* **2002**, *80* (6), 509-19, DOI: 10.1046/j.1440-1711.2002.01114.x.

(214) Legoux, F. P.; Lim, J. B.; Cauley, A. W.; Dikiy, S.; Ertelt, J.; Mariani, T. J.; Sparwasser, T.; Way, S. S.; Moon, J. J. CD4+ T Cell Tolerance to Tissue-Restricted Self Antigens Is Mediated by Antigen-Specific Regulatory T Cells Rather Than Deletion. *Immunity* **2015**, *43* (5), 896-908, DOI: 10.1016/j.immuni.2015.10.011.

(215) Iezzi, G.; Karjalainen, K.; Lanzavecchia, A. The duration of antigenic stimulation determines the fate of naive and effector T cells. *Immunity* **1998**, *8* (1), 89-95, DOI: 10.1016/s1074-7613(00)80461-6.

(216) Moyer, T. J.; Zmolek, A. C.; Irvine, D. J. Beyond antigens and adjuvants: formulating future vaccines. *J Clin Invest* **2016**, *126* (3), 799-808, DOI: 10.1172/JCI81083.

(217) Suri, A.; Levisetti, M. G.; Unanue, E. R. Do the peptide-binding properties of diabetogenic class II molecules explain autoreactivity? *Curr Opin Immunol* **2008**, *20* (1), 105-10, DOI: 10.1016/j.coi.2007.10.007.

(218) Levisetti, M. G.; Suri, A.; Petzold, S. J.; Unanue, E. R. The insulin-specific T cells of nonobese diabetic mice recognize a weak MHC-binding segment in more

than one form. *J Immunol* **2007**, *178* (10), 6051-7, DOI: 10.4049/jimmunol.178.10.6051.

(219) Daniel, D.; Gill, R. G.; Schloot, N.; Wegmann, D. Epitope specificity, cytokine production profile and diabetogenic activity of insulin-specific T cell clones isolated from NOD mice. *Eur J Immunol* **1995**, *25* (4), 1056-62, DOI: 10.1002/eji.1830250430.

(220) Stadinski, B. D.; Zhang, L.; Crawford, F.; Marrack, P.; Eisenbarth, G. S.; Kappler, J. W. Diabetogenic T cells recognize insulin bound to IAg7 in an unexpected, weakly binding register. *Proc Natl Acad Sci U S A* **2010**, *107* (24), 10978-83, DOI: 10.1073/pnas.1006545107.

(221) Sarikonda, G.; Fousteri, G.; Sachithanatham, S.; Miller, J. F.; Dave, A.; Juntti, T.; Coppieters, K. T.; von Herrath, M. BDC12-4.1 T-cell receptor transgenic insulin-specific CD4 T cells are resistant to in vitro differentiation into functional Foxp3+ T regulatory cells. *PLoS One* **2014**, *9* (11), e112242, DOI: 10.1371/journal.pone.0112242.

(222) Nakayama, M.; McDaniel, K.; Fitzgerald-Miller, L.; Kiekhäfer, C.; Snell-Bergeon, J. K.; Davidson, H. W.; Rewers, M.; Yu, L.; Gottlieb, P.; Kappler, J. W.; Michels, A. Regulatory vs. inflammatory cytokine T-cell responses to mutated insulin peptides in healthy and type 1 diabetic subjects. *Proc Natl Acad Sci U S A* **2015**, *112* (14), 4429-34, DOI: 10.1073/pnas.1502967112.

(223) Daniel, C.; Weigmann, B.; Bronson, R.; von Boehmer, H. Prevention of type 1 diabetes in mice by tolerogenic vaccination with a strong agonist insulin mimotope. *J Exp Med* **2011**, *208* (7), 1501-10, DOI: 10.1084/jem.20110574.

(224) Maldonado, R. A.; LaMothe, R. A.; Ferrari, J. D.; Zhang, A. H.; Rossi, R. J.; Kolte, P. N.; Griset, A. P.; O'Neil, C.; Altreuter, D. H.; Browning, E.; Johnston, L.; Farokhzad, O. C.; Langer, R.; Scott, D. W.; von Andrian, U. H.; Kishimoto, T. K. Polymeric synthetic nanoparticles for the induction of antigen-specific immunological tolerance. *Proc Natl Acad Sci U S A* **2015**, *112* (2), E156-65, DOI: 10.1073/pnas.1408686111.

(225) Yu, C.; Xi, J.; Li, M.; An, M.; Liu, H. Bioconjugate Strategies for the Induction of Antigen-Specific Tolerance in Autoimmune Diseases. *Bioconjug Chem* **2018**, *29* (3), 719-732, DOI: 10.1021/acs.bioconjchem.7b00632.

(226) Getts, D. R.; Martin, A. J.; McCarthy, D. P.; Terry, R. L.; Hunter, Z. N.; Yap, W. T.; Getts, M. T.; Pleiss, M.; Luo, X.; King, N. J.; Shea, L. D.; Miller, S. D. Microparticles bearing encephalitogenic peptides induce T-cell tolerance and ameliorate experimental autoimmune encephalomyelitis. *Nat Biotechnol* **2012**, *30* (12), 1217-24, DOI: 10.1038/nbt.2434.

(227) Yeste, A.; Nadeau, M.; Burns, E. J.; Weiner, H. L.; Quintana, F. J. Nanoparticle-mediated codelivery of myelin antigen and a tolerogenic small molecule suppresses experimental autoimmune encephalomyelitis. *Proc Natl Acad Sci U S A* **2012**, *109* (28), 11270-5, DOI: 10.1073/pnas.1120611109.

(228) Yamazaki, S.; Dudziak, D.; Heidkamp, G. F.; Fiorese, C.; Bonito, A. J.; Inaba, K.; Nussenzweig, M. C.; Steinman, R. M. CD8⁺ CD205⁺ splenic dendritic cells are specialized to induce Foxp3⁺ regulatory T cells. *J Immunol* **2008**, *181* (10), 6923-33, DOI: 10.4049/jimmunol.181.10.6923.

- (229) Loschko, J.; Heink, S.; Hackl, D.; Dudziak, D.; Reindl, W.; Korn, T.; Krug, A. B. Antigen targeting to plasmacytoid dendritic cells via Siglec-H inhibits Th cell-dependent autoimmunity. *J Immunol* **2011**, *187* (12), 6346-56, DOI: 10.4049/jimmunol.1102307.
- (230) Gottschalk, R. A.; Corse, E.; Allison, J. P. TCR ligand density and affinity determine peripheral induction of Foxp3 in vivo. *J Exp Med* **2010**, *207* (8), 1701-11, DOI: 10.1084/jem.20091999.
- (231) Jamison, B.; Neef, T.; Miller, S. D.; Haskins, K. Induction of antigen-specific tolerance with Hybrid Insulin Peptides in the NOD mouse model of autoimmune diabetes. *Journal of Immunology* **2017**, *198* (1).
- (232) Liu, H.; Moynihan, K. D.; Zheng, Y.; Szeto, G. L.; Li, A. V.; Huang, B.; Van Egeren, D. S.; Park, C.; Irvine, D. J. Structure-based programming of lymph-node targeting in molecular vaccines. *Nature* **2014**, *507* (7493), 519-522.
- (233) Chen-Woan, M.; Delaney, C. P.; Fournier, V.; Wakizaka, Y.; Murase, N.; Fung, J.; Starzl, T. E.; Demetris, A. J. A new protocol for the propagation of dendritic cells from rat bone marrow using recombinant GM-CSF, and their quantification using the mAb OX-62. *J Immunol Methods* **1995**, *178* (2), 157-71, DOI: 10.1016/0022-1759(94)00253-s.
- (234) Tesfa, L.; Volk, H. D.; Kern, F. A protocol for combining proliferation, tetramer staining and intracellular cytokine detection for the flow-cytometric analysis of antigen specific T-cells. *J Biol Regul Homeost Agents* **2003**, *17* (4), 366-70.

- (235) Fontenot, J. D.; Gavin, M. A.; Rudensky, A. Y. Pillars Article: Foxp3 Programs the Development and Function of CD4+CD25+ Regulatory T Cells. *Nat. Immunol.* 2003. 4: 330-336. *J Immunol* **2017**, 198 (3), 986-992.
- (236) Cella, M.; Sallusto, F.; Lanzavecchia, A. Origin, maturation and antigen presenting function of dendritic cells. *Curr Opin Immunol* **1997**, 9 (1), 10-6, DOI: 10.1016/s0952-7915(97)80153-7.
- (237) McHugh, N. J.; Owen, P.; Cox, B.; Dunphy, J.; Welsh, K. MHC class II, tumour necrosis factor alpha, and lymphotoxin alpha gene haplotype associations with serological subsets of systemic lupus erythematosus. *Ann Rheum Dis* **2006**, 65 (4), 488-94, DOI: 10.1136/ard.2005.039842.
- (238) Antunes, R. F.; Kaski, J. C.; Dumitriu, I. E. The role of costimulatory receptors of the tumour necrosis factor receptor family in atherosclerosis. *J Biomed Biotechnol* **2012**, 2012, 464532, DOI: 10.1155/2012/464532.
- (239) Cua, D. J.; Sherlock, J.; Chen, Y.; Murphy, C. A.; Joyce, B.; Seymour, B.; Lucian, L.; To, W.; Kwan, S.; Churakova, T.; Zurawski, S.; Wiekowski, M.; Lira, S. A.; Gorman, D.; Kastelein, R. A.; Sedgwick, J. D. Interleukin-23 rather than interleukin-12 is the critical cytokine for autoimmune inflammation of the brain. *Nature* **2003**, 421 (6924), 744-8, DOI: 10.1038/nature01355.
- (240) Johnson, L. E.; Olson, B. M.; McNeel, D. G. Pretreatment antigen-specific immunity and regulation - association with subsequent immune response to anti-tumor DNA vaccination. *J Immunother Cancer* **2017**, 5 (1), 56, DOI: 10.1186/s40425-017-0260-3.

(241) Szabo, S. J.; Sullivan, B. M.; Stemmann, C.; Satoskar, A. R.; Sleckman, B. P.; Glimcher, L. H. Distinct effects of T-bet in TH1 lineage commitment and IFN-gamma production in CD4 and CD8 T cells. *Science* **2002**, *295* (5553), 338-42, DOI: 10.1126/science.1065543.

(242) Chu, S. T.; Chien, K. H.; Lin, H. H.; Wu, W. H.; Jian, J. Y.; Tzeng, W. F.; Chiou, T. J. Using marker gene analysis instead of mixed lymphocyte reaction assay for identification of functional CD4+FOXP3+ regulatory T cells. *Biotechnol Lett* **2018**, *40* (3), 535-542, DOI: 10.1007/s10529-017-2498-8.

(243) Hellman, L. M.; Fried, M. G. Electrophoretic mobility shift assay (EMSA) for detecting protein-nucleic acid interactions. *Nat Protoc* **2007**, *2* (8), 1849-61, DOI: 10.1038/nprot.2007.249.

(244) Inoue, H.; Fukuizumi, T.; Tsujisawa, T.; Uchiyama, C. Simultaneous induction of specific immunoglobulin A--producing cells in major and minor salivary glands after tonsillar application of antigen in rabbits. *Oral Microbiol Immunol* **1999**, *14* (1), 21-6.

(245) Purcell, A. W.; Gorman, J. J. Immunoproteomics: Mass spectrometry-based methods to study the targets of the immune response. *Mol Cell Proteomics* **2004**, *3* (3), 193-208, DOI: 10.1074/mcp.R300013-MCP200.

(246) Tobian, A. A.; Canaday, D. H.; Harding, C. V. Bacterial heat shock proteins enhance class II MHC antigen processing and presentation of chaperoned peptides to CD4+ T cells. *J Immunol* **2004**, *173* (8), 5130-7, DOI: 10.4049/jimmunol.173.8.5130.

(247) Lazarski, C. A.; Chaves, F. A.; Sant, A. J. The impact of DM on MHC class II-restricted antigen presentation can be altered by manipulation of MHC-peptide kinetic stability. *J Exp Med* **2006**, *203* (5), 1319-28, DOI: 10.1084/jem.20060058.

(248) Laurence, A.; Tato, C. M.; Davidson, T. S.; Kanno, Y.; Chen, Z.; Yao, Z.; Blank, R. B.; Meylan, F.; Siegel, R.; Hennighausen, L.; Shevach, E. M.; O'Shea J, J. Interleukin-2 signaling via STAT5 constrains T helper 17 cell generation. *Immunity* **2007**, *26* (3), 371-81, DOI: 10.1016/j.immuni.2007.02.009.

(249) Medzhitov, R. Recognition of microorganisms and activation of the immune response. *Nature* **2007**, *449* (7164), 819-26, DOI: 10.1038/nature06246.

(250) Lee, H. K.; Mattei, L. M.; Steinberg, B. E.; Alberts, P.; Lee, Y. H.; Chervonsky, A.; Mizushima, N.; Grinstein, S.; Iwasaki, A. In vivo requirement for Atg5 in antigen presentation by dendritic cells. *Immunity* **2010**, *32* (2), 227-39, DOI: 10.1016/j.immuni.2009.12.006.

(251) Yamaguchi, T.; Teraguchi, S.; Furusawa, C.; Machiyama, H.; Watanabe, T. M.; Fujita, H.; Sakaguchi, S.; Yanagida, T. Theoretical modeling reveals that regulatory T cells increase T cell-interaction with antigen-presenting cells for stable immune-tolerance. *Int Immunol* **2019**, DOI: 10.1093/intimm/dxz043.

(252) Furtado, G. C.; Curotto de Lafaille, M. A.; Kutchukhidze, N.; Lafaille, J. J. Interleukin 2 signaling is required for CD4(+) regulatory T cell function. *J Exp Med* **2002**, *196* (6), 851-7, DOI: 10.1084/jem.20020190.

(253) Corse, E.; Gottschalk, R. A.; Allison, J. P. Strength of TCR-peptide/MHC interactions and in vivo T cell responses. *J Immunol* **2011**, *186* (9), 5039-45, DOI: 10.4049/jimmunol.1003650.

(254) Rocha, B.; Grandien, A.; Freitas, A. A. Anergy and exhaustion are independent mechanisms of peripheral T cell tolerance. *J Exp Med* **1995**, *181* (3), 993-1003, DOI: 10.1084/jem.181.3.993.

(255) Alleva, D. G.; Gaur, A.; Jin, L.; Wegmann, D.; Gottlieb, P. A.; Pahuja, A.; Johnson, E. B.; Motheral, T.; Putnam, A.; Crowe, P. D.; Ling, N.; Boehme, S. A.; Conlon, P. J. Immunological characterization and therapeutic activity of an altered-peptide ligand, NBI-6024, based on the immunodominant type 1 diabetes autoantigen insulin B-chain (9-23) peptide. *Diabetes* **2002**, *51* (7), 2126-34, DOI: 10.2337/diabetes.51.7.2126.

(256) Alleva, D. G.; Crowe, P. D.; Jin, L.; Kwok, W. W.; Ling, N.; Gottschalk, M.; Conlon, P. J.; Gottlieb, P. A.; Putnam, A. L.; Gaur, A. A disease-associated cellular immune response in type 1 diabetics to an immunodominant epitope of insulin. *J Clin Invest* **2001**, *107* (2), 173-80, DOI: 10.1172/JCI8525.

(257) Culina, S.; Boitard, C.; Mallone, R. Antigen-based immune therapeutics for type 1 diabetes: magic bullets or ordinary blanks? *Clin Dev Immunol* **2011**, *2011*, 286248, DOI: 10.1155/2011/286248.

(258) Zhang, L.; Londono, P.; Yu, L.; Grimes, S.; Blackburn, P.; Gottlieb, P.; Eisenbarth, G. S. MAS-1 adjuvant immunotherapy generates robust Th2 type and regulatory immune responses providing long-term protection from diabetes in late-stage pre-diabetic NOD mice. *Autoimmunity* **2014**, *47* (5), 341-50, DOI: 10.3109/08916934.2014.910768.

(259) Manetti, R.; Parronchi, P.; Giudizi, M. G.; Piccinni, M. P.; Maggi, E.; Trinchieri, G.; Romagnani, S. Natural killer cell stimulatory factor (interleukin 12 [IL-12])

induces T helper type 1 (Th1)-specific immune responses and inhibits the development of IL-4-producing Th cells. *J Exp Med* **1993**, *177* (4), 1199-204, DOI: 10.1084/jem.177.4.1199.

(260) Bucht, A.; Larsson, P.; Weisbrot, L.; Thorne, C.; Pisa, P.; Smedegard, G.; Keystone, E. C.; Gronberg, A. Expression of interferon-gamma (IFN-gamma), IL-10, IL-12 and transforming growth factor-beta (TGF-beta) mRNA in synovial fluid cells from patients in the early and late phases of rheumatoid arthritis (RA). *Clin Exp Immunol* **1996**, *103* (3), 357-67, DOI: 10.1111/j.1365-2249.1996.tb08288.x.

(261) Jensen, L.; Kuff, E. L.; Wilson, S. H.; Steinberg, A. D.; Klinman, D. M. Antibodies from patients and mice with autoimmune diseases react with recombinant hnRNP core protein A1. *J Autoimmun* **1988**, *1* (1), 73-83.

(262) Fantini, M. C.; Becker, C.; Tubbe, I.; Nikolaev, A.; Lehr, H. A.; Galle, P.; Neurath, M. F. Transforming growth factor beta induced FoxP3+ regulatory T cells suppress Th1 mediated experimental colitis. *Gut* **2006**, *55* (5), 671-80, DOI: 10.1136/gut.2005.072801.

ABSTRACT**SELF-DELIVERY DRUG AMPHIPHILIES IN CHEMOTHERAPY AND IMMUNOTHERAPY****by****JINGCHAO XI****December 2019****Advisor:** Dr. Haipeng Liu**Major:** Chemical Engineering**Degree:** Doctor of Philosophy

Eliminating the need for external delivery systems, self-delivery drug amphiphiles represent a simple yet effective approach designed to overcome the various biological barriers for drug delivery. The ability to program the molecular structures and the physicochemical properties, which control the interactions between the drug amphiphiles and their biological surroundings has attracted significant research interests. In this work, we constructed several amphiphilic drugs including chemotherapeutic and immunotherapeutic agents. These amphiphiles exhibited interesting interactions with their biological surroundings. Amphiphiles self-assemble into spherical micelle structures in aqueous solution. However, in the presence of complexed biological fluids, they also possess a strong affinity toward albumin protein and plasma membrane. By controlling the molecular structures which govern the three-way equilibrium, self-delivery drugs/vaccines overcoming multiple biological barriers were designed and tested *in vitro* and *in vivo*. Employed endogenous albumin protein as a drug carrier, self-delivery chemotherapeutic drug amphiphiles (e.g. amphiphilic doxorubicin) were

firstly investigated. High levels of tumor-specific and extended circulating half-life facilitated doxorubicin-induced cytotoxicity and anti-cancer efficacy. Importantly, it was the first report on lipid-based targeting subcellular mitochondria which filled the gap of intracellular tracking using lipoplex approaches. Translating from albumin-based self-delivery strategy, amphiphilic lipid-based immunosuppressive drugs and peptides were studied on several immune disease models. Amphiphilic peptides were observed to accumulate in the antigen presenting cells (APCs) in the lymph nodes (LNs), enhance the potency and duration of peptide antigen presentation by APCs, and induce antigen-specific immune tolerance that controlled both T-cell- and B-cell-mediated immunity. Moreover, immunization with an amphiphilic insulin B chain 9-23 peptide, an immunodominant CD4⁺ T cell epitope in non-obese diabetic (NOD) mice successfully restored antigen-specific immune tolerance delaying the onset of Type 1 Diabetes (T1Ds). Overall, those self-delivery amphiphilic drugs provided a simple approach to improve the bioavailability, bioaccessibility, and biocompatibility of the pharmaceutical payloads, which will be emerged as a novel design principle for drug delivery in the future.

Autobiographical Statement

Jingchao Xi received her B.S. degree (Bachelor of Science) in Chemistry from Fuzhou University (Fuzhou, Fujian, China) in 2014. She joined department of Chemical Engineering and Materials Science at Wayne State University, MI, US in fall of 2014 to pursue a degree of Doctor of Philosophy in Chemical Engineering. Her research, under the guidance of Dr. Haipeng Liu is focused on strategies to develop self-delivery drug amphiphiles nanomedicines for cancer chemotherapy and autoimmune disease immunotherapy. She has authored one publication as the first author and coauthored four peer reviewed publications. She also has industrial experience as an internship in AstraZeneca (South San Francisco, CA) in 2019 and focused on immunogenicity evaluation.